MULTIPOINT HUMIDITY SENSING BASED UPON A MULTIPLEXED FIBRE OPTIC SENSOR

By Stefan Mc MURTRY

PhD thesis submitted at the
University of Kent
1999

Thesis supervisors:

Pr. David Jackson

Professor of Applied Optics, School of Physical Science, University of Kent

Dr. John Wright

Reader in Materials Chemistry, School of Physical Science, University of Kent

Acknowledgements

I would like to thank David Jackson for his guidance and support over the project during these three years leading to successful results, also for all the useful and interesting long discussions on the field of optical sensing and finally for allowing me to work in a prestigious and internationally known research group.

I would like to thank John Wright for his constant help in chemistry during the project, for spending time, and for providing me advice on the best way to produce the required chemical samples.

I wish also to thank Malcolm Joyce and Simon Port for their contribution to the project, and especially for allowing me some access to the super-critical drying apparatus at Preston in BNFL's laboratories.

I wish to thank BNFL for financially supporting the project.

I wish to thank Joseph L. Keddie from the University of Surrey for collaborating in the project by supplying the PMMA-PMTGA-PMMA films.

I wish to thank my mother for her support during the last three years, and also the rest of my family.

Finally, I wish to thank my girl friend Sophie for providing me care, affection and support during my whole Phd.

Abstract

This thesis describes different interferometric systems, including a final prototype, used to characterise and sense humidity either by using materials or by measuring the refractive index of air.

A low cost humidity generator was built to permit the evaluation of the effect of humidity on the refractive index of air and on the different tested samples. This system allows the humidity to be tuned over the full range in a test chamber at a constant flow.

The effect of humidity on the refractive index of air was studied. This showed that for standard air, a full range humidity change could provoke a 171 nm optical path change in a 10 cm long Michelson interferometer. A fiberised dual tandem interferometric system based on a low coherence source was developed using a remote Michelson interferometric probe. This novel method allows humidity to be sensed remotely with a 1.6 %RH accuracy, a fast response time and no ageing.

To evaluate the response of materials when submitted to humidity, an accurate fiberised dual tandem interferometric system using a low coherence source was built. The accuracy of the measurement was 5 nm. The responses to humidity of sol-gel and aerogel samples were tested using this system.

Finally, a multiplexed fiberised dual tandem interferometric system based on a low coherence source was built allowing humidity sensing on different optical lines with an accuracy of 50 nm, by using Fabry-Perot interferometric probes. This system allowed the characterisation of various polymers when submitted to humidity.

Based on this system a final prototype using a PMMA-PMTGA-PMMA polymer film was demonstrated and an accuracy of 1.2 %RH was achieved. This polymer had a repeatable response to humidity and did not suffer from ageing. This system allowed an absolute measurement and was very close to a commercial device.

Table of contents

1

Introduction

1.1 Humidity sensing

1.1.1 The use of measuring humidity

1.1.2 Definition of humidity

1.1.3 BNFL's requirements

1.1.4 Outline of the thesis

1.2 Review of conventional methods of measuring humidity

1.2.1 Mechanical type humidity sensors

1.2.2 Wet and dry bulb thermometric sensors

1.2.3 Resistive sensors

1.2.4 Capacitive sensors

1.2.5 Dew point sensors

1.2.6 Saturated lithium chloride (LiCl) sensors

1.2.7 Phosphorous pentoxide (P_2O_5) sensors

1.2.8 Spectroscopic methods

1.2.9 Colour change

1.3 Measuring relative humidity with specific materials

1.3.1 Introduction

1.3.2 The sol-gel material

1.3.3 Aerogels

1.3.4 Hydrophilic polymers

1.4 References

1.1 Humidity sensing

1.1.1 The use of measuring humidity

The development of new technologies has resulted in the need for sophisticated humidity sensors. This is the case, for example, in electronic device manufacture where a dry atmosphere is required. Wet atmospheres are important for the growth of plants, and a constant monitoring of humidity is required in warehouses. Humidity being an environmental factor, it is useful to measure it not only for industrial applications but also for common household appliances such as in air conditioners, microwave ovens, photographic cameras, and dew sensing on VTR's heads (or video camera recorders). In fact in most high tech electronic devices that we use the measurement of humidity is required. Humidity sensors are also widely used in weather forecasting, allowing better prediction when combined with temperature and pressure measurements. Finally the determination of humidity is crucial in nuclear fuel depositories as the atmospheric conditions must be controlled to avoid any supercritical transitions resulting in neutron flows.

The following table shows the different areas where humidity sensors can be usefully applied.

Industry	**Application**	**Operation range**
Community safety	Nuclear power reactor	above 80°C, 80% RH
	Thermoelectric power plant	above 100°C
	Humidity in boiler	100-400°C
	Water in gas	city gas atmosphere
Domestic electric	Desiccator	50–100 % RH
appliance	Air conditioner	30–100% RH
	control of cooking	5-200°C, humidity
	various kind of conditioner	5-40 °C, 40–70 %RH
	Reprographic machine	150°C, humidity
Medical Equipment	Sterilizer	Humidity above 100°C
	Medical equipment for	20–30°C, above 90%RH
	Respiratory organs	
	Incubator	10-300°C, 50-80%RH
	Paper manufacture	10-30°C, 50-100%RH
	Oven	100-500°C, above 50%RH

		Film desiccation	20-60°C, below 20%RH
		Humidity control in factory	5-40°C,0-50%RH
		Humidifier for industry	30-300°C, above 50%RH
		Refrigerated Show case	below 8°C,below 30%RH
		Printing	20-25°C, 90%RH
	Agriculture	Observation robot for agriculture	open air
		Green house	5-40°C,0-100%RH
		Protection of plantations	-10-60°C,50-100% RH

1.1.2 Definition of humidity

Humidity is equivalent to the presence of water vapour in air in any arbitrary proportion. It can be considered as a gas formed of water molecules. This gas is normally transparent and its typical composition in air is to about 1 percent. Water vapour results from the evaporation of liquid or solid water (ice).

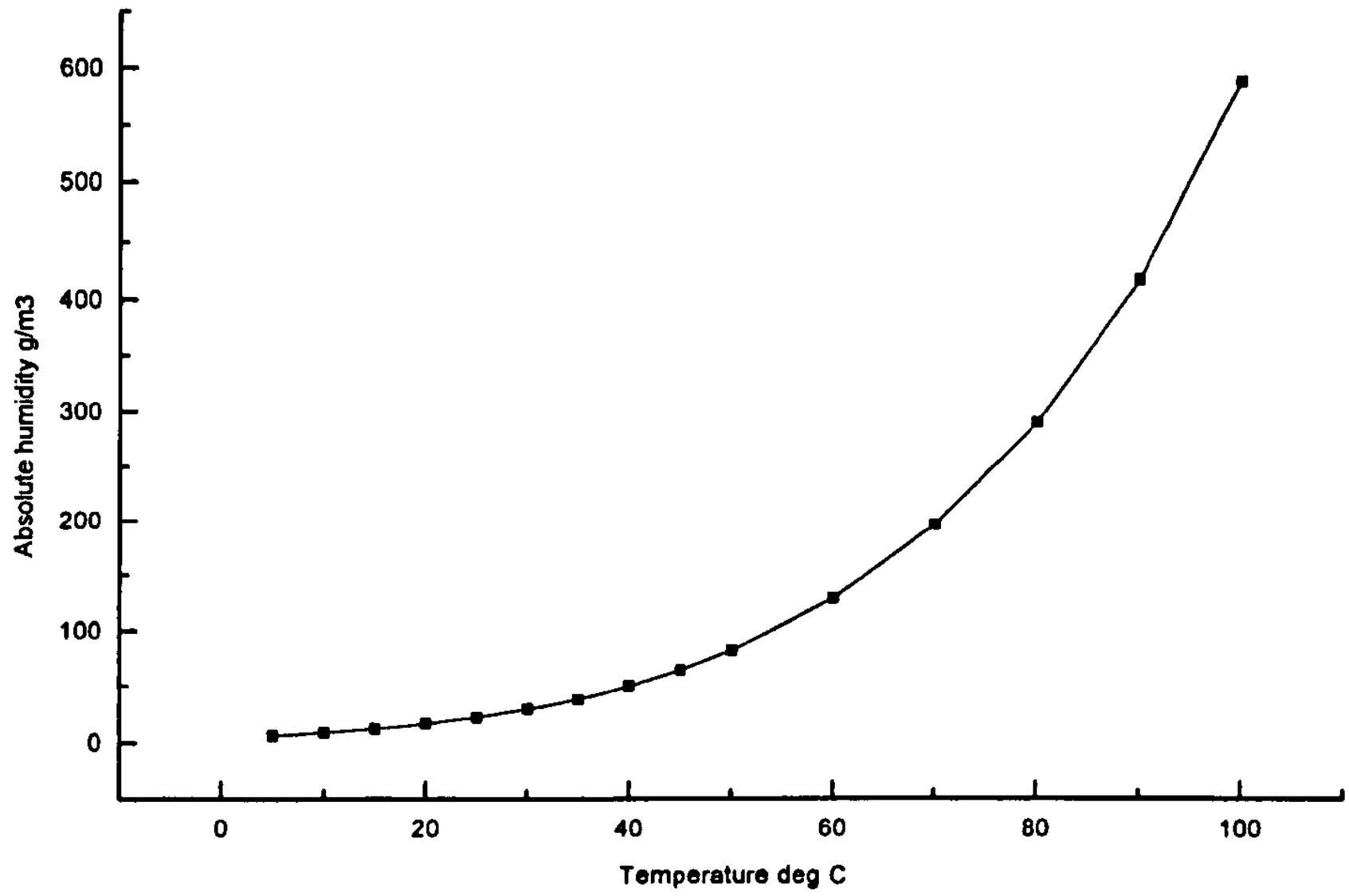

Figure 1.1 shows the maximum absolute humidity of air with temperature at one atmosphere

In fact when equilibrium between the different phases (gas, liquid, and solid) occurs evaporation and condensation are present at the same time. When the three phases are

present at the same time at equilibrium, the triple point of water is reached. This only occurs for fixed values of pressure and temperature, this is P= 4.57 mmHg and T= -0.15 °C. The extent of evaporation or condensation depends mainly on temperature. The higher the temperature the more water vapour can be contained in the air. This is quantified in figure 1.1. When the air is at maximum humidity, it is said that the air is saturated. Also the relative humidity indicates how saturated the air is at one given temperature, thus 50 %RH means that the air contains 50% of the maximum possible humidity. It is also possible to measure humidity using its absolute value, this measurement is dependent on temperature and quantifies the weight of the number of molecules held in one cube meter (g/m^3), but is not often used because it is less easy to understand than a percentage of the maximum humidity.

1.1.3 BNFL's requirements

The requirements defined by British Nuclear Fuels at the beginning of the project were the following. The sensing of humidity should be over the full range of humidity (0-100 %RH) with an accuracy similar to electronic devices (1-2 %RH), at normal temperatures and under atmospheric pressures. The sensor system should use fibre optic technology as it offers many advantages such as electromagnetic immunity, smaller dimensions, low weight and cost of fibres compared to electric cables, the capacity of multiplexing many sensors and finally the possibility to be deployed in harsh environments. The system should be composed of a central unit with various sensors placed remotely at the end of optical fibre links and allow the multiplexing of a large number of sensors. As the system is to be used in industry, the probes should be small enough to be used in all configurations and be sufficiently robust to allow handling. Finally the prototype should have the facility to display the measurements on a computer screen.

1.1.4 Outline of the thesis

This thesis describes novel interferometric systems and materials suitable for humidity sensing. After a description of conventional humidity sensors and possible materials for humidity sensing, the emphasis will be made on interferometry and the results obtained using the different sensing approaches (sensing humidity by measuring the refractive

index of air or by using specific materials such as aerogels). Finally the description of a final prototype based on a polymer film will be given.

1.2 Review of conventional methods of measuring humidity

1.2.1 Mechanical type humidity sensors

Mechanical humidity sensors are based on organic materials that expand or contract with humidity. In most cases the movement induced by the material is amplified by a lever to move a needle or a pen of a chart recorder. Some commonly used materials are hair, catgut, goldbeater's skin (cows intestine), textile or plastic, but this list is not exhaustive and any material can be used provided that the response to humidity is repeatable. This type of humidity sensor has usually a range of 20-80 %RH at room temperature with an accuracy of 5-15% RH. The advantages of such sensors are the lack of electric power (batteries or mains), the possibility of a permanent record and their low cost, while their weaknesses are a slow response, possible hysteresis and their fragility to vibrations and impact.

1.2.2 Wet and dry bulb thermometric sensors

A wet and dry bulb thermometric sensor is composed of two temperature sensors, one of which is inserted into a porous medium constantly held wet by a capillary action circulating water from a reservoir. The water enclosed in the porous medium evaporates and provokes a fall in temperature. For better precision a fan usually allows a constant evaporation of the water which depends on the humidity levels to be measured. The humidity measurement is obtained by comparing the temperature of both sensors. The water vapour pressure e is found from the two temperatures t_d and t_w respectively for the dry and wet bulbs by:

$$e = e_s - AP(t_d - t_w) \qquad (1\text{-}1)$$

Where P is the barometric pressure, and e_s the saturation vapour pressure at t_w. For ventilated systems as in the 'Assman' type $A = 6.66 \times 10^{-4}\ °C^{-1}$ but this value can vary between $A = 6.64 \times 10^{-4}\ °C^{-1}$ and $A = 6.68 \times 10^{-4}\ °C^{-1}$ depending on the design. This kind of humidity sensor covers the 5-100 %RH range with an accuracy of 2-5 %RH between 0-100 °C. The advantages of such system are the simplicity of the sensor, its robustness,

a good stability and the coverage of a wide range of humidity while tolerating high temperatures and condensation. However these instrument may be difficult to maintain, a large sample of air is required, this sample will be humidified by the evaporation process, and particles may obstruct the porous medium. Finally the measurement may be difficult below 10 °C especially due to the presence of water or ice at 0 °C.

1.2.3 Resistive sensors

These sensors use a hydrophilic polymer [1-5] such polystyrene-sulfonate [1] which modifies its electrical properties when water is absorbed. They do not support condensation that can alter the sensor properties except if equipped with a "saturation guard" heating system that avoids any condensation on the probe. The response is fast and the structure of the sensor simple. The resistance of the sensor decreases with humidity because the ionic pair of the polymer electrolytes is dissociated. However some polymers [6,7] such as polyethyleneoxide-sorbitol [6] swell and a resistive change is obtained due to a spread of carbon or metal powder on the film. Resistive humidity sensors are usually in the 5-99 %RH range for temperatures from –50 °C to 200 °C with an accuracy of 2-3 %RH.

1.2.4 Capacitive sensors

Similar to resistive sensors, a polymer film modifies its dielectric properties in presence of humidity. A capacitive sensor developed by Vaisala, is based on a cellulose acetate film dissolved in ethylene dichloride [8]. This sensor shows a linear relation between 0-100 %RH [9] and has a good accuracy, low hysteresis, and fast response time. Other humidity sensors based on a capacitive effect use polyimide [10] and crosslinked cellulose acetate butylate (CAB) [11,12]. Generally speaking these sensors are not damaged by condensation but a shift in the calibration may occur. The covered range is 0-100 %RH between –40 °C and 200 °C and for an accuracy of 1-2 %RH.

1.2.5 Dew point sensors

Dew point sensors are based on the reflection of light from a metal mirror. When dew appears, the sensor detects how the mirror reflects or scatters light. This type of sensor does not need to be linear over the full range of humidity, but only over 90 %RH. They are used for example to detect dew on VCR heads. These sensors usually have long life times and provide an accurate measurement. However a contamination of the mirror could affect the measurement, the mirror should then be cleaned with pure water. The temperature range of operation is –85 °C to 100 °C with an accuracy of 0.2-1 °C on the dew point temperature. A dew point sensor based on a vibrating quartz crystal has also been developed. The vibration amplitude of such resonant crystal is sensitive to a very small mass loading while its resonant frequency depends on the temperature. Thus when coupled to a Peltier cooled plate, the sensor can be used to measure the ambient relative humidity using the temperature of the room and the dew point temperature. This sensor can measure relative humidity with an accuracy better than 1.8 %RH [13].

1.2.6 Saturated lithium chloride (LiCl) sensors

Lithium chloride is an hydrophilic salt. The salt absorbs the humidity in the air and changes its electrical properties. A voltage is applied to the salt and the current is directly related to the amount of water absorbed. When the current flows the salt is slightly heated until an equilibrium is reached, the measuring process is therefore quite slow. These sensors cannot be used in automatic systems but are suitable for meteorological observation. Dunmore developed such a sensor in 1939 [14] which is still widely used, the range of operation is 20-90 %RH. The advantage of this sensor is its low cost. However it does not function under 10 %RH and will not tolerate condensation or contamination by solvent. Other chemicals such potassium metaphosphate [15] and barium fluorite [16] are also used as thin films for humidity sensing.

1.2.7 Phosphorous pentoxide (P_2O_5) sensors

This sensor is similar to the previous one except that, when the voltage is applied on the thin film of P_2O_5 (a powerful dessicant) a process of water dissociation into oxygen and hydrogen takes place. The current corresponds to the power needed for the dissociation of the water vapour and not to the change of resistivity of the film as in section 1.2.6. These sensors are suitable for the measurement of low levels of humidity but require a known flow of air. The measurement is read in ppm (part per million) and the accuracy is 3-10 % of the reading. The advantages are good sensitivity and resistance to some corrosive gases but the air flow is critical and the sensor can be damaged in the case of very low humidity levels (<1 ppm). An error on the reading can also be induced by the inherent presence of oxygen and hydrogen.

1.2.8 Spectroscopic methods

By using various spectroscopic methods it is possible to isolate the "signature" of the water vapour of air by comparison with a reference. This technique allows a resolution of a few parts per billion. There are several versions of this technique such as APIMS (atmospheric pressure ionisation mass spectrometry), FT-IR (Fourier transform infrared spectroscopy), and TDLAS (tuneable diode laser absorption spectroscopy). The range is usually wide depending on the type of device and the accuracy is 3-10 % of the readings. The advantage is that the technique can be used with any gas, at any temperature with a fast response, but these systems need sophisticated technology and calibration, and are therefore expensive.

1.2.9 Colour change

Cobalt chloride is inserted into a sensing medium (as a film) and reacts with humidity. The effect is a visible change of colour of the chemical. The range is 20-80 %RH at room temperature for an accuracy of 10-20 %RH. The advantage is the lack of power (batteries or mains), low cost and simplicity, but this sensor is difficult to calibrate and only gives a poor estimate on the humidity levels.

1.3 Measuring relative humidity with specific materials

1.3.1 Introduction

To constitute a good humidity sensor the material should give reproducible dimensional changes when exposed to different humidity levels. In the case of optical sensing, transparency is also a useful property. Thus this work has explored the use of polymer, sol-gel and aerogels samples all of which can be transparent materials with appropriate swelling properties. Some key aspects will now be reviewed.

1.3.2 The sol-gel material

1.3.2.1 Introduction to sol-gels

In 1846 Ebelmen [17] prepared the first metal alkoxide from $SiCl_4$ when the solution gelled with the humidity of the atmosphere. The interest for this material remained to the chemists, until Geffcken [18] found in the 1930's that alkoxides could be used in the preparation of oxide films. Then the process was understood as described in a review from Schroeder [19]. Sol-gels are oxide glasses that result from a chemical reaction that can be done at room temperature or slightly above. The first solution is a mixture of several compounds forming a solution. This solution then becomes a 'sol' by the process of hydrolysis and condensation. At this stage the sol is a colloidal suspension composed of solid particles in a liquid. Then if these particles can form further cross links a gel appears that can lead to a rigid glassy gel. The starting compounds for preparation of a sol gel solution consist of a 'metal' or 'metalloid' element (such as Al,Si,Ti…) coupled with various ligands. A ligand being a molecule or ion that donates an electron pair to an atom or ion forming a complex. The following sketch gives a representation of three different possible structures of porous sol gel using TMOS (tetramethoxysilane):

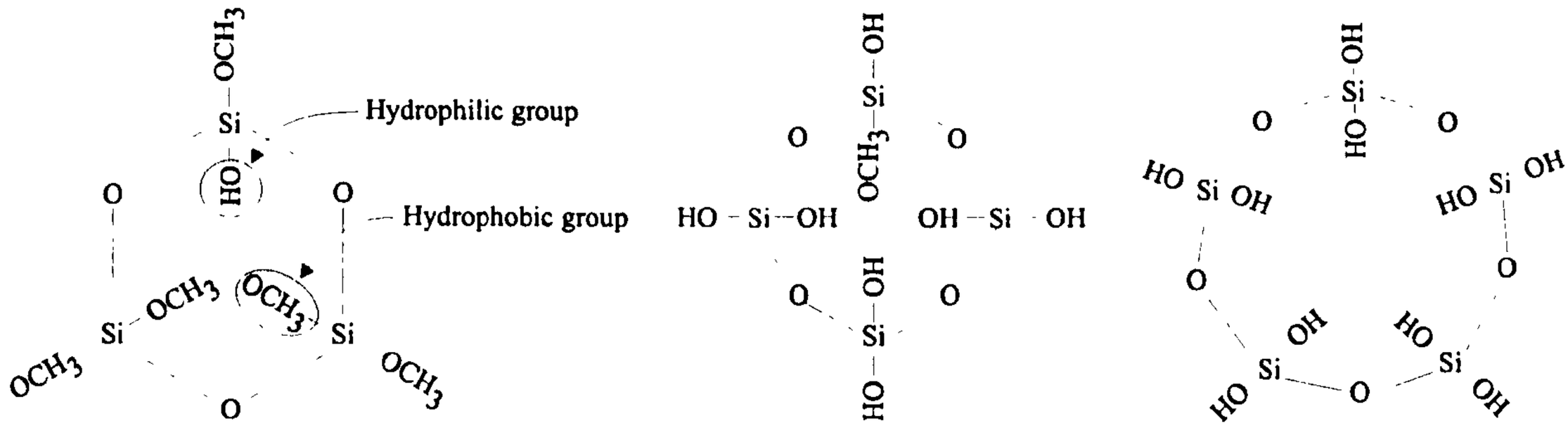

Figure 1.2 shows three of the possible different structures of sol-gel using tetramethoxysilane (TMOS)

1.3.2.2 Fabrication of sol-gels

The mixture chosen to give a transparent porous sol gel using TMOS during this project was:

3 ml	ethanol	(EtOH) $CH_3.CH_2.OH$
2.5ml	tetramethoxysilane (TMOS)	$Si.(OCH_3)_4$
1.6 ml	water	H_2O
2 drops	hydrochloric acid	HCl (pH 2.2)

The components are added in the order of the list and mixed for a period of 5 minutes at room temperature. Once the mixture was made several transformations described below occurred.

1.3.2.2.1 Hydrolysis

Hydrolysis is the main reaction of the process, here a hydroxyl ion links to the 'metal' atom, as in the following reaction:

$$Si(OR)_4+H_2O \rightarrow HO\text{-}Si(OR)_3+ROH$$

Where R represents the ligand which in our case is $-CH_3$

Thus the reaction is:

$$Si(OCH_3)_4+H_2O \rightarrow HO\text{-}Si(OCH_3)_3+CH_3\text{-}OH$$

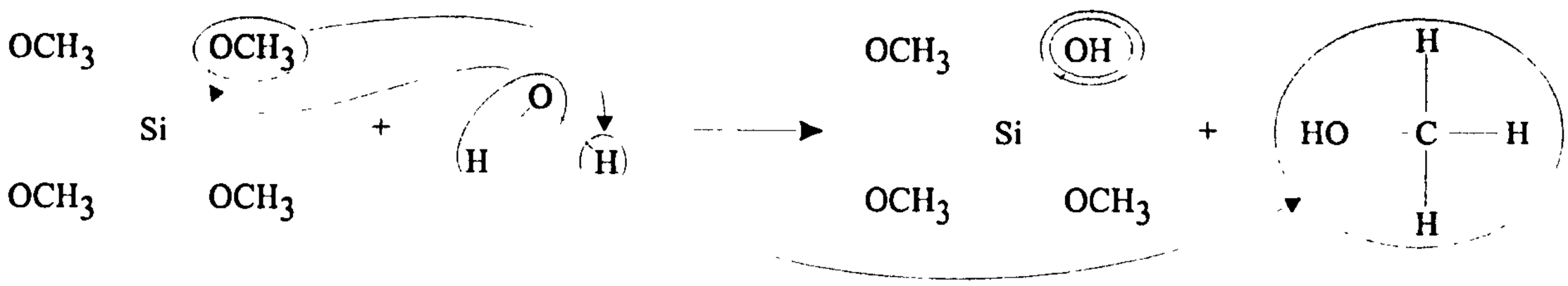

If the amount of water is sufficient and depending on the catalyst (HCl) in the solution, the hydrolysis may go to completion. In this case all the -OCH_3 groups are replaced by -OH groups

$$Si(OCH_3)_4+4\ H_2O \rightarrow Si(OH)_4+4\ CH_3\text{-}OH$$

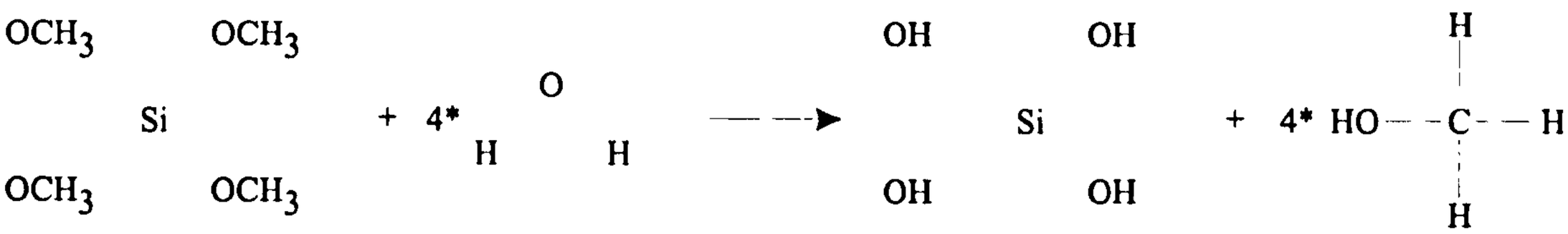

1.3.2.2.2 Condensation

The condensation process links two partially (or totally) hydrolysed molecules and liberates a molecule such as -ROH, in our case water.

$$(OCH_3)_3Si\text{-}OH + HO\text{-}Si(OCH_3)_3 \rightarrow (OCH_3)_3Si\text{-}O\text{-}Si(OCH_3)_3 + H_2O$$

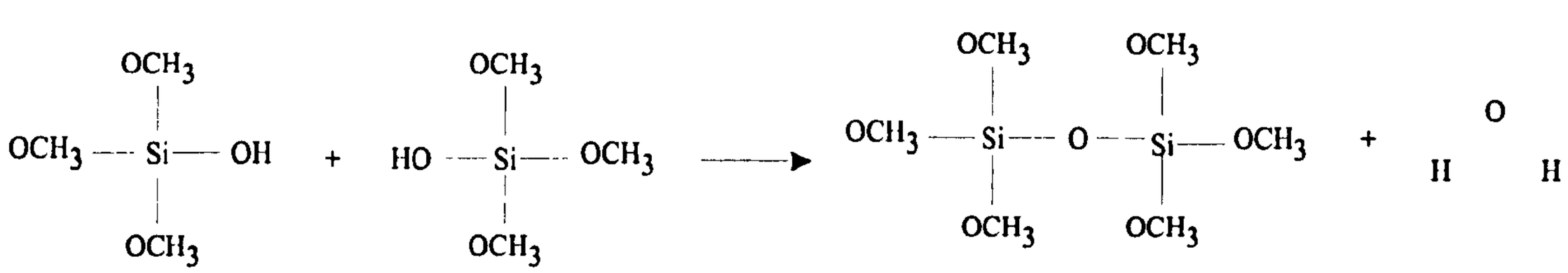

or

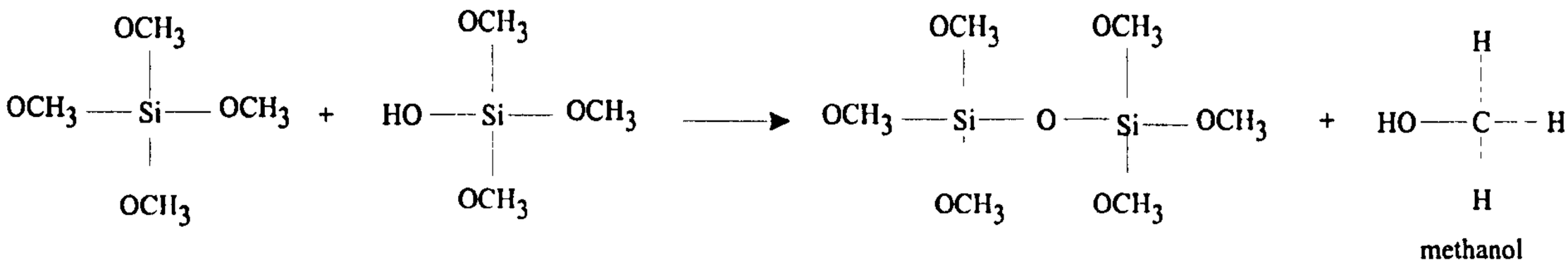

The condensation process can continue, and build up larger and larger molecules that end up in clusters capable of linking together in the gelation process. Usually the condensation process begins before the hydrolysis ends.

1.3.2.2.3 Gelation

Gelation occurs when condensation has proceeded far enough to form a continuous spanning cluster across the whole reaction vessel. At this point the viscosity and viscoelastic modulus increase rapidly, but condensation can still continue after the gel point, to give more and more links between the clusters (see ageing below). Increasing slightly the temperature of the sol can reduce the gelation time.

1.3.2.2.4 Ageing process

In this process, the obtained gel left in its liquid strengthens its lattice. During this phase three processes occur: polymerisation, coarsening, and phase transformation. The polymerisation results from further condensation reactions [20-22] that can occur several months after the gelation of the gel depending on the pH of the solution and the temperature. The coarsening process is a process of dissolution and precipitation linked to the solubility of the particles in the solution. The particles with a positive radius of curvature dissolve more easily than those that are flat. The effect is that the smaller particles tend to dissolve while the solute precipitates into larger particles filling the small pores and increasing the pore size [23]. The phase transformation process is the separation in two phases of the liquid followed by a crystallisation. The changes induced by the ageing process on the lattice are important, such as the shrinkage of the gel (syneresis) expelling the liquid out of the pores.

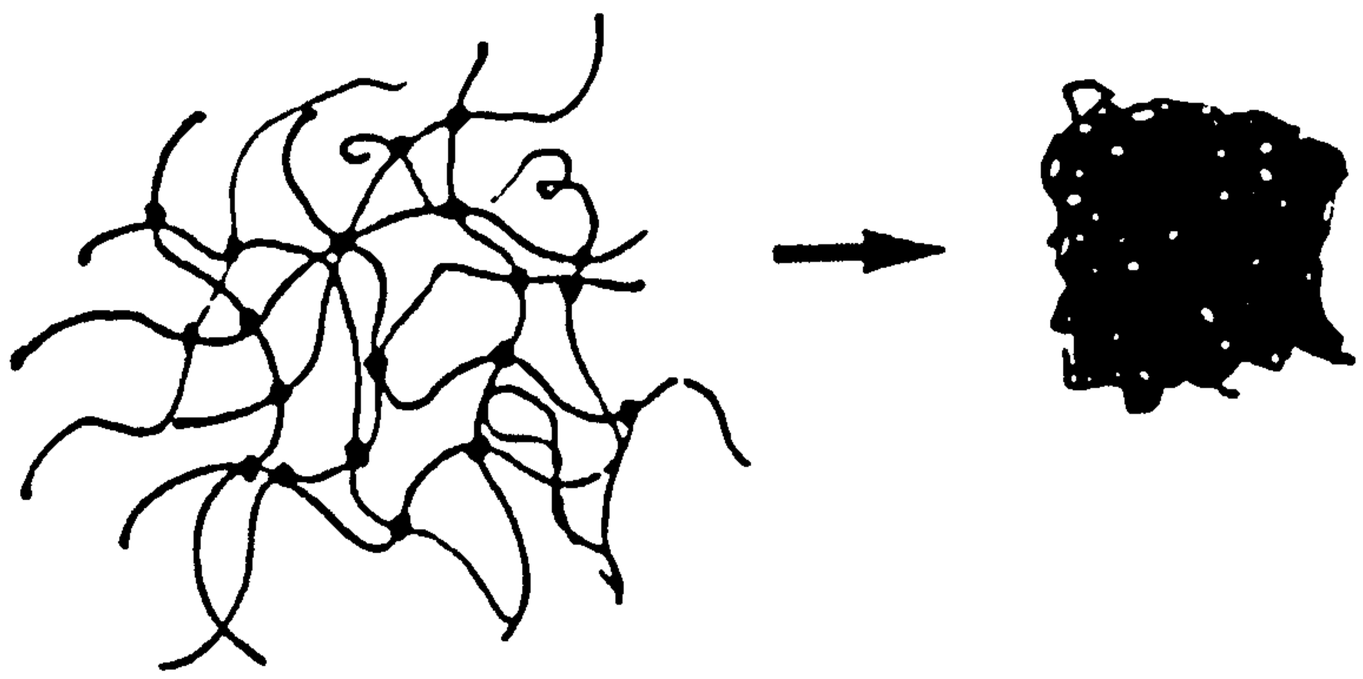

Figure 1.3 shows the ageing process for an acid catalysed sol-gel

1.3.2.2.5 Drying

The problem of drying sol-gel has been well described [24] because of the difficulty of obtaining crack free sol-gels. The main reason cracks appear in a gel is the tension due to the capillary pressure on the lattice of the gel. The pressure due to the meniscus of curvature seen in figure 1.4 is given by Kelvin's equation.

$$RT \ln \frac{P_r}{P_0} = \frac{2\gamma M}{\rho r} \qquad (1\text{-}2)$$

Where P_r is the pressure over a surface of radius of curvature r, P_0 the pressure over a flat surface, γ the surface tension, M the molecular mass and ρ the density of the liquid. This equation shows that the size of the pores is crucial, the smaller the pores the higher the pressure stress. The first stage is the constant rate period where the gel shrinks by the same amount of liquid that evaporates. Therefore the interface liquid-vapour remains at the exterior of the gel inducing no stress to the lattice. Following this critical point the meniscus enters the lattice and the tension reaches its maximum value. The following stage is the falling rate period where the rate of evaporation falls while the temperature of the surface rises but is still below the ambient temperature. This is because most of the evaporation still occurs at the surface of the gel since the liquid flows along the pore walls.

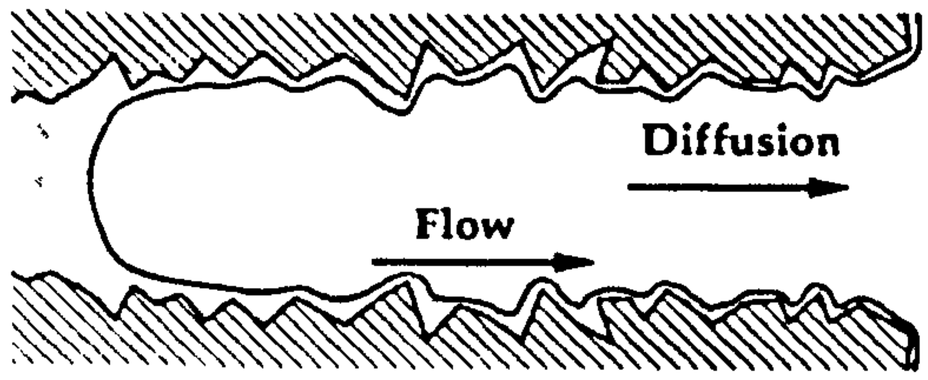

Figure 1.4 shows the meniscus penetrating into the pores in the falling rate period

The evaporation rate depends on the ambient temperature but also on the vapour pressure above the gel. Finally the second falling rate period occurs where the liquid in the pores stop flowing to the surface and is confined in little pockets. At this stage the liquid moves only by diffusion and the evaporation is very slow. One way to minimise the cracking of gels when drying is to use a DCCA (Drying control chemical agent) such as DMF (dimethylformamide) [25]. The effect is to reduce the surface tension at the liquid-vapour interface compared to water.

1.3.2.3 The hydrophilic property of sol-gels

TMOS based sol-gels are known for their hydrophilicity due to the presence of -OH groups at the surface of the pore walls. The hydrophilic property of the sol-gel depends on the present amount of these groups. Thus a well hydrolysed sol-gel (containing more -OH groups than, $-OCH_3$ groups as seen in section 1.3.2.1) will be more sensitive to humidity. Also the lack of pore liquid increases the sensitivity to water molecules, explaining the high hydrophilicity of aerogels.

1.3.3 Aerogels

1.3.3.1 Definition of aerogels

Aerogels are nanoporous materials obtained by supercritical drying. The first synthesis was made by Kistler [26] in the early 30's. Aerogels have been since, a source of interest [27] due to their low density, high porosity, large surface area, and low thermal conductivity. Many applications [28,29] have resulted from this material such as thermal insulation, supercapacitors, drug delivery systems, absorbents and particle trapping in space. The fabrication of aerogels necessitates two distinctive technologies,

the sol-gel processing and the supercritical drying. As described in the previous section the sol-gel synthesis does not require special instrumentation unlike the supercritical drying that necessitates a high pressure flow system. It is now possible to make aerogels with a density down to 0.003 g/cm^3 much more transparent than conventional ones [30].

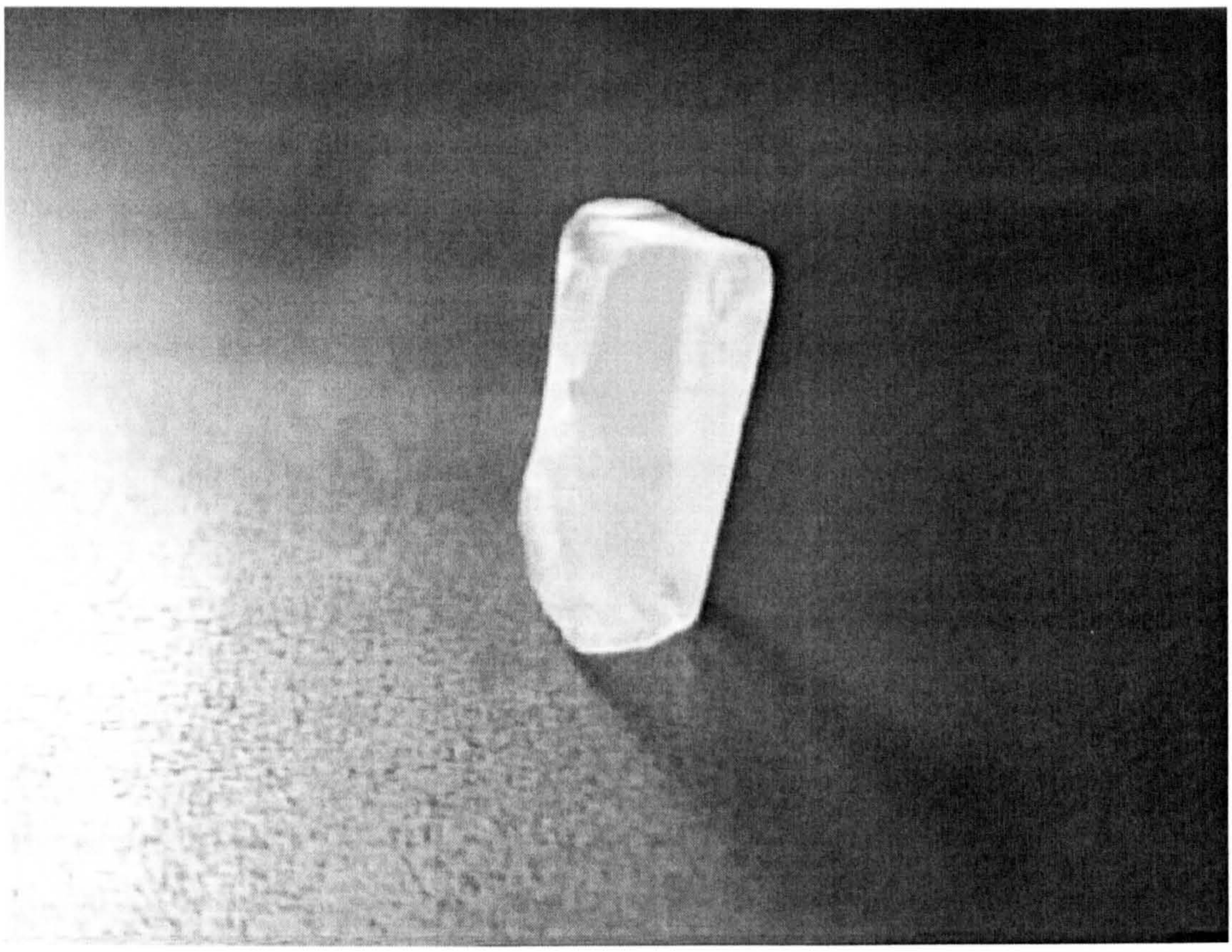

Figure 1.5 shows a typical bulk aerogel for use in industry

1.3.3.2 Fabrication of aerogels

As described in section 1.3.1.2.5 , the main problem when drying sol gels is to avoid cracking. The stress on the lattice of the gels is the result of the penetration of the meniscus at the interface gas-liquid into the gel while drying. The supercritical technique takes advantage of the fact that there is no distinction between liquid and vapour phases at the supercritical point [31-35]. As can be seen in figure 1.6, the process is therefore to reach the supercritical condition and to flow liquid CO_2 (T_c= 30.94 °C and P_c=73.75 bars) in the lattice to eliminate all pore liquid [36-39]. The sample is then brought back to atmospheric conditions.

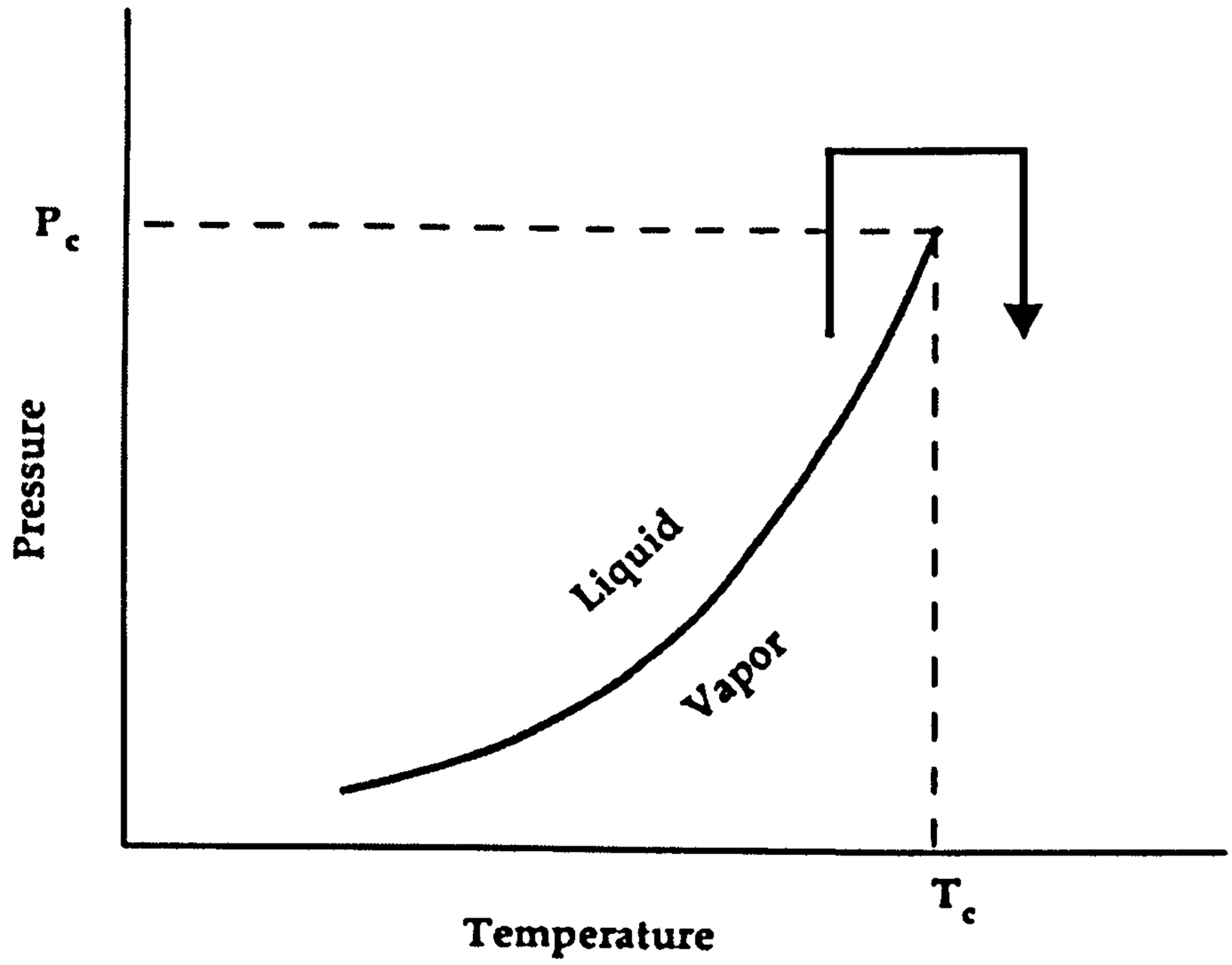

Figure 1.6 shows the supercritical point in the P, T diagram

1.3.3.3 Advantages of aerogels over sol-gels

The advantages of aerogels are clear. The fact the pores are empty of liquid reduces considerably any further reactions that could transform the gels structure such as hydrolysis, condensation, or ageing leading to stable gel. The second advantage is the increased amount of -OH groups present on the pore walls increasing the sensitivity of the gel. Finally the obtained sample isn't cracked and can be of any size.

1.3.4 Hydrophilic polymers

1.3.4.1 Definition

A polymer is the material resulting from the condensation or polymerisation of simple identical molecules such as monomers. They are described as a continuous three dimensional network held together by chemical or physical bonds. Sufficient space between the parts of the network allows solvents, here water, to penetrate the polymer and react with the structure [40]. Hydrophilic polymers are a particular group compatible with water. They are used for several applications such as thickeners or

additives in cosmetics. The use of hydrophilic polymers for humidity sensing is well known [41-46] due to the fact that their water content is directly related to the relative humidity of the surrounding atmosphere. The hydrophilicity of any polymer depends greatly on its structure. Usually the chain ensuring the stability of the polymer is composed of C-C bonds while the presence of oxygen contributes to the hydrophilicity of the material. This is due to the high electronegativity of the oxygen atom which still possess two pairs of electrons after forming two covalent bonds. Another element responsible for hydrophilicity of various polymers is nitrogen which after three covalent bonds still possess lone pair electrons. When water molecules penetrate the polymer they tend to separate the different adjacent chains. This may provoke the dissolution of non cross-linked polymer in water while cross-linked polymers have an increased resistance. However an increase of cross-linking or molecular weight of the polymer may reduce its swelling property and therefore its hydrophilicity.

1.3.4.2 Different types of hydrophilic polymers

The chemical process is the introduction of primary covalent cross-links, either by the polymerisation of water soluble monomers in presence of a cross-linking agent, or the cross-linking of an hydrophilic polymer with an cross-linking agent. Except if the covalent bonds are broken these polymers do not dissolve in water but usually swell. This technique is used for the production of Poly(hydroxyalkyl methacrylates) such as PHEMA, a component in the manufacture of contact lenses. Other techniques include gas phase and plasma-induced polymerisation. These techniques are usually expensive but produce pure and uniform gels [47-49].

In the case of physical polymers the network is composed of a hydrophilic polymer phase maintained together by polymer chain segments using Van der Waals type molecular forces. This type of polymer will eventually dissolve in water.

Finally the interpenetrating polymer network is based on two or more monomeric type polymers cured independently in juxtaposition [50]. By inserting an hydrophobic type polymer as the second network it is possible to increase the mechanical strength of the final polymer.

1.4 References

[1] M.Pope, U. S. Patent 2728831 (1955).

[2] D. C. Musa, and G. L. Schnable, Humidity and Moisture 1, (1965), 346.

[3] S. Miyoshi, et al., Proc. Int. Meet, Chemical Sensors, Fukuoka, (1983), 451.

[4] K. Otsuka, S. Kinoki, and T. Usui, Denshi-Zairyo 19, 9, (1980), 68.

[5] Y. Sakai, et al., proc. 4th Solid-State Sensors and Actuators (Transducers '87), Tokyo, (1987), 677.

[6] R Kanou, Sensa Gijyutsu Nyumon, Tokyo: Kogyo Chosakai, (1978), 131.

[7] S. L. Stine, Humidity and Moisture, 1, (1965), 436.

[8] Vaisala KK, Catalog, Ref. No. A 9371.

[9] Nakaasa Instrument Co. Ltd., Catalog, C911-84001-15K-2D, (1984), 78.

[10] T. Yamamoto, K. Kurakami, and T. Takai, Proc. 4th Solid-State Sensors and Actuators (Transducers '87), Tokyo, (1987), 658.

[11] M. Hijikigawa, et al., Proc. 4th Sensor Symp.; Tsukuba, (1984), 135.

[12] M. Hijikigawa, et al., Proc. 2nd Solid-State Sensors and Actuators (Transducers '85); Philadelphia, (1985), 221.

[13] H. Ziegler, K. Rolf, Sens. Actuators, 11 (1987) 37.

[14] F. W. J. Dunmore, Research National Bureau Standards, 23, (1939), 701.

[15] A. J. Wexler, Res. Natl. Bur. Standards 55, (1955), 71.

[16] N. Nakamura, Electroanalytical Chem. Interfacial Electro Chem., 47, (1974), 175.

[17] J. J. Ebelmen, Ann., 57, (1846), 331.

[18] W. Geffcken and E. Berger, German Patent 736 411, (May 1939).

[19] H. Schroeder, Phys. Thin Films, 5, (1969), 87-141.

[20] A. J. Vega and G. W. Scherer, J. Non-Cryst. Solids, 103, (1989), 153.

[21] T. W. Zerda, I. Artaki and J. J. Jonas, J.Non-Cryst. Solids, 81, (1986), 365.

[22] G. Orcel, L. L. Hench, J. Jonas and T. W. Zerda, J. Non-Cryst. Solids, 105, (1988), 223.

[23] R. K. Iler, 'Chemistry of Silica', Wiley, New-York, (1979).

[24] G. W. Scherer, J. Non-Cryst. Solids, 100, (1988), 77.

[25] T. Adachi and S. Sakka, J.Mat. Sci., 22, (1987), 4407.

[26] S. S. Kistler, Nature, 127, (1931), 741.

[27] For example, Science, 250, (1990), 1642.

[28] J. Fricke, Scientific American, May, (1988), 92.

[29] G. Carlson, D. Lewis, K. McKinley, J. Richardson and T. Tillotson, , J. Non-Cryst. Solids, 186, (1995), 372-379.

[30] T. M. Tillotson, and L. W. Hrubesh, J. Non-Cryst. Solids, 145, (1992), 44.

[31] B. Novak, D.Auerbach, and C. Verrier, Chem. Mater., 6, (1994), 282-286.

[32] F. Lu, S. Chen, and S. Peng, Cat. Today, 30, (1996), 183-188.

[33] J. Fricke and A. Emmerling, J. Sol-gel Science and Tech., 13, (1998), 299-303.

[34] G. Herrmann, R. Iden, M. Mielke, F. Teich, and B. Ziegler, J. Non-Cryst. Solids, 186, (1995), 380-387.

[35] K-H Lee, S-Y Kim and K-P Yoo J. Non-Cryst. Solids, 186, (1995), 18-22.

[36] M. J. Bommel, A. B. de Haan, J. Non-Cryst. Solids, 186, (1995), 78-82.

[37] N. Hüsing, F. Schwertfeger, W. Tappert and U. Schubert, J. Non-Cryst. Solids, 186, (1995), 37-43.

[38] G. Rogacki and P. Wawrzyniak, J. Non-Cryst. Solids, 186, (1995), 73-77.

[39] H. Yokogawa, M. Yokoyama, J. Non-Cryst. Solids, 186, (1995), 23-29.

[40] Shaw, Colloid and surface chemistry, op. cit.,8.

[41] S. D. Senturia, S. L. Garverick, and K. Togashi, Sens. Actuators, 2, (1981), 59.

[42] G. Delapierre, et al., Sens. Actuators, 4, (1983), 97.

[43] E. C. M. Hermans, Sens. Actuators, 5, (1984) 181.

[44] D. D. Denton, and S. D. Senturia, Proc. 2nd Solid-State Sensors and Actuators (Transducers '85); Philadelphia, (1985), 202.

[45] P. H. Huang, Sens. Actuators, 8, (1985), 23.

[46] Y. Sakai, and Y. Sadaoka, proc. 2nd Int. Meet. Chemical Sensors; Bordeaux, (1986), 353.

[47] Peppas and Mikos, op. cit., 7.

[48] R. E. Marchant, S. D. Johnson, B. H. Schneider, M. P. Agger, and J. M. Anderson, Journal of Biomedical.Materia1s Research, 24, John Wiley & Sons, Inc., (1990), 1521-1537.

[49] S. D. Johnson, J. M. Anderson, R. E. Marchant, Journal of Biomedical Materials Research, 26, John Wiley & Sons, Inc., (1992), 915-935.

[50] L. H. Sperling, Polymeric Materials Science and Engineering Symposium in Interpenetrating Polymer Networks, American Chemical Society, 65, (1991), 80.

2

Interferometry

2.1 Interferometry review

2.1.1 Advantages of optical sensors over electronics

2.1.2 Intensity, wavelength and interferometric optical fibre sensors

2.1.3 Dual tandem interferometry

2.1.4 The different multiplexing schemes

2.2 References

2.1 Interferometry review

2.1.1 Advantages of optical sensors over electronics

Optical sensors benefit from many advantages when compared with their electrical counterpart. They benefit from electromagnetic immunity, eliminating any error readings due to interference of current and voltages in the sensor head when inserted into high microwave and radio frequency fields. They also eliminate the influence of the probe on the measured parameter. This might happen when the temperature of a material is measured with a metallic probe when inserted into an electromagnetic field [1]. Optical fibre sensors, especially when implemented with Bragg gratings, are also small enough to be inserted into any material without disturbing its integrity such as its strength. This allows distributed sensors to be embedded into large structures, like bridges or buildings. Their small size also allows minimally invasive measurement when used in human tissue. They also benefit from low weight and cost increasing their interest for industry. Finally the possibility of multiplexing optical sensors also allows quasi-distributed measurement and the potential for mass production makes them competitive with electrical sensors.

2.1.2 Intensity, wavelength and interferometric optical fibre sensors

There are several books published in which fibre optic sensors are reviewed [2]. Here we present a few examples of fibre optic sensors which operate using different transduction mechanisms.

2.1.2.1 Intensity modulated optical fibre sensors

Intensity sensor systems are usually composed of cheap components making them attractive for industry. Intensity sensors are based on the modulation of light in response to a physical, chemical or biological effect. The measurement relies on the comparison of the intensity levels generated by a reference with that generated by the sensor. There are various ways to modulate the intensity. It can be modulated by microbending loss which transfers the light to higher modes having a higher propagation loss [3]. The

modulation can also be due to absorption or scattering of the light by the measurand due to the presence of say 'oil in water' [4], or simply by a loss of coupling when a reflective target moves away from the emitting fibre [5,6]. Many intensity optical sensors have also been based on the modulation of the guided light by variations of the evanescent field loss, both in fibre optic and bulk glass waveguides [7-9].

As an example we describe an intensity sensor based on optical loss used to detect liquid levels [10,11]. As seen in figure 2.1 the sensor is composed of two fibres attached to a prism. When the prism is not in contact with a liquid, the light from the LED is totally internally reflected and returns to the output fibre. However when the prism is immersed in the liquid, the light is refracted into the liquid and a loss of power in the output fibre occurs. The sensitivity of this liquid level device is determined by the contrast ratio which depends on the refractive index of the liquid.

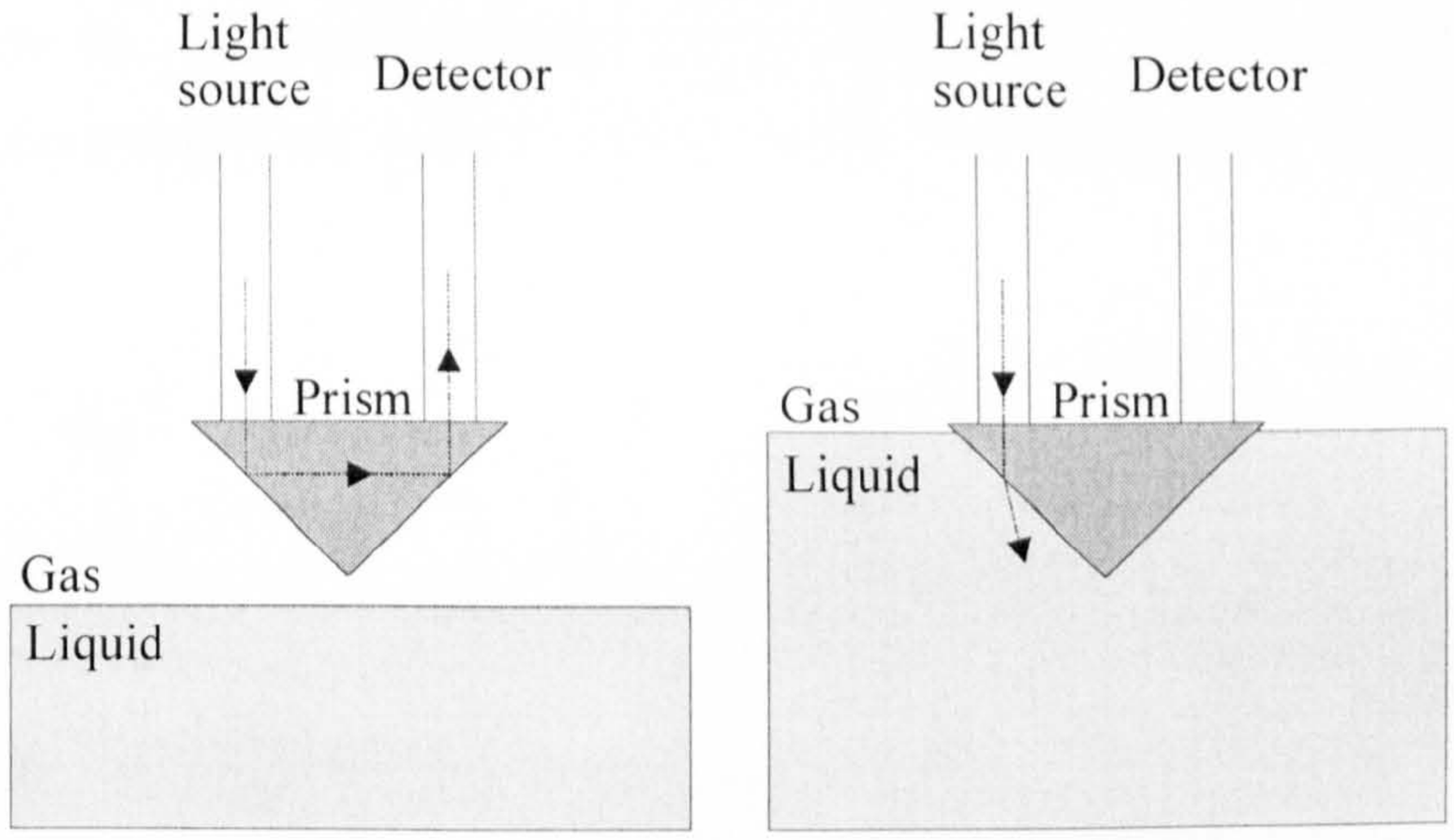

Figure 2.1 shows an intensity liquid level sensor

The change in loss varied from 2.1 dB to 31 dB using liquids with refractive indexes between 1.33 and 1.39. If well designed this type of sensor can detect level variations of 0.1 mm. Problems were experienced due to ripples at the liquid surface and bubbles for liquids at high temperatures. Due to its low cost and electrical isolation, these sensors can be used in petroleum and chemical plants where the hazardous environment makes it impossible to use conventional sensors.

2.1.2.2 Wavelength modulated optical fibre sensors

Wavelength modulated optical fibre sensors are based on the modification of the wavelength of the input light in response to the measurand. A range of optical sensors are based on this principle, such as pollution monitoring by fluorescence spectroscopy [12-14] or temperature via Raman scattering in the optical fibre [15]. For physical measurements the recent developments of fibre Bragg gratings offers several sensing opportunities as it can be used to measure temperature, strain, are easily multiplexed and coated for chemical sensing via induced strain [16]. Fibre Bragg gratings can be written in the fibre by exposure to a spatial pattern of ultraviolet light which produces a permanent periodic change in the local refractive index of the fibre. Thus, the fibre Bragg grating will reflect a light at a specific wavelength when, for example, illuminated by a broadband source. If the grating is subject to a change in temperature or strain then the mean reflected wavelength will change. As many gratings can be encrypted sequentially on a fibre, multiplexing techniques allow quasi distributed sensing [17].

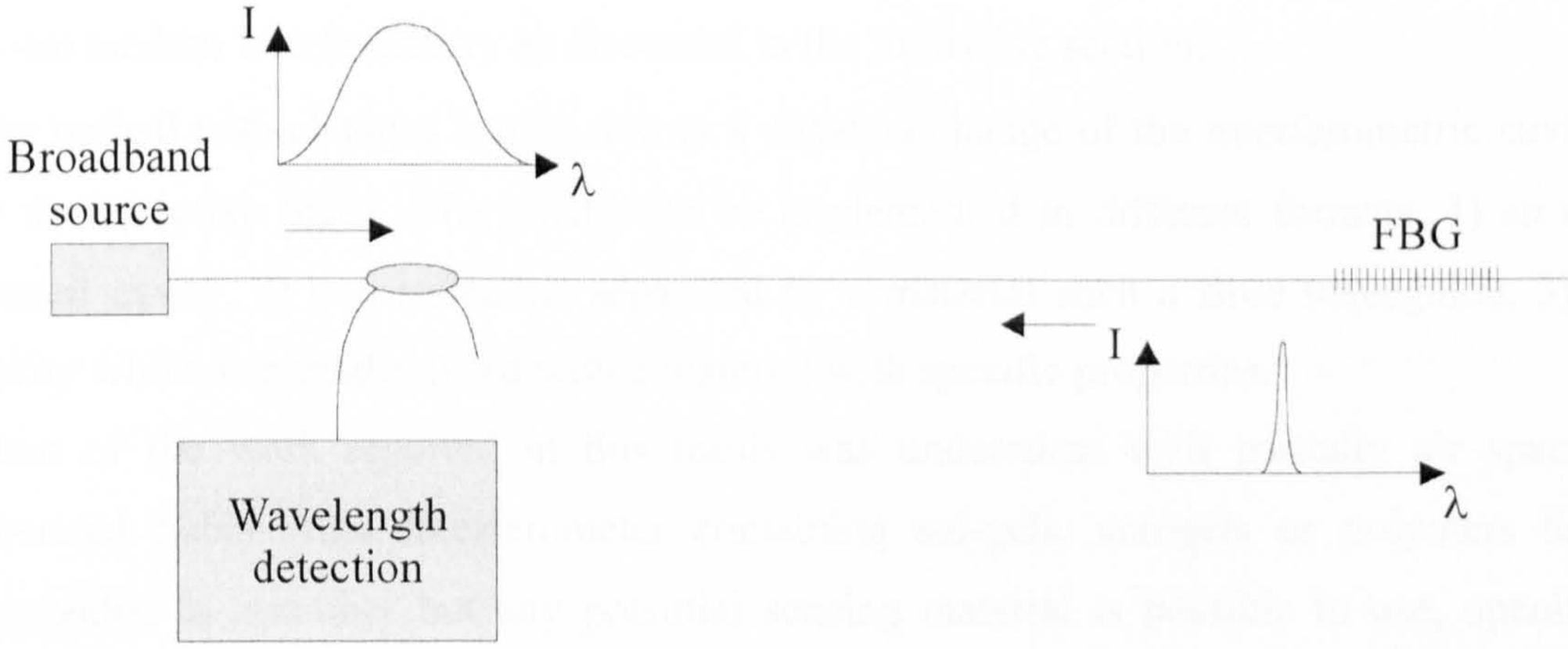

Figure 2.2 shows a simple method of interrogating a fibre Bragg grating

Figure 2.2 shows a simple scheme for temperature and strain sensing [17]. The system is illuminated using a broadband source. The light is then reflected by the fibre Bragg grating and directed to a wavelength detection system, here a Fabry-Perot filter. The Fabry-Perot filter can be operated either in a tracking or in a scanning mode for an interrogation of a single or multiplexed fibre Bragg grating configuration. This sensor

was used for strain detection and a shift of 0.75 nm in wavelength corresponded to 700 μstrain applied to the grating. The resolution obtained with this system was better than 0.3 μstrain.

2.1.2.3 Interferometric optical fibre sensors

Interferometers are well known for their ability to measure optical path changes with very high precision. Interferometers were primarily used to study the spectra of optical sources. The implementation of the classical interferometer in a fibre optic format has lead to many new types of optical sensors.

For sensor applications it is convenient to classify the measurement as quasi-static/absolute or periodic. Although all interferometers can be used to make path length change measurements, problems occur if the measurement must be absolute due to the periodic nature of the transfer function. For periodic measurements such as vibrations high coherence lasers can be used. For absolute measurement, currently the only successful method, is based upon low coherence interferometry, where the system is illuminated by a LED or SLD. For remote absolute sensing, the only reported method is to use tandem interferometry as discussed in the following sections.

The optical path changes can be due to a physical change of the interferometric cavity or its refractive index. The cavity can be implemented in different formats, 1) an air spaced cavity, 2) two reflectors separated by a material such a fibre waveguide, 3) a cavity which is partially filled with a material with specific properties.

Most of the work reported in this thesis was undertaken with partially air spaced fiberised Fabry-Perot interferometer containing sol-gels, aerogels or polymers that responded to humidity but any potential sensing material is possible to use, opening many possibilities for general sensing. Fabry-Perot sensors containing a responsive material are convenient to use due to their small size, high sensitivity, low cost, and minimum cross sensitivity to temperature [18,19]. In many cases it is required that the sensor system allows multiplexing, remote and absolute measurements [20].

An example of an air spaced cavity acting as a low pressure sensor designed for medical applications is shown in figure 2.3 [21].

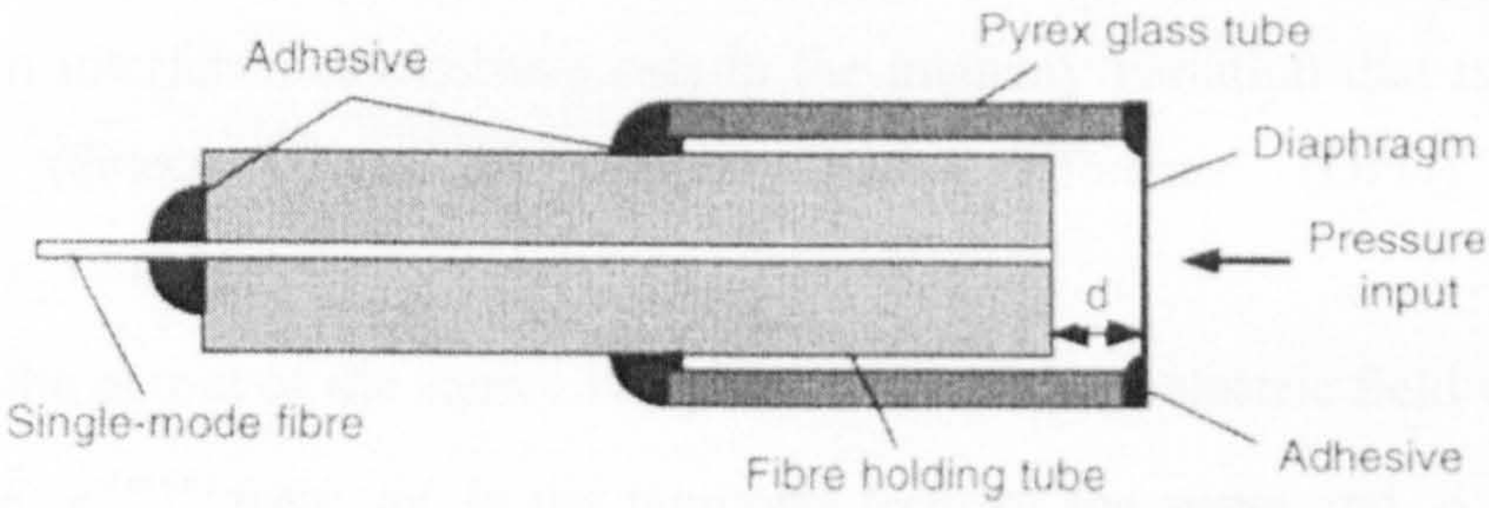

Figure 2.3 shows an interferometric low pressure probe

The basic principle of the sensor is that when the pressure increases, the membrane is displaced reducing the cavity length 'd' formed between the fibre end and the diaphragm. The probe was interrogated by a local processing interferometer composed of a bulk Michelson interferometer, this concept is described in detail in the following section. The results showed that the sensor had a range to resolution ratio of 6.7×10^3:1 over a pressure range of 0-0.48 bar.

In this thesis we describe the feasibility of using low coherence interferometry to measure relative humidity from the induced phase change in a remote Fabry-Perot interferometer containing specific materials. Suitable materials for humidity sensing such as sol-gels [22,23], polymers [24,25] or other materials have been reported in the literature. Relatively few studies have been reported on humidity sensing based on fibre sensors [26,27] and none were multiplexed to suit industrial needs.

2.1.3 Dual tandem interferometry

2.1.3.1 Transfer function of an all fibre Michelson interferometer using a laser and a low coherence source

Standard interferometry using a laser is well known and offers a means to make accurate measurements. However, such system is limited to relative measurements unsuitable in a prototype configuration as required in this project. The use of a low coherence source allows to make absolute measurements by locating the maximum of the transfer function of the interferometer. Furthermore, such source allows remote

sensing by the means of dual tandem interferometry as described here. The transfer function of an interferometer corresponds to the intensity variation that is observed at the output (detector) as the optical path difference (OPD) is varied, ($\Delta x = 2.(x_1 - x_2) = OPD$).

Assume that the output of the source is a plane wave with an electric field which can be written $\vec{E} = \vec{E}_0.e^{i(\omega t+\phi)}$ were ωt is the temporal term of the wave and ϕ is the phase change induced by the elements in the system such as fibre or a coupler.

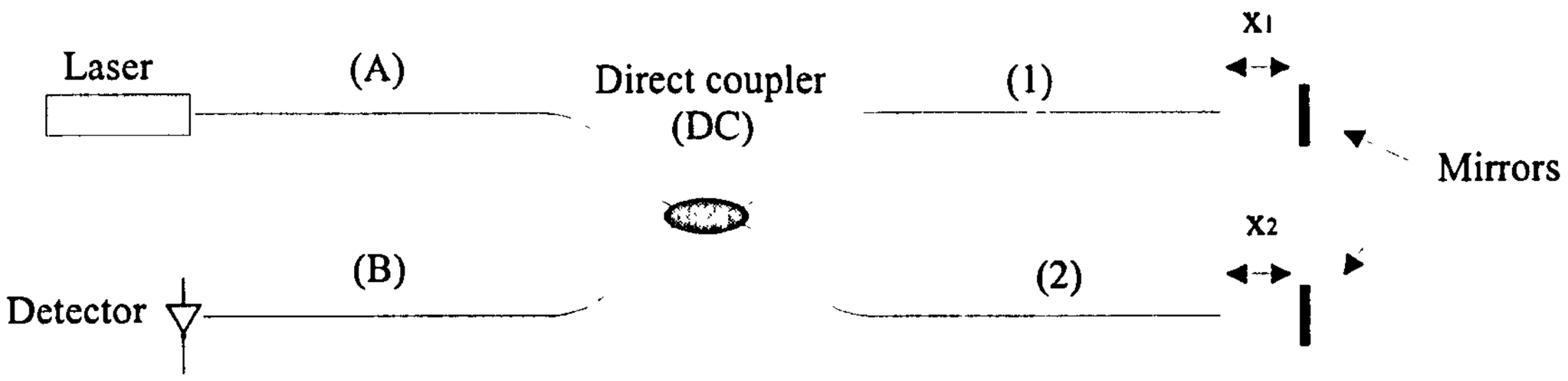

Figure 2.4 shows an all fiberised Michelson interferometer

We will also consider that the two arms (1) and (2) of the interferometer have exactly the same length inducing the same phase change ϕ_f and that the OPD changes only as a result of the variation of x_1 and x_2. Finally we will neglect losses due to the coupling of the laser into the fibre and the fibres with the mirrors. The directional coupler (DC) acts as a beam splitter and thus distributes the light equally in the two arms (1) and (2). The light then gets reflected at the mirrors and part of the returned signal is directed to the detector arm (b) where interference takes place. The electric field amplitude in arm (b) can be written:

$$\begin{cases} \vec{E}_1 = \vec{E}_0/2.e^{i(\omega t+2\phi_f+2kx_1+\pi/2)} \\ \vec{E}_2 = \vec{E}_0/2.e^{i(\omega t+2\phi_f+2kx_2+\pi/2)} \end{cases} \quad (2\text{-}1)$$

The terms $2kx_1$ and $2kx_2$ represent the phase induced by the distance x_1 and x_2 between the fibre and the mirror whilst the $\pi/2$ term is due to the crossing through the coupler. In order to find the transfer function of the interferometer, we note that the electric field at the output is $\vec{E} = \vec{E}_1 + \vec{E}_2$. The intensity of the output is then obtained by taking the

time average of the above equation which is the product of the overall output electric field $\vec{E}$ and its complex conjugate.

$$I = \vec{E}.\vec{E}^{*} \tag{2-2}$$

$$I = \left(\vec{E}_1 + \vec{E}_2\right).\left(\vec{E}^{*}{}_1 + \vec{E}^{*}{}_2\right) \tag{2-3}$$

This leads directly to the intensity function of the OPD,

$$I = I_0/2.\left[1 + \cos\left(2k.\Delta x\right)\right] \tag{2-4}$$

If a low coherence source (I_0 = 2 mw, λ = 825 nm, $\Delta\lambda$ = 22.2 nm) is used instead of the laser an additional factor should be considered. Because the correlation function of the source has a gaussian profile determined by the form of the spontaneous emission, a correction to the modulating term of the transfer function is given by $e^{-[2|\Delta x|/Lc]^2}$.

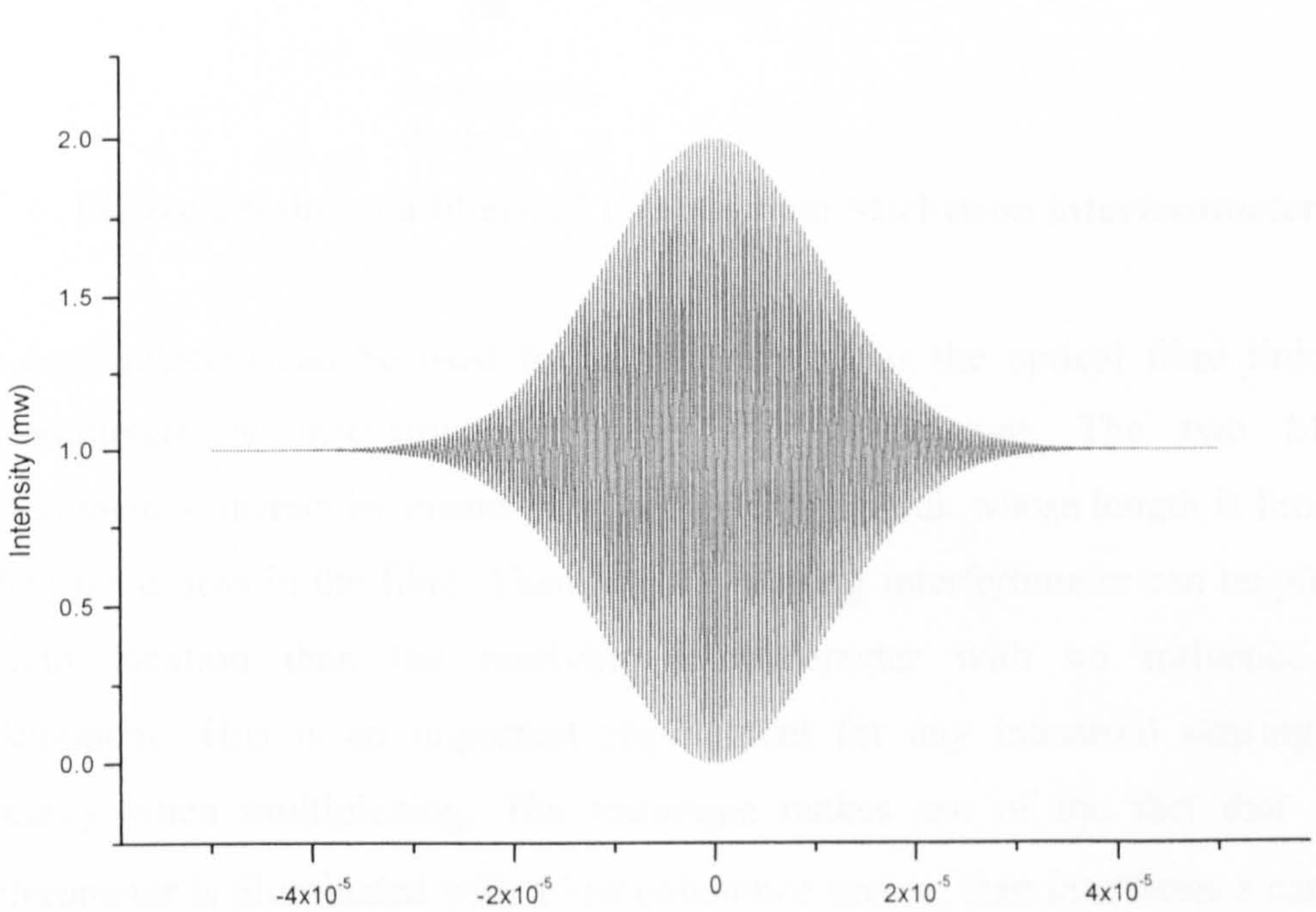

Figure 2.5 shows the transfer function of a simple Michelson interferometer using a low coherence source

Thus,

$$I = I_0/2.\left[1+\cos\,(2k.\Delta x).e^{-\left[2|\Delta x|/Lc\right]^2}\right] \qquad (2\text{-}5)$$

Where $Lc = \lambda^2 / \Delta\lambda$ is the coherence length of the source and $\Delta\lambda$ its spectral width. The graph of this transfer function can be seen in figure 2.5.

2.1.3.2 Transfer function of two Michelson interferometers in tandem using a low coherence source

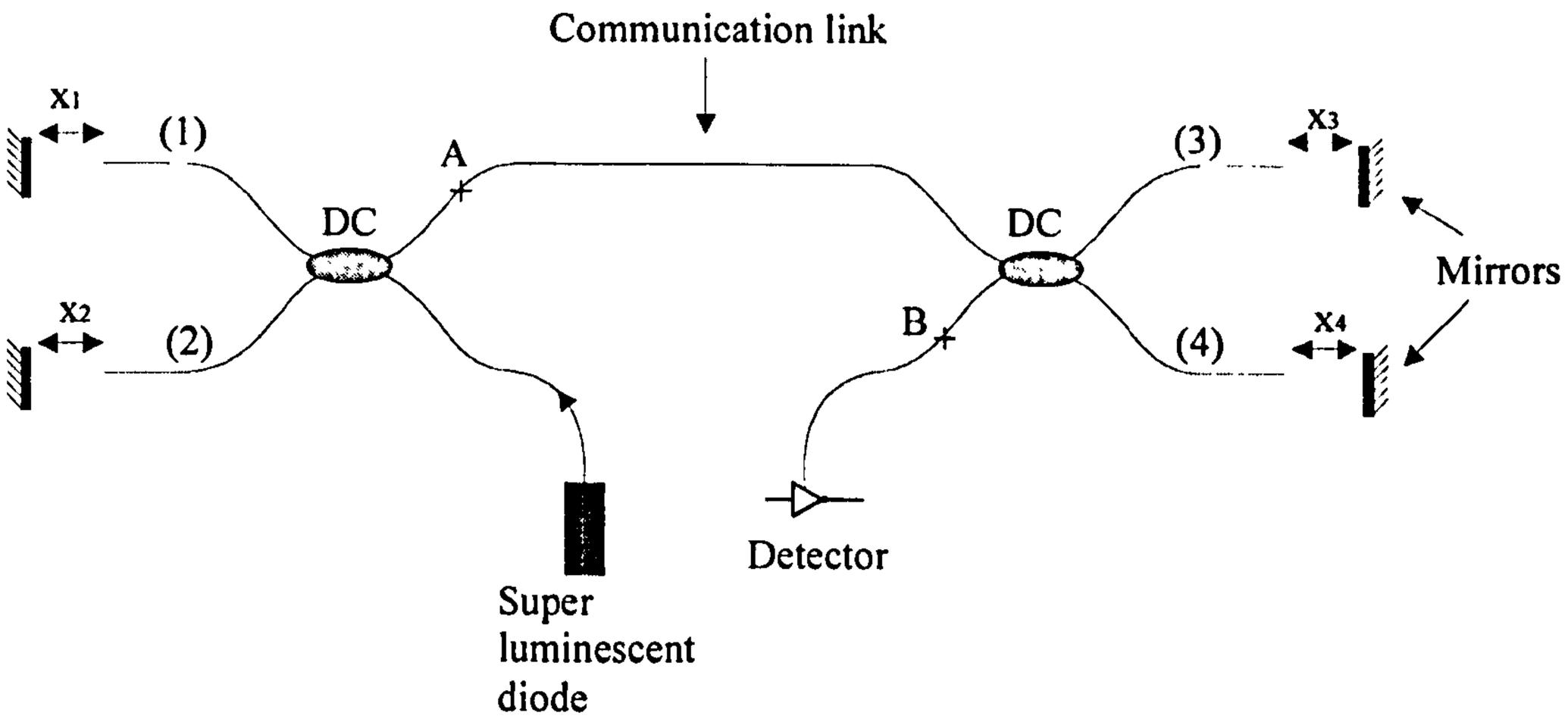

Figure 2.6 shows a fiberised dual tandem Michelson interferometer

This configuration can be used for remote sensing as the optical fibre linking both interferometers is insensitive to strain and temperature. The two Michelson interferometers interact by means of a communication link whose length is limited only by the optical loss in the fibre. Therefore the sensing interferometer can be placed in a different location than the receiving interferometer with no influence on the measurement. This is an important requirement for any industrial sensing system, especially when multiplexing. The technique makes use of the fact that when an interferometer is illuminated with a low coherence source, then interference can only be observed when the optical path differences within the interferometers are well balanced. Thus if x_4 changes, fringes can only be seen if x_1 or x_2 changes by the same amount. This constitutes the basis of the absolute measurement. Using the same starting hypothesis as in the previous section (2.1.3.1) we can write the two electric fields at point A resulting from the arms (1) and (2).

$$\begin{cases} \vec{E}_1 = \vec{E}_0/2.e^{i(\omega t+2\phi_f+2kx_1+\pi/2)} \\ \vec{E}_2 = \vec{E}_0/2.e^{i(\omega t+2\phi_f+2kx_2+\pi/2)} \end{cases} \quad (2\text{-}6)$$

Then each of these electric fields will travel in arm (3) and (4), the result being the four following equations.

$$\begin{cases} \vec{E}_{13} = \vec{E}_0/4.e^{i(\omega t+4\phi_f+2kX_1+2kX_3+\pi)} \\ \vec{E}_{14} = \vec{E}_0/4.e^{i(\omega t+4\phi_f+2kX_1+2kX_4+\pi)} \\ \vec{E}_{23} = \vec{E}_0/4.e^{i(\omega t+4\phi_f+2kX_2+2kX_3+\pi)} \\ \vec{E}_{24} = \vec{E}_0/4.e^{i(\omega t+4\phi_f+2kX_2+2kX_4+\pi)} \end{cases} \quad (2\text{-}7)$$

As previously stated $\vec{E} = \vec{E}_{13} + \vec{E}_{14} + \vec{E}_{23} + \vec{E}_{24}$ and $I = \vec{E}.\vec{E}^*$.

Using the same technique as in 2.1.3.1 the final transfer function is given by :

$$I = I_0/4.\begin{bmatrix} 1+\cos\left(2k.(x_1-x_2)\right).e^{-\left[2|x_1-x_2|/Lc\right]^2} \\ +\cos\left(2k.(x_3-x_4)\right).e^{-\left[2|x_3-x_4|/Lc\right]^2} \\ +\frac{1}{2}\cos\left(2k.((x_1-x_2)+(x_3-x_4))\right).e^{-\left[2|(x_1-x_2)+(x_3-x_4)|/Lc\right]^2} \\ +\frac{1}{2}\cos\left(2k.((x_1-x_2)-(x_3-x_4))\right).e^{-\left[2|(x_1-x_2)-(x_3-x_4)|/Lc\right]^2} \end{bmatrix} \quad (2\text{-}8)$$

Several cases can occur:

If $x_1 = x_2$ and $x_3 = x_4$ that is $(x_1\text{-}x_2) = (x_3\text{-}x_4) = 0$ the two interferometers are balanced and $I = I_0/4$ (central lobe of Figure 2.6).

If $(x_3\text{-}x_4) >> Lc$ and $(x_1\text{-}x_2) \approx 0$ then

$$I = I_0/4.\left[1+\cos\left(2k.(x_1-x_2)\right).e^{-\left[2|x_1-x_2|/Lc\right]^2}\right] \quad (2\text{-}9)$$

which contains no information related to x_3 and x_4 and is again the central fringe.

Finally if $(x_1-x_2) = (x_3-x_4) \neq 0$, then the two interferometers are balanced and the central lobe remains in addition to two side lobes containing all information on the position of the four mirrors. In the case of an experimental system the tracking will therefore be made on one of the side lobes as its position depends on the optical path difference of the sensor (x_3-x_4).

Information about (x_3-x_4) can then be obtained by varying (x_1-x_2).

$$I = I_0/4.\left[1+\frac{1}{2}\cos\left(2k.\left((x_1-x_2)\pm(x_3-x_4)\right)\right).e^{-\left[2\left|(x_1-x_2)\pm(x_3-x_4)\right|/Lc\right]^2}\right] \quad (2\text{-}10)$$

The plot of this transfer function is given below.

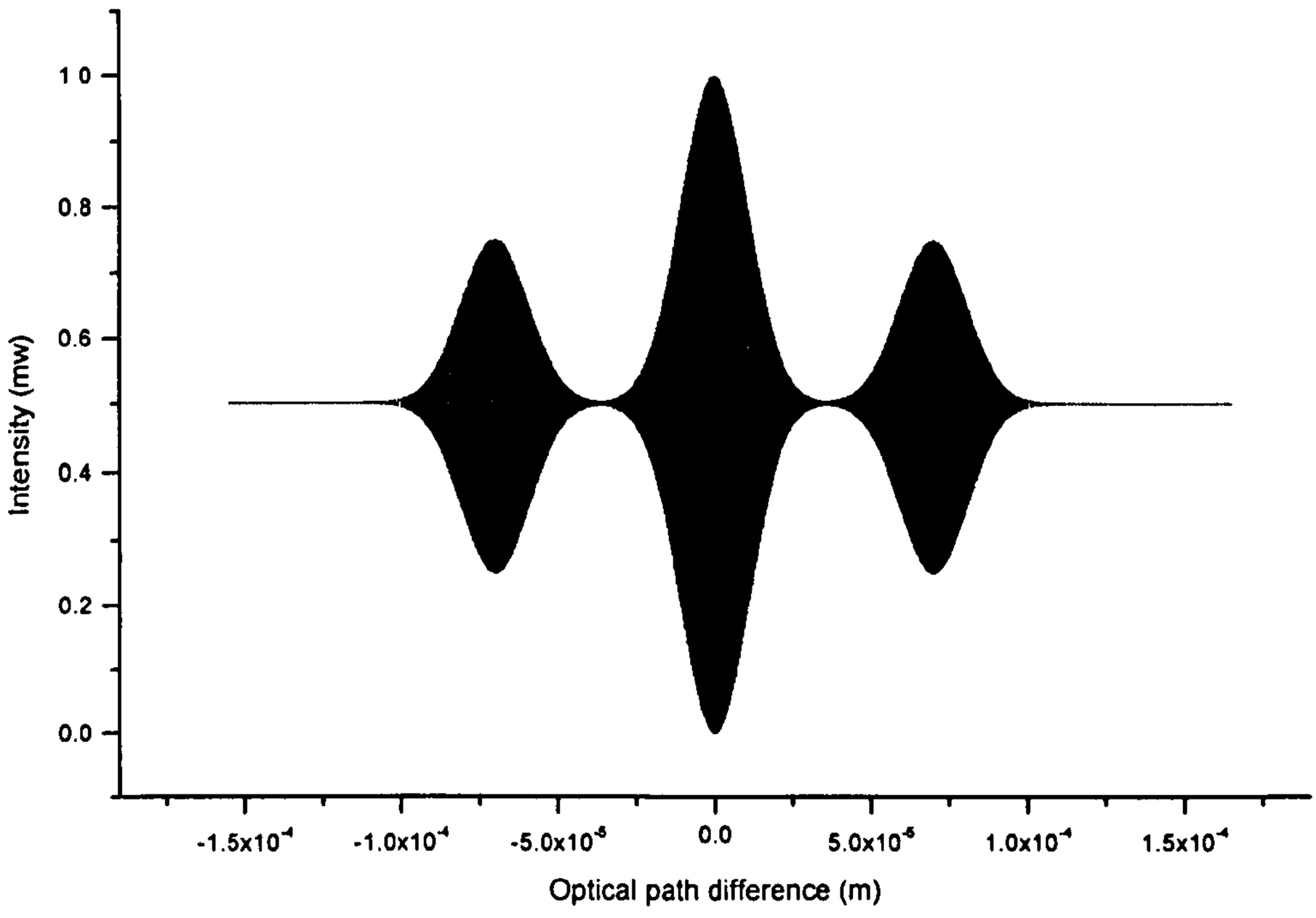

Figure 2.7 shows the transfer function of a tandem Michelson interferometer using a low coherence source

2.1.3.3 Transfer function of a Michelson interferometer in tandem with a Fabry-Perot cavity using a low coherence source

Using the previous paragraph as an introduction to tandem interferometry, this configuration has the advantage of being easily multiplexed, can be designed to be

relatively temperature insensitive and will be the basis of the final system discussed in chapter 7.

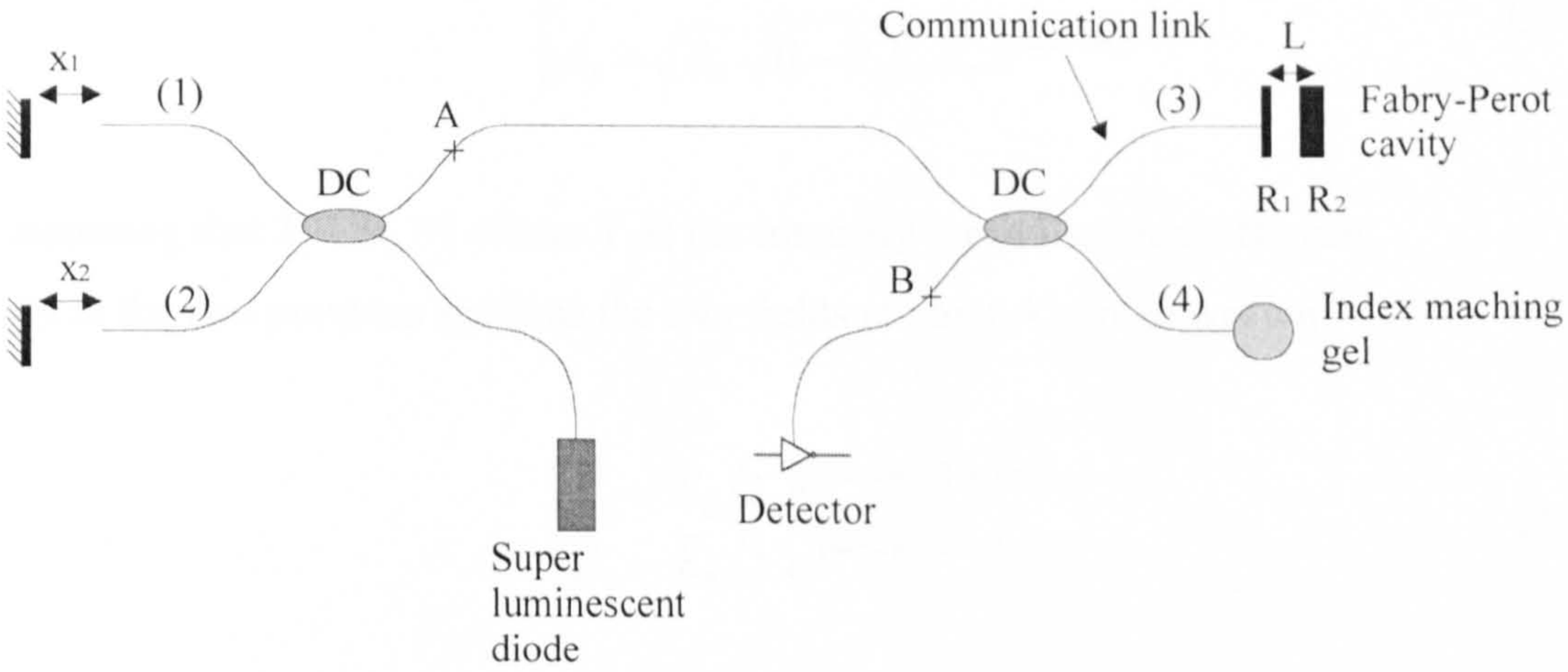

Figure 2.8 shows a fiberised dual tandem Fabry-Perot and Michelson interferometer

The sensing interferometer is here localised in the Fabry-Perot cavity resulting in a temperature insensitive arm 3, which serves as the transceiver link. The interferometric processing will be similar except that the final transfer function can be slightly different. The same hypothesis as in previous sections will be made and a low reflectivity Fabry-Perot cavity will here be considered.

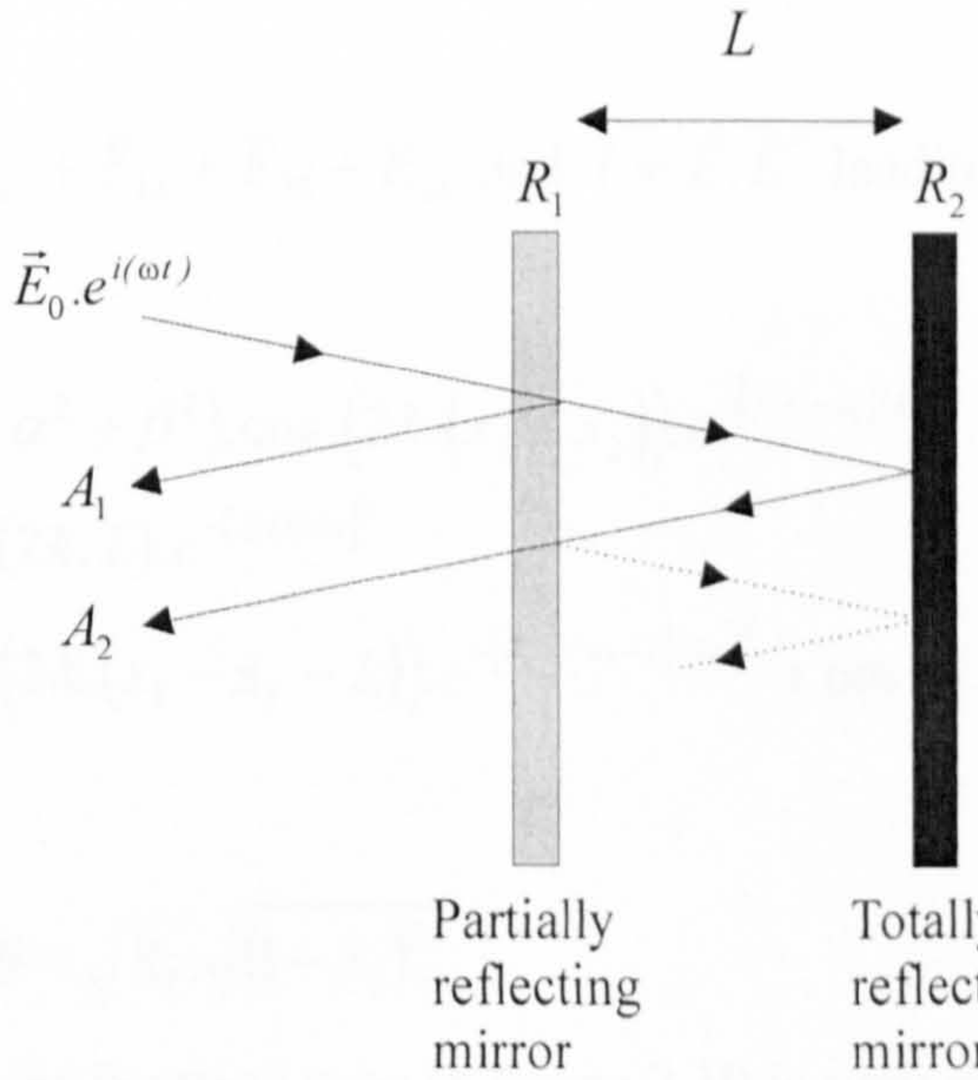

Figure 2.9 shows a Fabry-Perot interferometer

If R_1, R_2 are the intensity reflection coefficients, then we have for this cavity

$$\begin{cases} A_1 = \sqrt{R_1}.E_0.e^{i\omega t} \\ A_2 = \sqrt{R_2}.\sqrt{(1-R_1)^2}.E_0.e^{i(\omega t+2kL)} \end{cases} \quad (2\text{-}11)$$

assuming that $T_i + R_i = 1$ where T_i is the intensity transmission coefficient.

As in the two previous sections the two fields at point A can be written

$$\begin{cases} \vec{E}_1 = \vec{E}_0/2.e^{i(\omega t+2\phi_f+2kx_1+\pi/2)} \\ \vec{E}_2 = \vec{E}_0/2.e^{i(\omega t+2\phi_f+2kx_2+\pi/2)} \end{cases} \quad (2\text{-}12)$$

Each of which will generate two different fields in the Fabry-Perot interferometer and at point B we will have:

$$\begin{cases} \vec{E}_{13} = \sqrt{R_1}.\vec{E}_0/4.e^{i(\omega t+4\phi_f+2kX_1+\pi)} \\ \vec{E}_{14} = \sqrt{R_2}.\sqrt{(1-R_1)^2}.\vec{E}_0/4.e^{i(\omega t+4\phi_f+2kX_1+2kL+\pi)} \\ \vec{E}_{23} = \sqrt{R_1}.\vec{E}_0/4.e^{i(\omega t+4\phi_f+2kX_2+\pi)} \\ \vec{E}_{24} = \sqrt{R_2}.\sqrt{(1-R_1)^2}.\vec{E}_0/4.e^{i(\omega t+4\phi_f+2kX_2+2kL+\pi)} \end{cases} \quad (2\text{-}13)$$

Then as usual, $\vec{E} = \vec{E}_{13} + \vec{E}_{14} + \vec{E}_{23} + \vec{E}_{24}$ and $I = \vec{E}.\vec{E}^*$ leading to,

$$I = I_0/8.\left[\begin{array}{l} \alpha^2 + \beta^2 + (\alpha^2 + \beta^2).\cos\left(2k.(x_1 - x_2)\right).e^{-[2|x_1-x_2|/Lc]^2} \\ + 2\alpha\beta\cos(2k.L).e^{-[2|L|/Lc]^2} \\ + \alpha\beta.\left\{\cos\left(2k.(x_1 - x_2 - L)\right).e^{-[2|x_1-x_2-L|/Lc]^2} + \cos\left(2k.(x_2 - x_1 - L)\right).e^{-[2|x_2-x_1-L|/Lc]^2}\right\} \end{array}\right] \quad (2\text{-}14)$$

where $\alpha = \sqrt{R_1}$ and $\beta = \sqrt{R_2}.\sqrt{(1-R_1)^2}$.

The shape of the transfer function seen in figure 2.10 is very similar to the one in figure 2.7 except that it now depends on α and β.

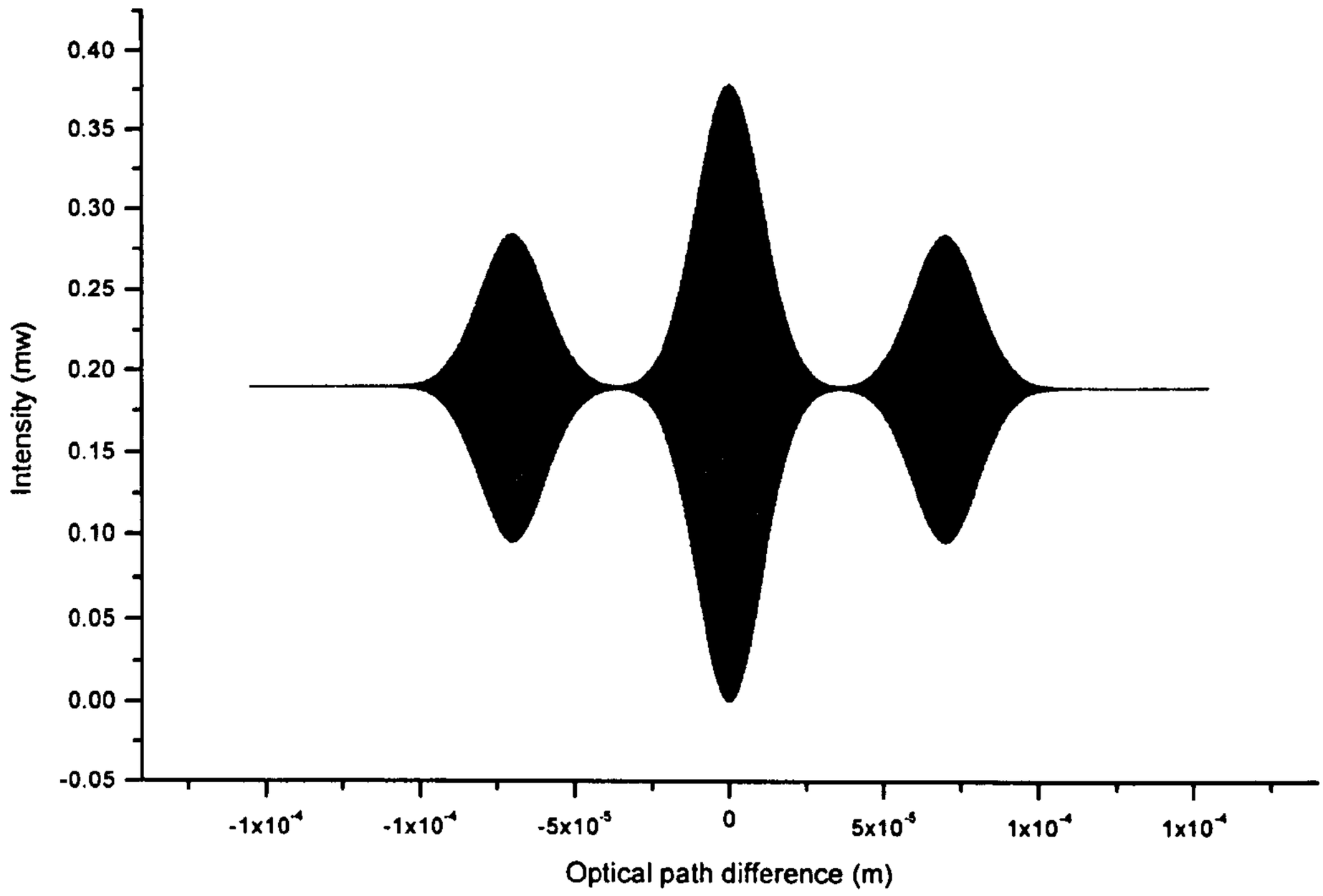

Figure 2.10 shows the transfer function of a tandem Michelson and Fabry-Perot interferometer using a low coherence source

2.1.4 The different multiplexing schemes

Interferometric fibre sensors have been developed for a wide range of application areas where high sensitivity is required. Intensive research during the last 15 years has resulted in the introduction of a large number of sensors operating on a large variety of principles. In most cases optical sensors benefit from better performance than conventional sensors. It is important for industry to multiplex the sensors in order to reduce costs and allow multipoint measurements. Four multiplexed systems will be described here.

2.1.4.1 Frequency multiplexing

Frequency multiplexing can be used with intensity [28-29] and interferometric sensors. This multiplexing scheme relies on the modulation of the source generating a high frequency carrier in a series of sensors. The sensors can be set in series or parallel.

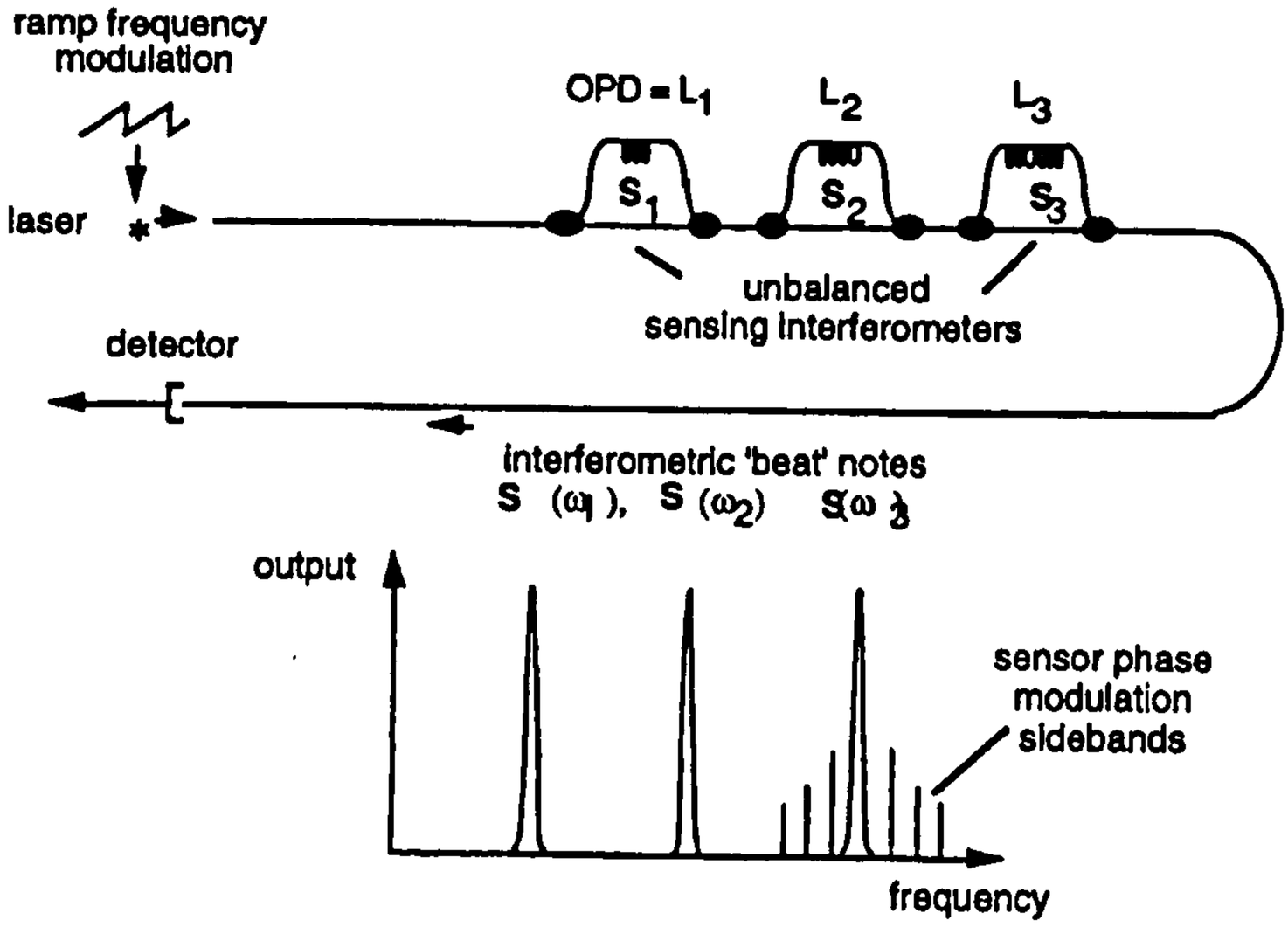

Figure 2.11 shows a frequency division multiplexing scheme

Figure 2.11 shows a possible arrangement of a frequency multiplexing scheme. The unbalanced interferometers being extremely sensitive, a beat frequency is generated at each sensor output. The period of the beat frequency depends on the frequency excursion of the chirp, the chirp rate and the interferometers optical path difference (OPD). If each interferometer has a different OPD, the generated beat frequency of each sensor will be unique. In this case the phase change of the output signal $\partial\phi$ is given by:

$$\partial\phi = \frac{2\pi n \Delta l \Delta \nu}{c} \tag{2-15}$$

where Δl is the path imbalance, $\Delta \nu$ the frequency change and n the refractive index. The information on the OPD can then be recovered by band filtering. Finally the interferometric phase of each sensor can be recovered using a phase locked loop system or an other phase analysis technique. The problems associated with this technique are the limitation of the number of sensors since the length of each sensor has to be different (the length of the sensors rapidly increases) and the difficulty of building a system having the same sensitivity for each sensor.

2.1.4.2 Time multiplexing

In the case of time multiplexing the sensors are placed at different distance from the source and the detector. The emission of a single pulse of a suitable duration then results in a series of pulses corresponding to each detector. The duration of the pulse is fixed by the optical delay of the fibre linking the different sensor elements. Each sensor is then interrogated by gating the series of pulses. It is necessary to repeat the pulsing as many times as there are sensors to achieve a measurement of the whole ladder. Concerning the time addressing, two conditions must be completed. The duration 'μ' of the pulses injected in the system must be sufficiently short, to avoid any overlapping on the detectors, and the periodicity 'T' of the pulses must long enough so that the pulse coming from the farthest sensor location of the system reaches the detector before the next pulse coming from the nearest sensor location.

These two conditions are expressed by:

$$\frac{2n\tau}{c} \geq \mu \qquad (2\text{-}16)$$

$$T \geq \frac{2(N-1)n\tau}{c} + \mu \qquad (2\text{-}17)$$

Where N is the total number of sensors and τ the delay between each sensor.

It is possible to use interferometric sensors provided a means for demodulating the different interferometers is inserted into the system. The different phases of the interferometric sensors are then recovered by using a phase carrier demodulation technique if configured as path unbalanced interferometers. It is possible to build an array based on Mach-Zender interferometers but the use of Michelson interferometers was also successfully demonstrated [30]

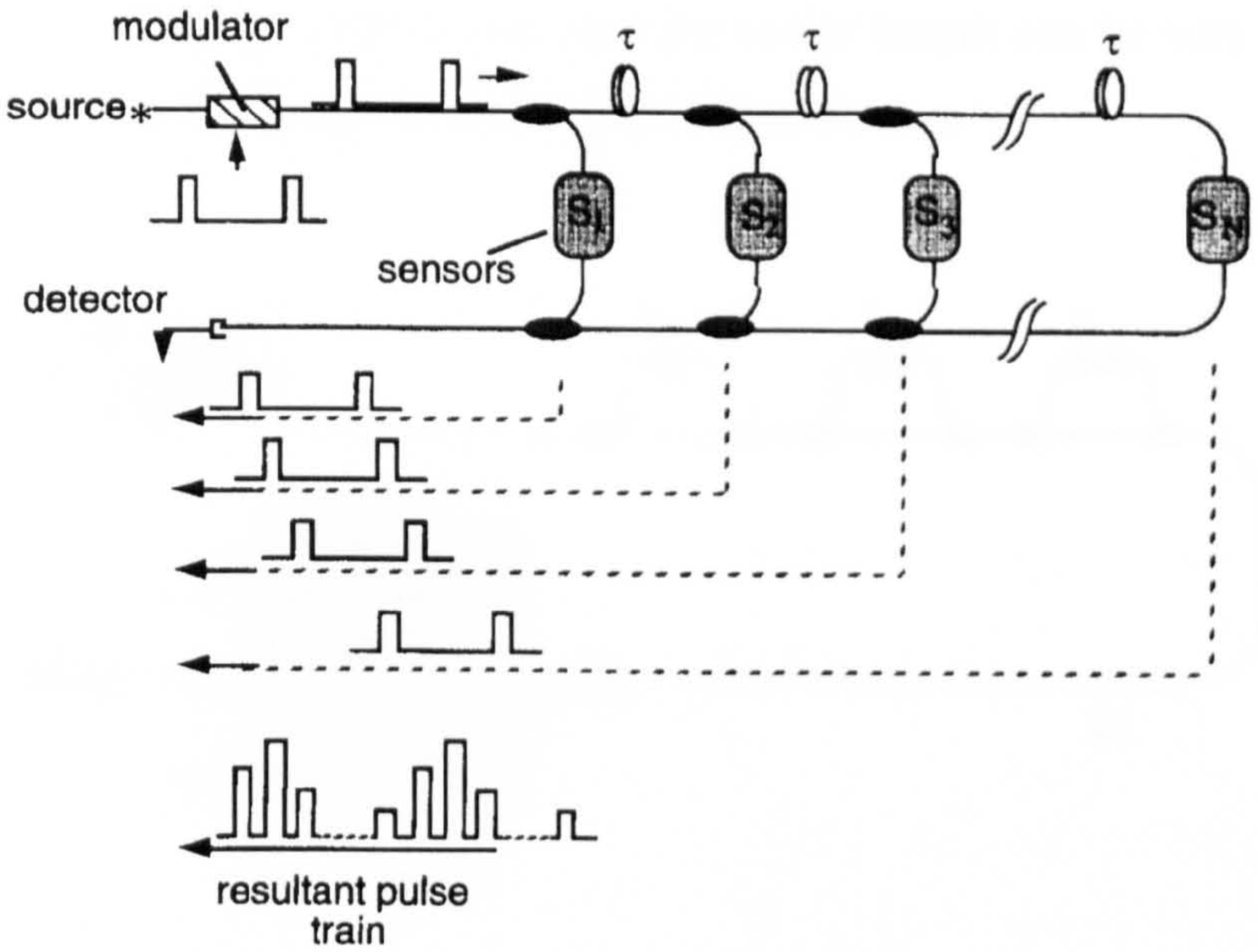

Figure 2.12 shows a time division multiplexing scheme

2.1.4.3 Coherence multiplexing

When using the coherence multiplexing scheme an unbalanced interferometer is illuminated with a low coherence source. The optical path difference between the two arms of the processing interferometer is greater than the coherence length of the source and no interference pattern is observed. The resulting light is then coupled to a second interferometer (the sensing interferometer) where the optical path difference is matched to the previous interferometer within the coherence length of the source [31-33]. An interference pattern is then visible, its phase depends on both, the processing interferometer and the sensing interferometer. Multiplexing using this scheme can be achieved by coherence matching the different processing and sensing interferometers within the coherence length of the source as seen in figure 2.13. In the case of a measurand slowly varying it is possible to use only one processing interferometer interrogating successively the different sensors. In this case, the OPD of the processing interferometer is ramped over the different OPDs of the sensors to coherence tune successively. The information on the OPD of the sensors is then recovered by locating the maximum of the obtained transfer function. In the first case low signal to noise ratio may occur for a large number of sensors (>10) because each sensor has to be of a different cavity length and because cross sensitivity with temperature increases with the

length of the cavities but in the second case the cavity length can be very close or even the same provided each sensor is read by a different detector.

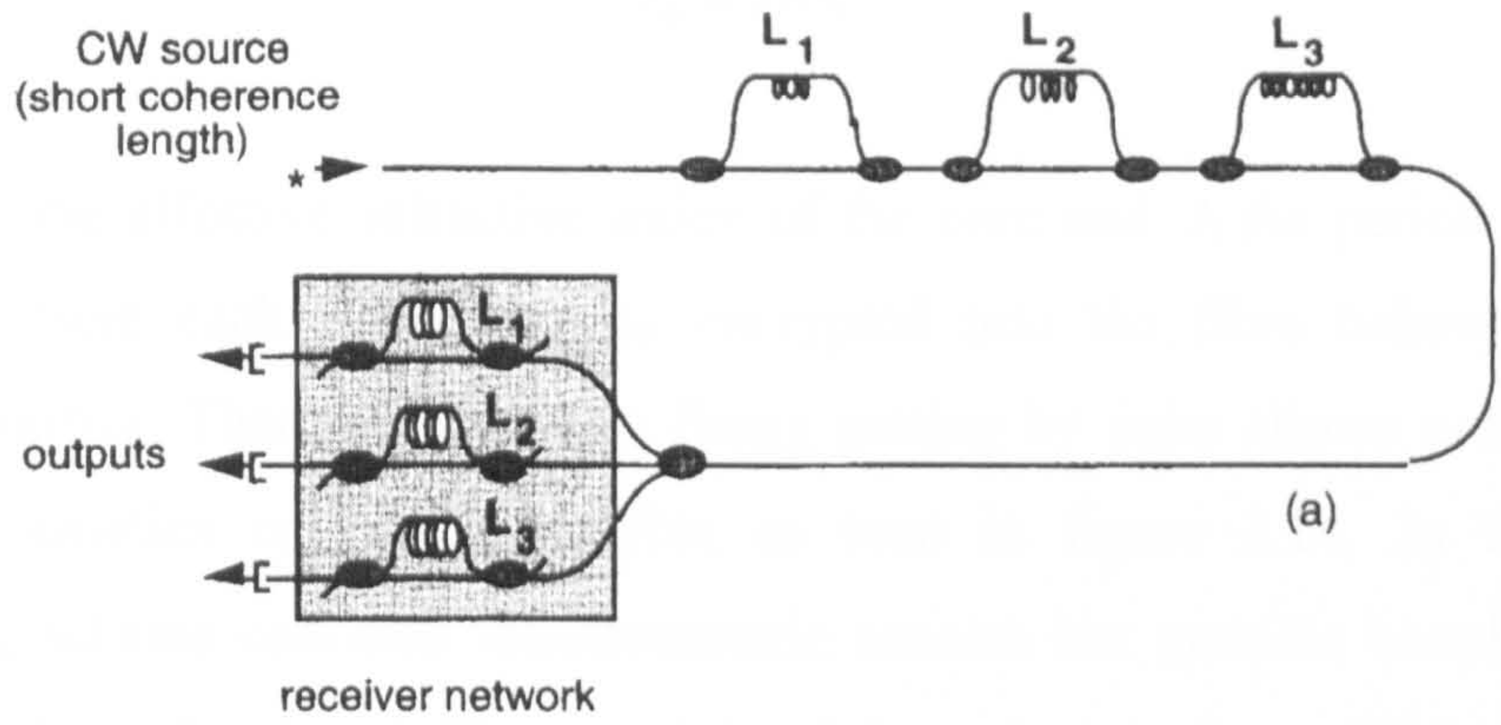

Figure 2.13 shows a coherence multiplexing scheme

This difficulty can be overcome by using a power distributor linking all the return lines to one detector sequentially. In this case one scan is necessary for each sensor. This coherence tracking technique was used in the final system described in chapter 7.

2.1.4.4 Wavelength multiplexing

This multiplexing technique is theoretically the most efficient since it is possible to direct the light from the source to a specific sensor and then to a particular detector with minimal loss. An important element in this type of multiplexing scheme is the fibre Bragg grating. A fibre Bragg grating is written into a Ge-doped single mode fibre. The periodic modulation written in the core of the fibre is achieved by exposure of a spatial pattern of ultraviolet light in the region of 244-248 nm. The size of a fibre Bragg grating

is around 1-20 mm and their reflectivities can approach 100%. When illuminated with a broadband source a fibre Bragg grating reflects at the Bragg wavelength defined by:

$$\lambda_b = 2n\Lambda \tag{2-18}$$

Where n is the effective refractive index of the core and Λ the period of the index modulation. Here each Bragg grating encrypted into the fibre behaves as a semi transparent mirror. Therefore coupling Bragg grating by pairs allows a distribution of Fabry-Perot cavities on the same fibre as seen in figure 2.14. In this case the multiplexing scheme concerns interferometric sensors but systems based on intensity sensors have been developed. The principle of the system in figure 2.14 is to modulate the light with an unbalanced Mach-Zender interferometer and then demodulate the signal with a Fabry-Perot interferometer of a similar OPD that of the Mach-Zender and composed of two Bragg gratings [34,35].

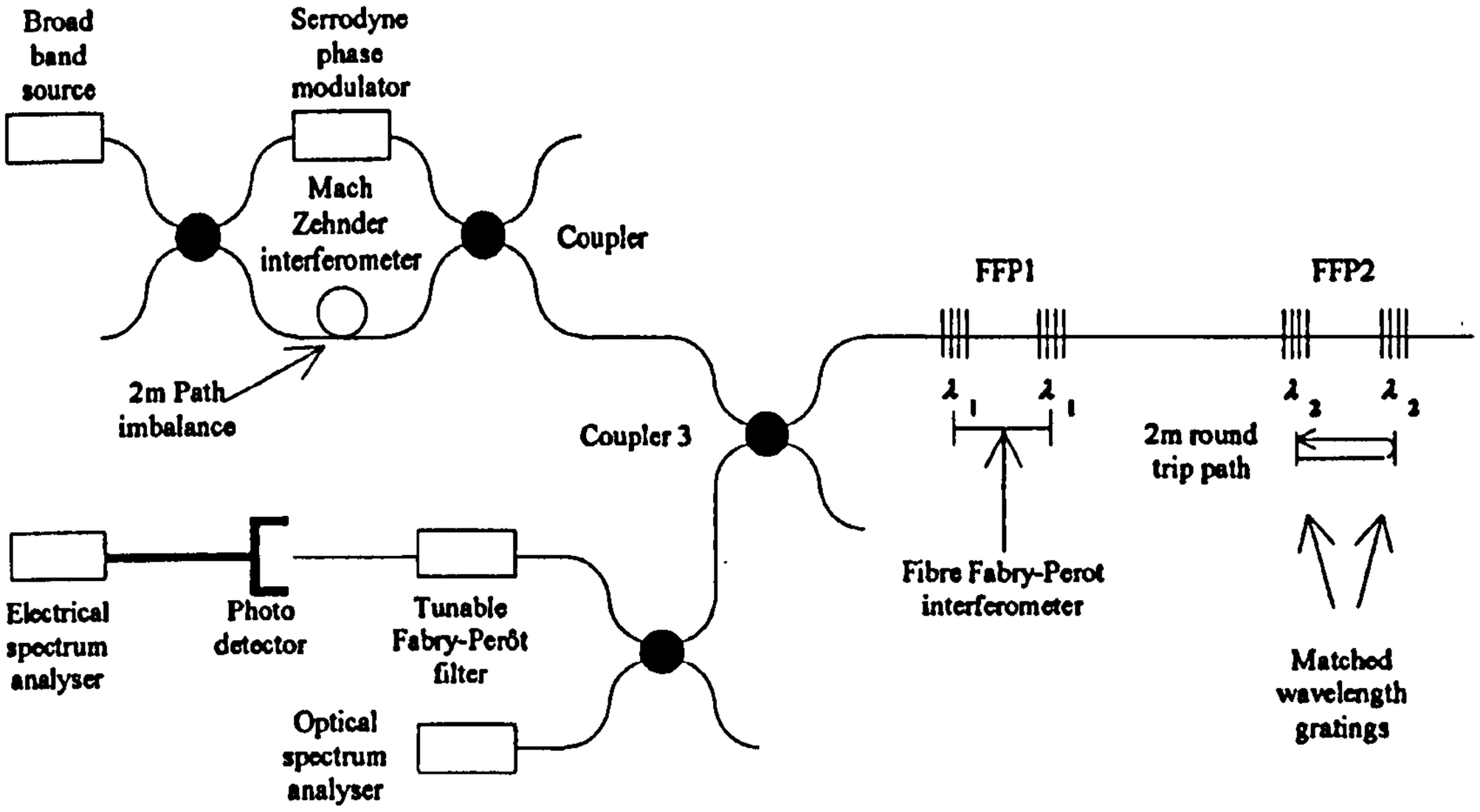

Figure 2.14 shows a wavelength multiplexing scheme

The response of each sensor, reflecting at different wavelengths, is read by the tuneable final Fabry-Perot acting as a filter. This tuneable Fabry-Perot cavity allows the interrogation of each sensor uniquely and is the base of the demultiplexing scheme. This multiplexed system allows good sensitivity for strain and temperature measurement but also permits dual simultaneous measurand sensing. In this particular case, dynamic

strain induced an OPD change in the Fabry-Perot sensor, while temperature was encoded as a change in the reflected wavelength.

2.2 References

[1] Y. J. Rao, D. J. Webb, D. A. Jackson, L. Zhang, and L. Bennion, Journal of lightwave Technology, 15, (1997), 779-785.

[2] B. Culshaw and J. Dakin, Optical fibre sensors, Vol.1&2, Artech House, Boston, (1989).

[3] D. C. Marvin, and N. A. Yves, Appl. Optics, 23, (1984), 4212-4217.

[4] D. Snell, and G. D. Pitt, Proc. BHRA Int. Conf. Opt. Tech. in process control, (1983), 27-41.

[5] W.E. Frank, US patent No. 3,273,447 (1966).

[6] C. Menadier, C. Kissinger, and H. Adkins, Instr. Contr. Sys.,40, (1967), 114-120.

[7] H. Franke, D. Wagner, T. Kleckers, R. Reuter, H. V. Rohitkumar, and B. A. Blech, Appl. opt., 32,(1993), 2927-2935.

[8] W. Lukosz, CH. Stamm, Sens. and Actuators, 25, (1991), 185-188.

[9] G. T. Sincerbox and J. G. Gordon, Laser focus, (1981), 55-58.

[10] G. D. Pitt, Elect. Comm., 57, (1982), 102.

[11] A. L. Harmer, Proc. Int Conf OFS, (1986), VI1-VI18.

[12] R. Kotzick, and R. Niessner, J. Anal Chem., 354, (1996), 72-76.

[13] P. Karlitschek, F. Lewitzka, U. Bünting, M. Niederkrüger, and G. Marowsky, Appl. Phys.,67, (1998), 497-504.

[14] S. Draxler and M. E. Lippitsch, Appl. Opt., 35, (1996), 4117-4123.

[15] J. P. Dakin, D. J. Pratt, G. W. Bibby, and J. N. Ross, Electron. Lett., 21, (1985), 569-570.

[16] Y. T. Peng, Y. Tang and J. S. Sirkis, Proc. Conf. on Optical Fibre Sensors, 13, (1999), 171-174.

[17] A. D. Kersey, Proc. SPIE, 2071, (1993), 30-48.

[18] D. A. Jackson and J. D. C. Jones, Opt. Acta., 33, (1987), 1469-1503.

[19] Y. J. Rao, D. J. Webb, D. A. Jackson, Proc. SPIE, 2070, (1993), 35.

[20] Y. J. Rao, D. A. Jackson, J. Lightwave Tech., 14, (1996), 592-600.

[21] Y. J. Rao, D. A. Jackson, R. Jones and C. Shannon, J. Lightwave Technol., 12, (1994), 1685-1695.

[22] A. Matsuda, Y. Matsuno, S. Katayama, T. Tsuno, N. Tohge, and T. Minami, Journ. of the Ceram. Soc. of Jap., 102, (1994), 330-335.

[23] G. Gusmano, G. Montesperelli, P. Nunziante, E. Traversa, A. Montenero, M. Braghini, G. Mattogno and A. Bearzotti, Journ. of the Ceram. Soc. of Jap., 101, (1993), 1095-1100.

[24] T. Kurroiwa, T. Hayashi, A. Ito, M. Matsuguchi, Y. Sadaoka, and Y. Sakai, Sens. Actuators, 13, (1993), 89-91.

[25] Y. Sakai, Sens. Actuators, 13, (1993), 82-85.

[26] G. Xin, and H. Shanglian, Proc. SPIE, 1169, (1989), 582-585.

[27] F. Mitschke, Opt. Letters, 14, (1989), 967-969.

[28] J. Mlodzianowski, et al., IEEE. Lightwave Technol., LT-5, (1987), 1002.

[29] K. I. Mallalieu et al., Electron. Lett., 22, (1986), 809.

[30] M.J. Marrone, et al., Proc. 8th Int. Conf on Optical Fiber Sensors, Monterey, Ca., (1992), 69.

[31] S. A. Al–Chalabi, B. Culshaw, and D. E. N. Davies, Proceedings of the first international conference on optical fibre sensors (IEEE), (1983), 132.

[32] J. L. Brooks, et al., IEEE J. Lightwave Technol., 3, (1985), 1062.

[33] F. Farahi, T. P. Newson, J. D. C Jones and D. A. Jackson, Opt. Commun., 65, (1988), 319-21.

[34] J. Meyer, S. J. Spammer, and P. L. Swart, Proc SPIE, 2071, (1993), 169-179.

[35] Y. J. Rao, D. A. Jackson, Meas. Sci. Technol, 7, (1996), 981-999.

3

Humidity generation

3.1 Humidity generation

3.2 References

3.1 Humidity generation

3.1.1 Commercial solution for humidity generation

When studying the effect of humidity on various materials it is important to have access to a humidity generator capable of varying the humidity over a wide range, as fast as possible with a minimum of temperature fluctuation. This is important since the measured speed of response of the material will be limited by the speed of response of the humidity generator. It is also important that the generator covers the full range of humidity at more or less 1-2 % RH at a reasonable flow of ~10 l/min. The system should be robust, requiring little maintenance and be small enough to fit easily in a laboratory.

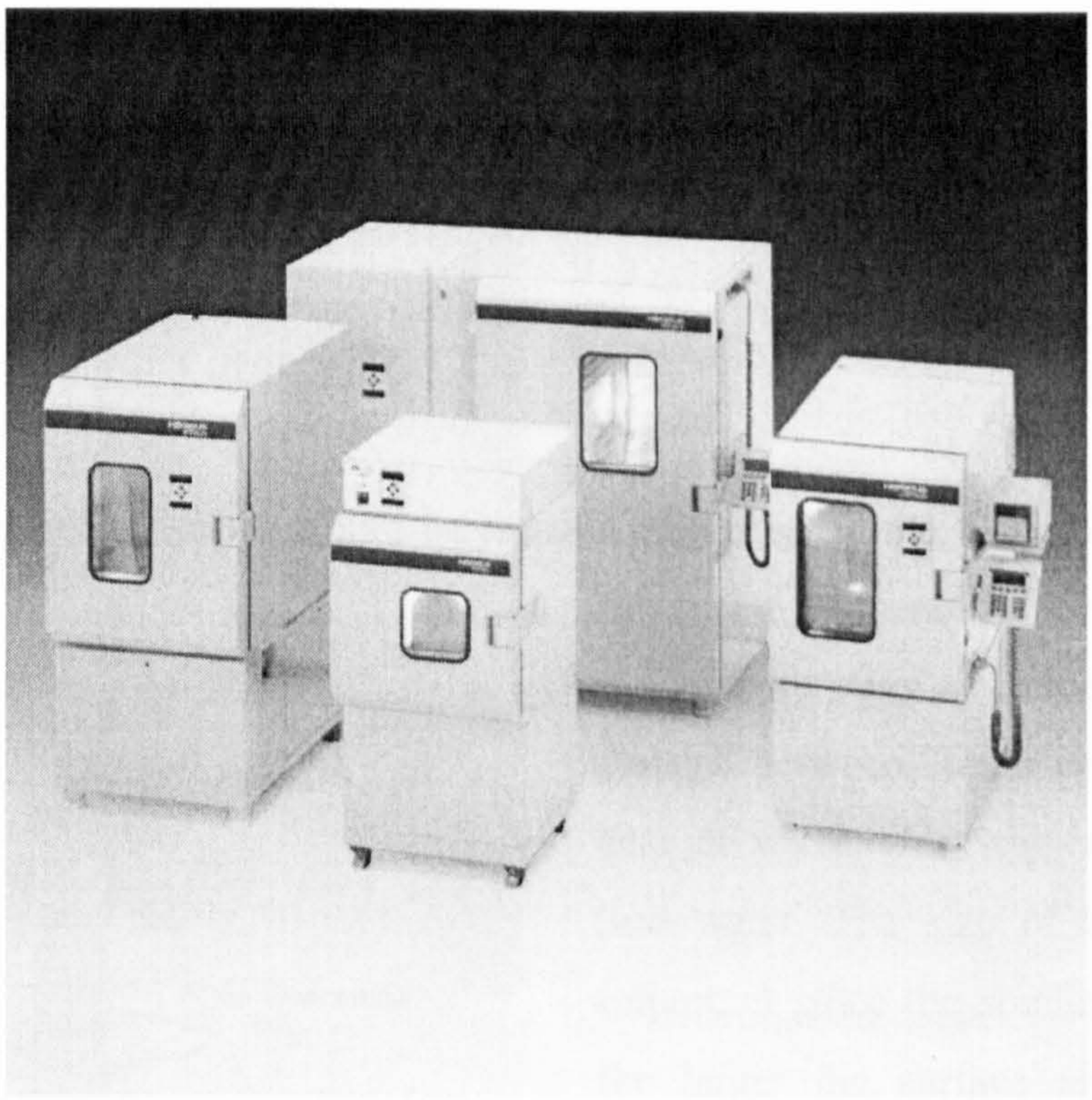

Figure 3.1 shows a typical set of climatic test chambers distributed by Weiss Technique Ltd

Ideally this generator would allow the degree of humidity to be tuned using one or two simple valves, with an output pipe feeding the humid air into a test chamber. Most available commercial devices do not meet these requirements. They are usually

designed to allow samples to be stored in the device to permit the testing of samples over long periods. This is the case of climatic tests chambers distributed by various companies. A typical example is shown in figure 3.1 [1]. These climatic chambers usually allow variation of relative humidity and temperature between 10-95 % RH and 10-90 °C respectively. Despite the important range of temperature covered by these chambers the lack at low humidities is critical as the detection is required over the full range of humidity. These humidity chambers are also difficult to modify to suit general experimentation. For example in the case of test on remote humidity sensor using fibres it would be necessary to make holes in the front window to permit the probes to be inserted. This would lead to an immediate loss of warranty and might critically affect the performance of the apparatus. The size of these chambers is also a problem, as it should be placed close to the end of the optical bench, which was not possible due to the restricted space in the laboratory. Finally these chambers are extremely costly ~£ 10 000 and beyond the resources available for the project.

It was therefore decided to construct a humidity generator specifically for our studies on materials suitable for optical humidity sensors.

3.1.2 In house humidity generator

The ideal humidity generator would be capable of producing the 0-100% range, with a minimum temperature variations. There are several ways of inducing the phase change between liquid and gas in the case of water. One way is to bubble air into water. The size of the bubbles is important since the smaller the bubbles, the larger the surface area of contact between the air and water. The bubblers were originally made by fusing commercial glass sinter filter tubes to a Dreschel bottle head. A saturation of ~80% RH was achieved. The disadvantage of such bottles is their fragility and cost. This problem was overcome using simple Erlenmeyer flasks as shown in figure 3.2. All

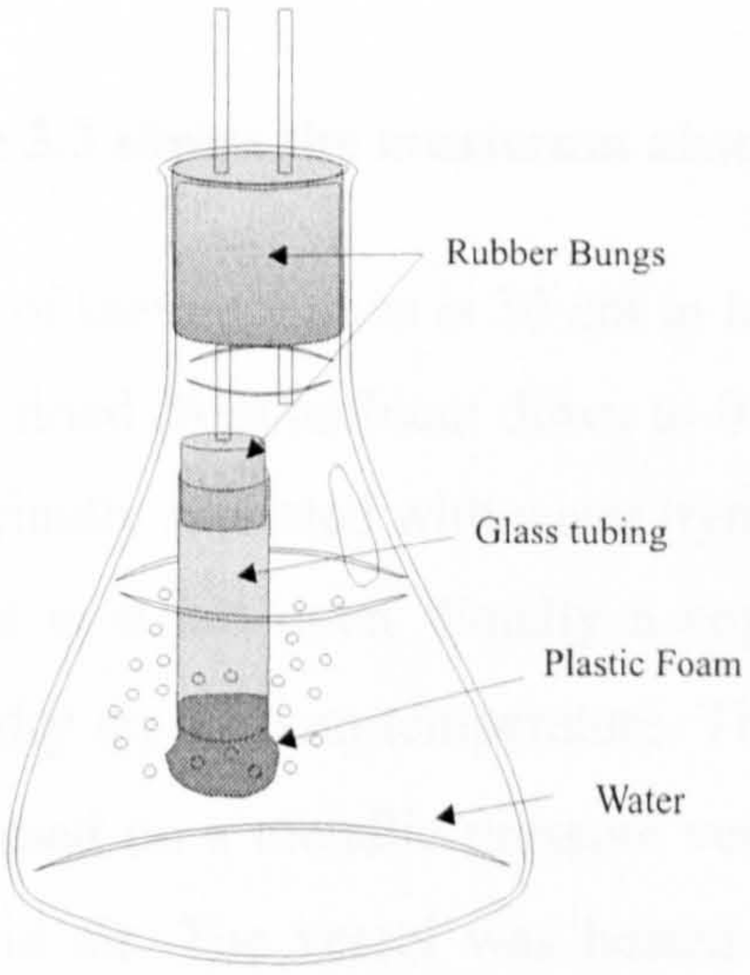

Figure 3.2. Converted Erlenmeyer Flask

parts of this bubbler are readily available, cheap, and it generates small bubbles allowing an equivalent humidity generation. The use of several humidifying bottles in series did not drastically increase the humidity levels as each added bottle increased the relative humidity by only one percent, hence a heating alternative was used. The humidity held by air varies with temperature as seen in figure 3.3. If the air is heated at the temperature T and saturated at 80% RH, a decrease of 2°C is sufficient to saturate the air at 100 % RH in the 20°C region. It is thus possible to obtain a flow of fully saturated air by heating the air by a few degrees followed by a cooling to room temperature. The full system described in figure 3.4 shows two separate lines. The dry line was built using silica-gel towers in which the air is simply circulated.

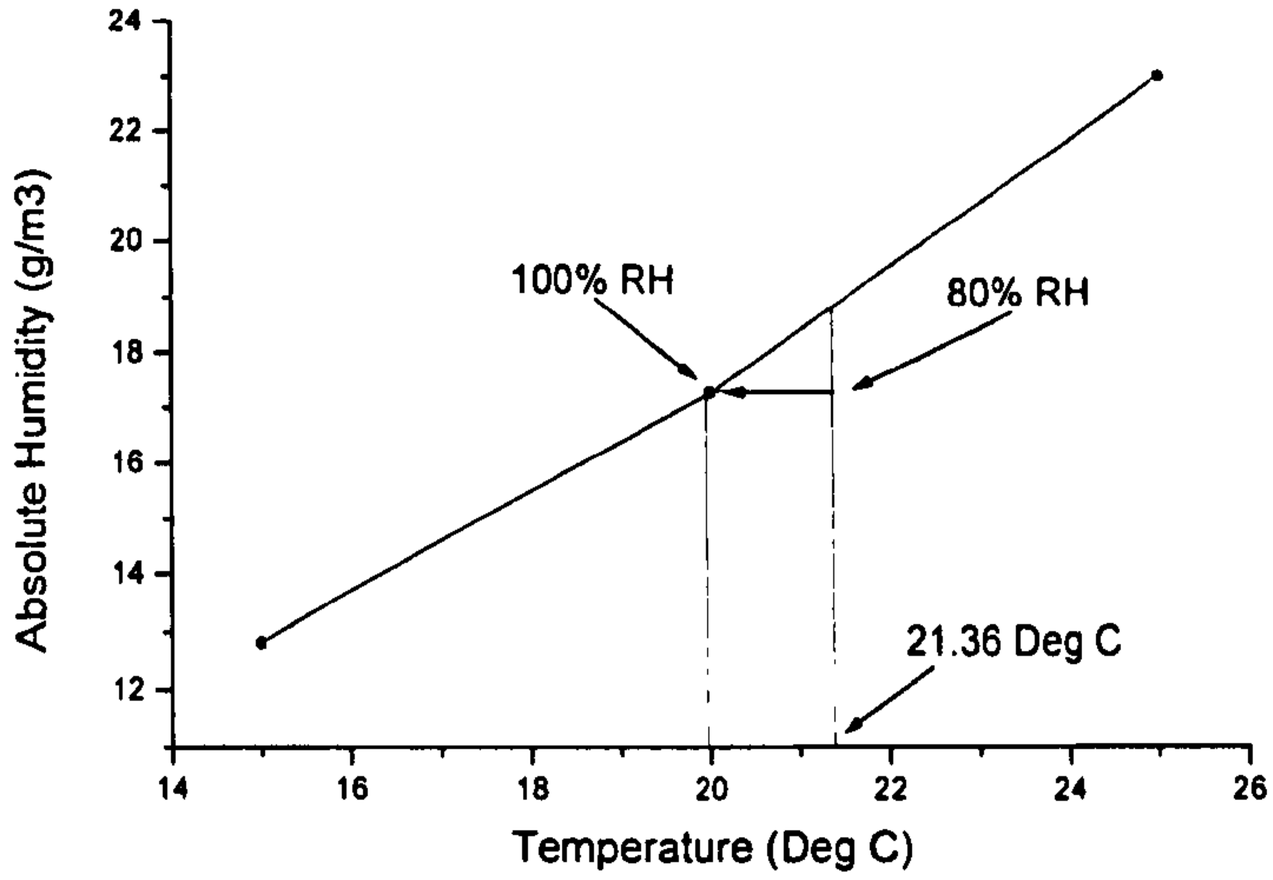

Figure 3.3 shows the maximum absolute humidity possible against temperature

The size of these columns is 30 cm in length and 9 cm in diameter. This system allows air to be dried from ambient down to 0.1% RH at a 10 l/min air flow. When the silica gels are finally saturated with water (typically one week) the gels are removed and dried overnight in a hot oven. Finally a copper coil placed in a thermostated water bath ensured dry air at room temperature. The humidity line consists of two parts. The first part is based on a metallic pressure vessel (a customised pressure cooker) to generate hot humid air. The vessel was heated using a standard laboratory hot plate while a copper tube was generating bubbles inside the vessel. The result was a flow of fairly saturated air (10 l/min) which was then directed to the second part of the line. As explained earlier this hot humid air had to be cooled to room temperature to obtain the 100% RH required. This was done using a set of three bubblers shown in figure 3.4

allowing the hot air to have a maximum and efficient surface exchange when cooled while maintaining its humidity levels. Because the water container was placed on the floor the water was found to be at a lower temperature than that of the room, and was hence slightly heated to compensate this effect. Finally a water pump was inserted to allow a good circulation of water in the container allowing a higher cooling efficiency. To obtain 100 % RH at room temperature, the temperature of the hot plate and the water in the cooling container were perfectly matched, by fine tuning. If the system is not set correctly two effects are possible: 1) the relative humidity is lower than maximum because of an excess of cooling and 2) the humidity is maximum but at a higher temperature than that of the laboratory. In this case, if the temperature exceeds the temperature of the laboratory by one degree, dew is observed in the tubes and on windows of the test chamber which can lead to severe condensation if the temperature increases even more. Both lines were fitted with escape lines. These lines would release the excess of air unused by a closed line by using pressure relief valves. As these valves are usually expensive a series of Erlenmeyer flasks full of water were used.

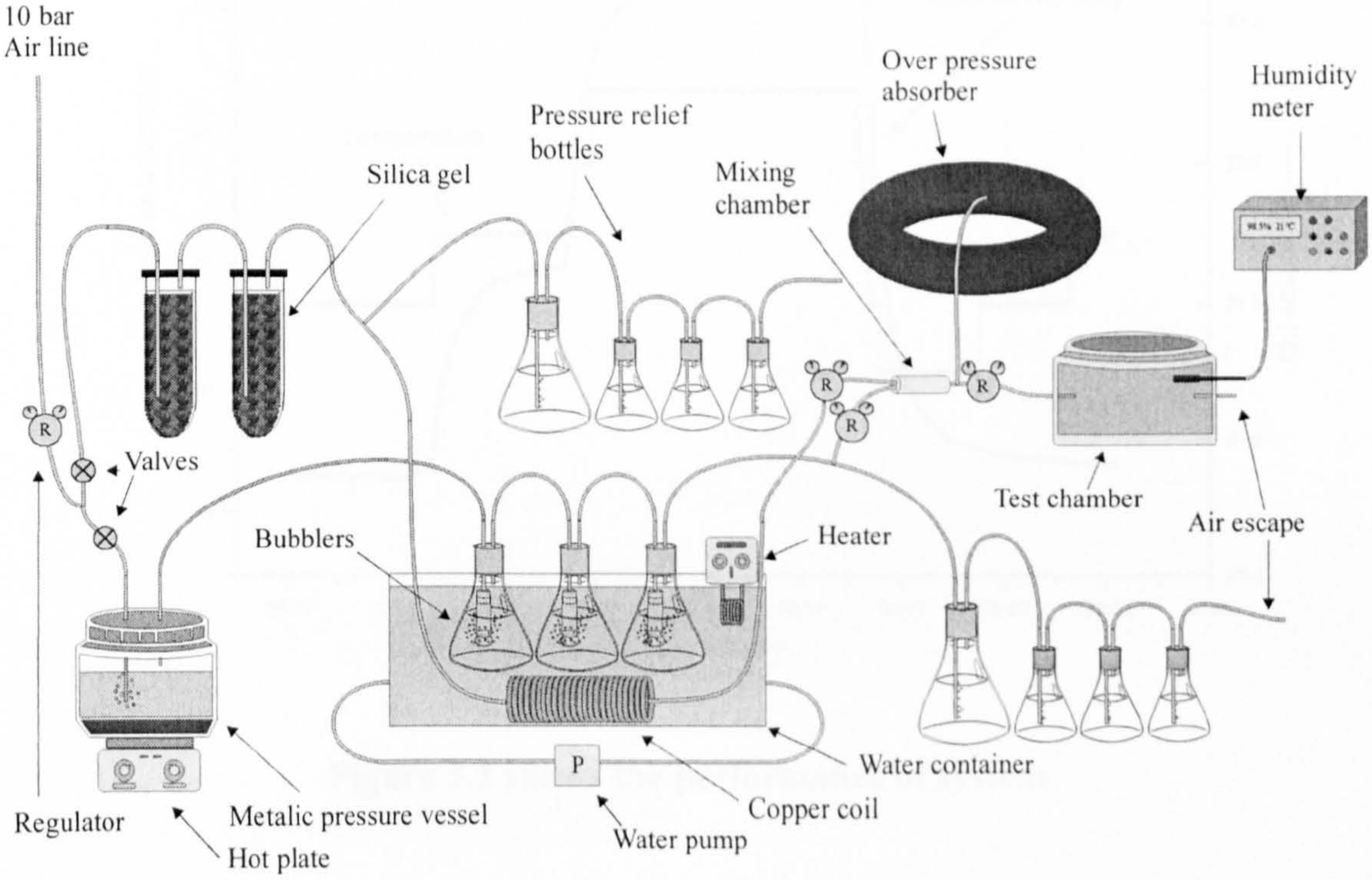

Figure 3.4 shows the humidity generator

The principle is that as at a given pressure corresponds a water level that will be compensated exactly due to its weight. If this pressure is exceeded then the air simply

circulates through the bottles and escapes. Typically three or four flasks were used including one 5 litres and 1 litre for the others in each line. These simple relief valves had also the great advantage of being tuneable by modifying the heights of the tubes in the flasks or by simply adding or subtracting flasks. At the end of both lines, two regulators were used to set the ratio of humid and dry air so as to obtain the maximum humidity range possible. Finally a flexible inner reservoir consisting of a car tyre inner tube was used to average any pressure fluctuations when commuting from one line to the other. The mixed flow was then directed to the test chamber and a final regulator ensured a constant 10 l/min humid air flow. Finally measurements of the humidity levels in the chamber were made by using a commercial Vaisala humidity transmitter.

3.1.3 Results of humidity generating system

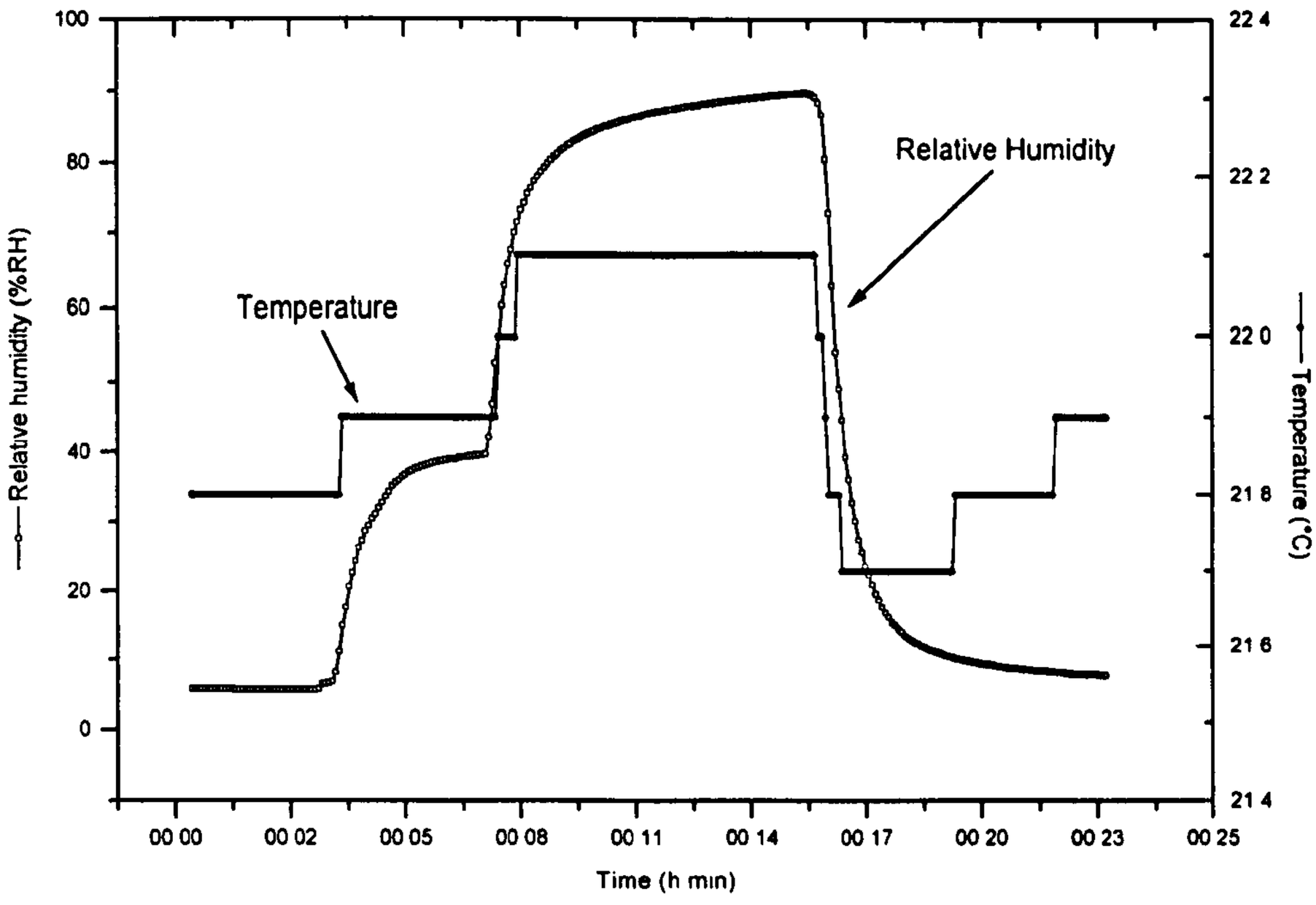

Figure 3.5 shows the performance of system

The different steps of the humidity curve of figure 3.5 were obtained by changing the ratio of humid and dry air in the mixing chamber. Using the two appropriate regulators it is possible to set any relative humidity in the chamber between 0.1% and 100% RH. The response time of this generator depends mainly on the flow and the size of the test

chamber (here 17.5 cm in diameter and 15 cm deep). As can be seen, an increase from 5 to 40 then to 90% RH was obtained in 15 minutes. It is possible to obtain a complete saturation from 0.1% RH within the same time. As seen in figure 3.5 the system performs extremely well. When changing the humidity levels, it is convenient to minimise any temperature fluctuations in the flow. Figure 3.5 shows a typical fluctuation of 0.4°C between 5% and 90% RH, this is uncorrelated with the humidity level curve. These fluctuations can be minimised by fine tuning of the temperature levels of the thermostated bath and the metallic vessel.

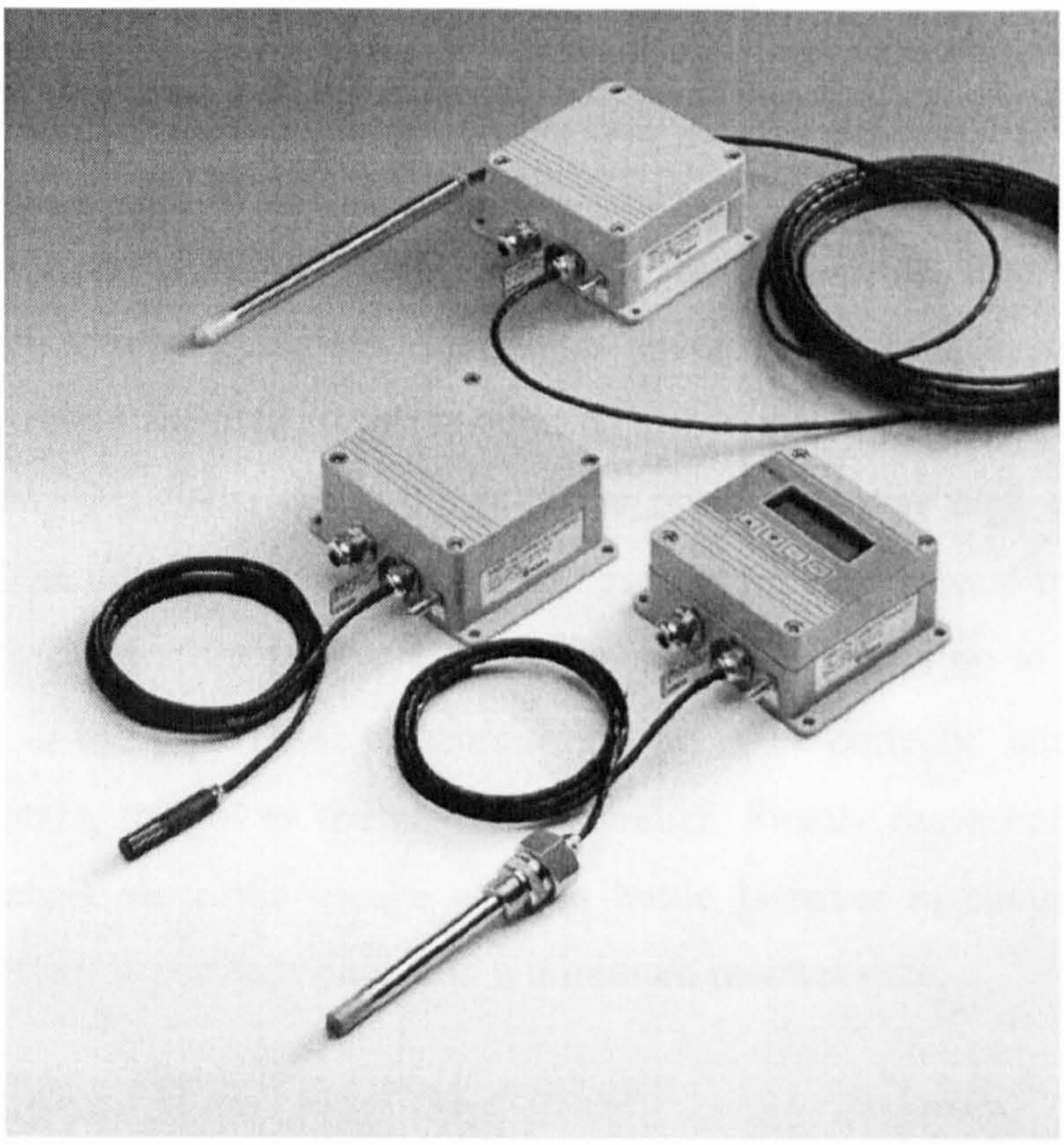

Figure 3.6 shows different Vaisala humidity transmitters

All humidity measurements were made using an electronic humidity sensor available from Vaisala [2]. This sensor was controlled using the RS232 interface of a computer. The unit also had a remote probe that sensed the humidity of the chamber. The sensor used in the experiment was composed of the top or middle unit shown in figure 3.6 coupled with the bottom probe. The accuracy of this sensor was 1% RH between 0 to 90 % relative humidity and 2% RH over 90 % relative humidity with a response speed of 15 seconds.

3.1.4 Maintenance and safety of the humidity generator system

During the three years of use of this humidity generator system little maintenance has been necessary. Due to the evaporation of the water in the air bubbling through the bottles the water levels had to be checked regularly to avoid any loss of performance of the system and refilling occurred typically once every month. The container in which the bubblers were placed had to be filled regularly (every 2 months) due to evaporation in the atmosphere. It is important that the bottles are placed in the water bath as this avoids the propagation of glass in the laboratory in the case of the breakage of an Erlenmeyer flask due to a failure or misuse of the system. The metallic heated vessel used to saturate the air with water had to be cleaned once a year due to deposition of chalk. Over long periods the rubber joint also may need to be changed. Most of the parts of this system were trouble free. This is due to the fact that, in normal use, the system is never under high pressure. The important points about safety of this system are the two pressure relief valves inserted in the system. The first one is located on the modified pressure cooker. This valve either bursts if the pressure is too high or melts if the temperature of the vessel exceeds a specified temperature. The second type of pressure relief valve is located at the end of each line avoiding any build up of pressure when closing the dry or wet line. These pressure relief valves are perfectly safe since the less water they contain, the lower the pressure of relief. Finally these bottles cannot be blocked with chalk since the escape of each bottle is never in contact with water. Overall, this system is perfectly safe with a minimum maintenance.

3.2 References

[1] Weiss Technik Ltd, (94), Cat. HVB-E 20000.

[2] Vaisala Ltd, (94), Cat. A576en.

4

Humidity sensing via the determination of the refractive index of air

4.1 Measurement of humidity via the determination of the refractive index of air

4.1.1 Theory of the refractive index of air

4.1.2 Effect of humidity on the refractive index of air

4.1.3 Effect of temperature on the refractive index of air

4.1.4 Effect of pressure on the refractive index of air

4.1.5 Effect of CO2 on the refractive index of air

4.1.6 Sensing the humidity of air by measuring its refractive index

4.1.7 Advantages of such measurement

4.2 Experimental verification of Edlen's equations

4.2.1 Comparison of Edlen's and Cauchy's equations

4.2.2 Experimental setup

4.2.3 Results of the comparison

4.3 Dual tandem interferometry for measuring the refractive index of air

4.3.1 Humidity sensing by measuring the refractive index of air

4.3.2 Sensor head design

4.3.3 System description

4.3.4 Results using this system

4.4 References

4.1 Measurement of humidity via the determination of the refractive index of air

4.1.1 Theory of the refractive index of air

In 1965 Bengt Edlen from the University of Lund in Sweden reviewed the theory of the refractive index of air [1]. A series of equations giving the refractive index (n) as a function of the temperature, pressure, humidity level and wavelength were based on the definition of standard air which had a composition by molar percentage of 78.09 % nitrogen, 20.95 % oxygen, 0.93 % argon and 0.03 % of carbon dioxide at 760 torr, 15 °C and 0 %RH [1]. An updated version of this equation was proposed in 1993 by K. Birch and M. Downs [2] converting all parameters to S.I units but also revising the notion of standard air including its CO_2 levels. Recent measurements of these levels [2] were found to be in excess of that assumed by Edlen and a new standard value of 450 ppm was adopted. The definition of standard air was also modified to 100 kPa, 20 °C and 50 %RH to match modern laboratory conditions.

The equations are:

$$(n-1)_s \times 10^8 = 8343.05 + 2406294 \times \left(130 - \sigma^2\right)^{-1} + 15999 \times \left(38.9 - \sigma^2\right)^{-1} \qquad (4\text{-}1)$$

with σ in μm^{-1} and 's' standing for 'standard'.

$$(n-1)_{tp} = p \times (n-1)_s / 96095.43 \times \left[1 + 10^{-8}(0.601 - 0.00972 \times t) \times p\right] / (1 + 0.0036610 \times t) \qquad (4\text{-}2)$$

with t in $^{\circ}C$, p in Pa and 'tp' standing for 'temperature' and 'pressure'. Finally,

$$n_{tpf} - n_{tp} = -f \times \left(3.7345 - 0.0401 \times \sigma^2\right) \times 10^{-10} \qquad (4\text{-}3)$$

f being the partial pressure of water in Pa.

Following this update, a sign error that occurred in the correction for the change from IPTS-1948 to the ITS-90 temperature scale, led to a published correction [3] changing the values in equation (4-1). The corrected equation is:

$$(n-1)_s \times 10^8 = 8342.54 + 2406147 \times \left(130 - \sigma^2\right)^{-1} + 15998 \times \left(38.9 - \sigma^2\right)^{-1} \qquad (4\text{-}4)$$

These equations have been shown to agree closely with the experimental data within an experimental uncertaincy of $\pm 3\times10^{-8}$.

4.1.2 Effect of humidity on the refractive index of air

Using the above equations it is possible to evaluate the effect of humidity levels on the refractive index of air. Edlen's equations contain two parameters, $\sigma = 1/\lambda$ which in this case is the wavelength of the source i.e. 825 nm in this project, and the second, f being the partial pressure of water vapour in Pa at a particular temperature. As this partial pressure depends only on the temperature it was possible to insert a polynomial interpolation in Edlen's equation. The final equation gave the refractive index as a function of the temperature, the pressure and the relative humidity. The effect of the relative humidity on the refractive index of air could therefore be quantified. At standard condition (according to K.P. Birch and M.J. Downs [2]: 100 kPa, 20 °C and 50 %RH) the refractive index of air is n = 1.0002662348. As the fluctuation around this values are small we will adopt the (n-1) notation which in this case gives (n-1) = 2.662348×10^{-4}. To determine the fluctuation due to relative humidity only, the same calculation was made for the two extremes RH = 0% and RH = 100%.
The values are:

(100 kPa, 20 °C and 0 % RH) $\quad (n-1) = 2.666644\times10^{-4}$

(100 kPa, 20 °C and 100 % RH) $\quad (n-1) = 2.658052\times10^{-4}$

The variation is then:

$$\{ (n-1)_{0\%} - (n-1)_{100\%} \} = 8.592626\times10^{-7}$$

This value represents the variation of the refractive index when the relative humidity is varied from 0 %RH to 100 %RH keeping the temperature and the pressure constant. This values corresponds to 0.32 % of the refractive index value (n-1) of standard air. To

appreciate these quantities it is convenient to convert these variation to an optical path change in an interferometer. In the case of a Michelson interferometer having a fixed reference arm of 20 cm of cavity length (10 cm of physical length) the optical path change will be given by $\Delta OPD = \Delta n \times L$ with L the length of the cavity. The result of this calculation gives: ΔOPD = 171 nm. This value is to be compared to the interfringe distance of this interferometer which is $\lambda/2 = 412.5$ nm in the precedent case of a source at 825 nm. As it is possible to obtain a resolution between 1/100 and 1/1000 of a fringe using an interferometric system, measuring the relative humidity down to 1 or 2 %RH by this mean is therefore feasible.

4.1.3 Effect of temperature on the refractive index of air

As in the case of the relative humidity, the temperature has an important effect on the refractive index of air. Using the same comparison as in the previous section the variation of the refractive index of air for a 0.1 °C temperature change at 20°C is $\Delta n = 9.386085 \times 10^{-8}$. This corresponds to a ΔOPD = 18.7 nm using the interferometric system described in section 4.1.2. It is obvious that if the relative humidity is to be recovered from the measurement of the refractive index of air, an accuracy of 0.01°C is required for the associated temperature measurement.

4.1.4 Effect of pressure on the refractive index of air

Pressure is also an important parameter when measuring the refractive index of air. A variation of pressure of 30 Pa will lead to a variation of the refractive index of air of $\Delta n = 8.003186 \times 10^{-8}$, which corresponds to 16 nm in the previously described interferometer (4.1.2). Therefore in order to determine the relative humidity by measuring the refractive index of air, the accuracy on the pressure measurement should be 3 Pa.

4.1.5 Effect of CO2 on the refractive index of air

As the air is composed of different gases, a source of error when measuring the refractive index of air may be the fluctuation of the composition of the air and

particularly its CO_2 concentration. It is known that CO_2 fluctuations do not constitute a great source of error [4] since its fluctuations remain small. As an example, in the event of an increase of 100 ppm, the variation of the refractive index would be $\Delta n = 14.5 \times 10^{-9}$ corresponding to an OPD change of 2.9 nm in the interferometer described in 4.1.2.

4.1.6 Sensing the humidity of air by measuring its refractive index

If the temperature and the pressure are measured with a sufficient accuracy, sensing the relative humidity by measuring the refractive index of air is thus possible. The principle is to invert Edlen's equation to obtain the function RH = f(T,P).

4.1.7 Advantages of such measurement

The advantage of such method is that no solid state material is needed. This implies that no drawback inherent to any material such as low response time and ageing is present. Also, an important advantage of a sensing probe using this principle is that no maintenance is required since it is composed of bulk material such as glass and metal. This kind of sensor could also be used for smoke detection since any opaque smoke would inevitably cause a loss of power on the return path.

4.2 Experimental verification of Edlen's equations

4.2.1 Comparison of Edlen's and Cauchy's equations

To estimate the effect of the relative humidity on the refractive index of air it was initially planned to use Edlen's equations. However a second set of equations was found in the 63rd edition of the handbook of Physics and Chemistry. These equations, called the Cauchy and Lorentz formulas, allow the calculation of the refractivity of air and a comparison with Edlen's equations was made. The Cauchy formula is given for dry air only and depends on the wavelength (in nm) only.

$$(n-1)\times 10^{7} = 2589.72 + \frac{12.259}{\lambda^{2}\times 10^{-8}} + \frac{0.2576}{\lambda^{4}\times 10^{-16}} \qquad (4\text{-}5)$$

This equation gives the refractivity of air at 30 °C and at a pressure of 760 mmHg. No indications are given on the exact composition of the air except for the 0.05% CO_2 amount.

The second formula is the Lorentz formula that allows one to calculate the variation of the refactive index of air by adding a correction to the previous equation. Both equations are given by:

$$(n-1) = \left(2589.72 + \frac{12.259}{\lambda^{2}\times 10^{-8}} + \frac{0.2576}{\lambda^{4}\times 10^{-16}}\right)\times 10^{-7} + 0.000041\frac{m}{760} \qquad (4\text{-}6)$$

The variable m is the water vapour partial pressure of the considered humid air. This value is linked to the relative humidity by:

$$m = \frac{RH}{100}\times m_s \qquad (4\text{-}7)$$

Where m_s is the saturated vapour pressure at a particular temperature. This value can be found in tables, here for 30°C the value is m_s = 31.824 mmHg. Considering the wavelength of an Helium-Neon laser at 632.8 nm the previous equations are condensed to:

$$(n-1) = 2.62194064004\times 10^{-4} + 1.71682105263\times 10^{-8}\times RH \qquad (4\text{-}8)$$

Using this equation we can plot the refractive index change against the relative humidity of the air (figure 4.1).

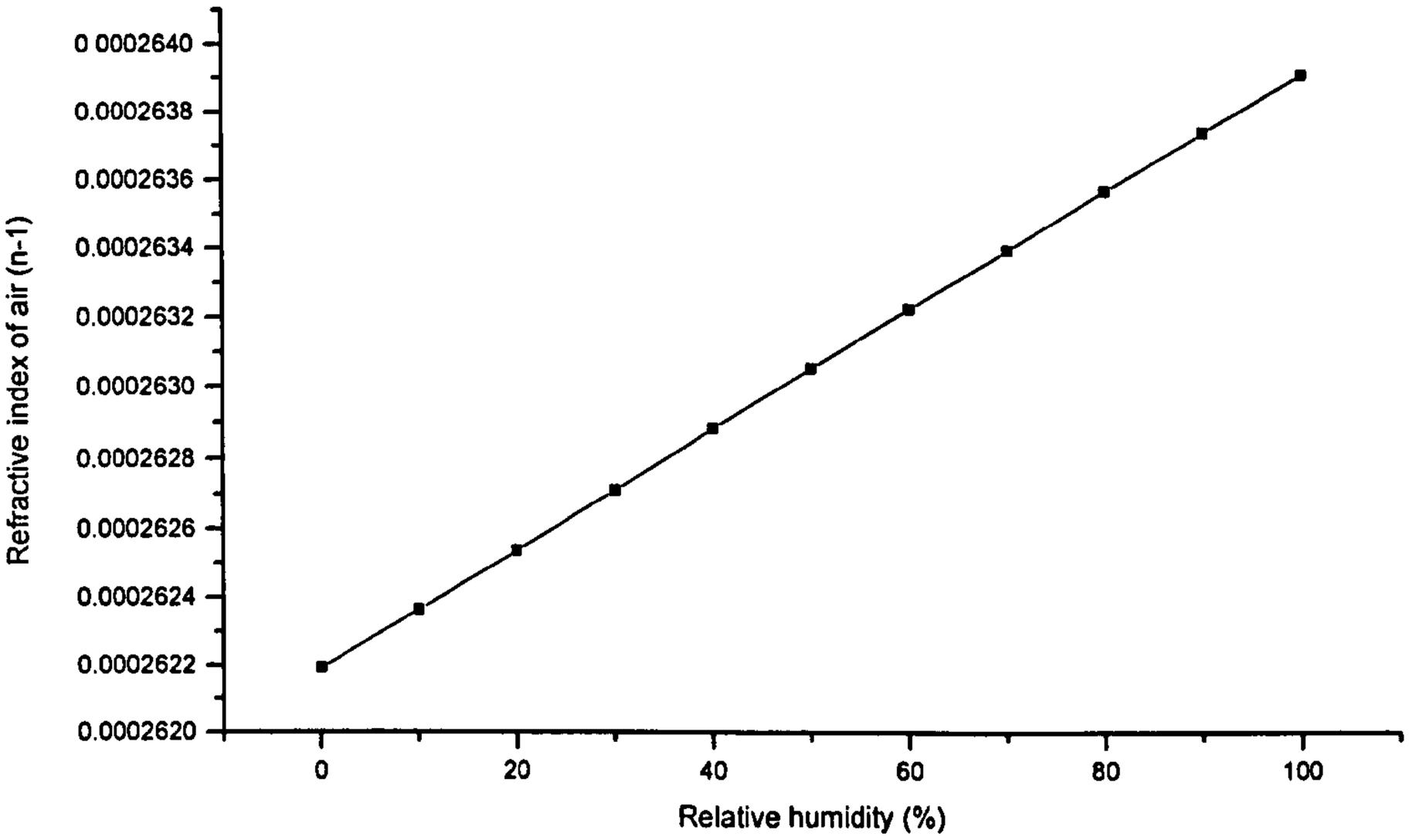

Figure 4.1 shows the variation of refractive index of air with relative humidity according to Cauchy's and Lorent'z formulas.

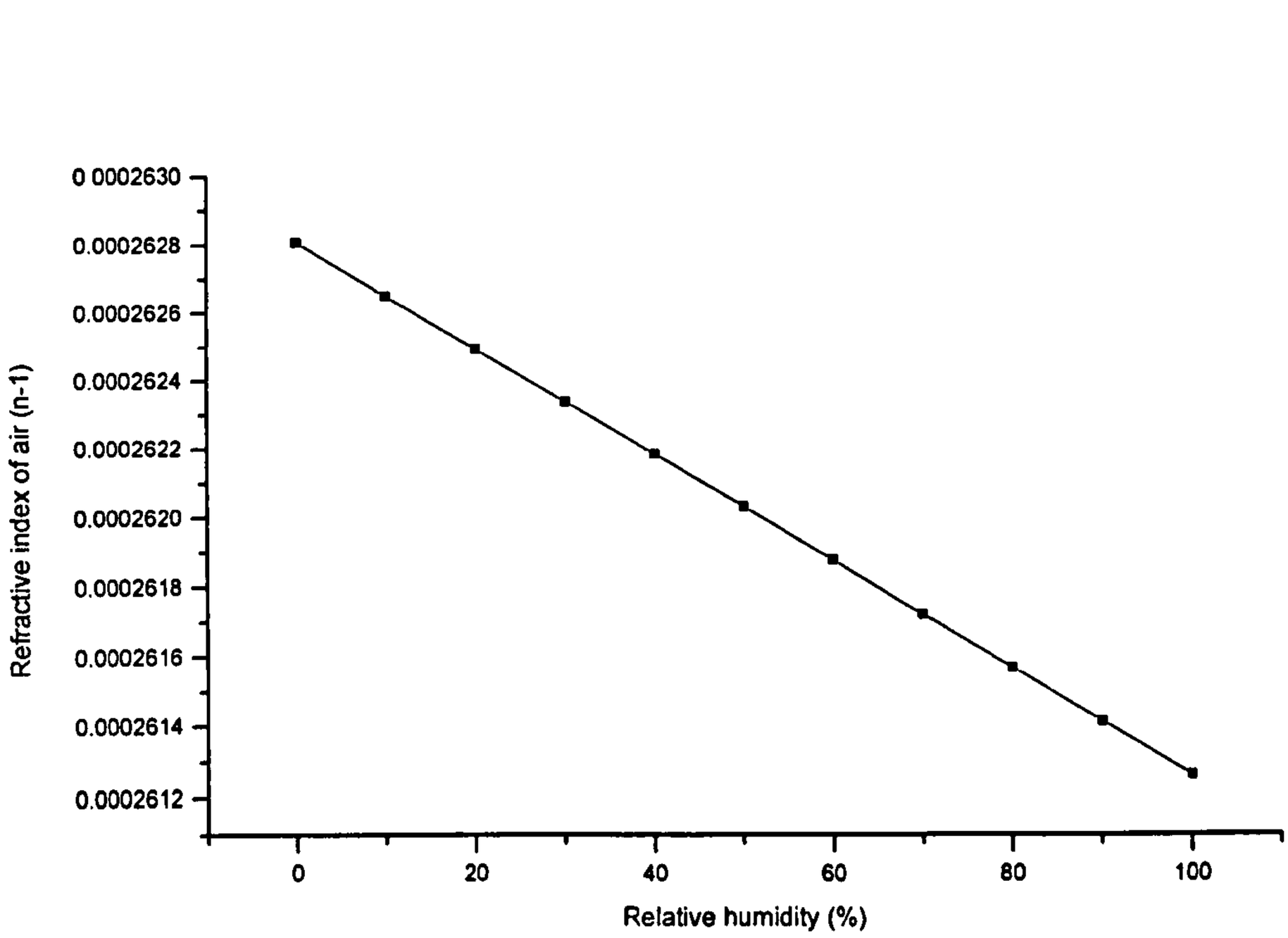

Figure 4.2 shows the variation of the refractive index of air with humidity according to the updated Edlen's equation

Under the same conditions, figure 4.2 shows the variation of the refractivity with humid air according to the updated Edlen's equation. The difference between the two is obvious. The slope of both curves are opposite and the values are different. Suspecting misprints in the handbook of Physics and Chemistry the decision was taken to build an experiment to confirm the validity of the work done by K. Birch, M. Down, and B. Edlen. The experiment was designed using a bulk interferometric system. The aim was to recover the refractive index of air from fringe movements in the interferometer. The results would then allow a comparison between the experimental and the theoretical value of n.

4.2.2 Experimental setup

The experimental setup seen in figure 4.3 was composed of a Michelson interferometer. Using a cube beam splitter it was possible to set the interferometer so that both arms would be parallel, this reduced any thermal effects. The interferometer was illuminated with a Helium-Neon laser and two simple mirrors returned the light to a detector.

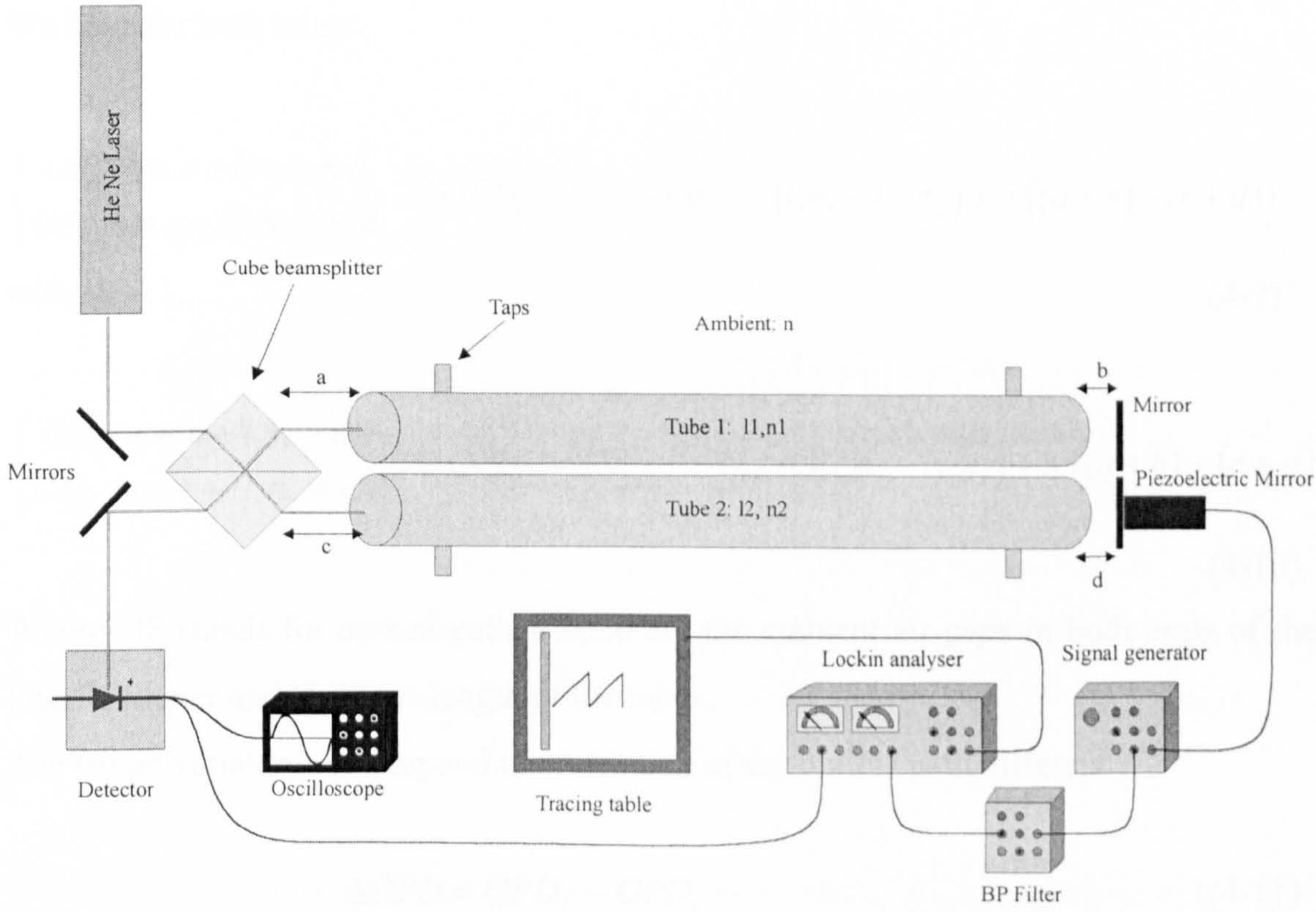

Figure 4.3 shows the experimental setup

One of the mirrors was coupled to a Piezoelectric actuator allowing a modulation of the transfer function. The signal from the detector was analysed by an oscilloscope and any change in the optical path difference in the interferometer resulted in a fringe movement. To measure the refractive index of air, two tubes of about one meter were inserted into both arms of the interferometer. The two tubes were sealed identically by two windows at each end. Each tube had two taps allowing air to be either inserted or evacuated, the tubes were totally air tight when the taps were closed. This system enables the measurement of the refractive index of humid air (n_1) in tube 1 whilst the gas in tube 2 is held at constant conditions, i.e. tube 2 is evacuated. At the beginning of the experiment tube 1 is evacuated, then a flow of air of constant relative humidity is injected into tube 1 by opening the inlet tap. The result is a movement of fringes due to the optical path change in tube 1. The fringe movements are then analysed by a lock-in amplifier and recorded using a chart recorder. The fringe counting was done by hand and the refractive index derived.

The optical path is defined by $OP = n \times d$ were n and d are the refractive index and a physical length of the medium respectively.

We have for both tubes:

$$\begin{cases} OP_{1i} = n.a + l_1 n_1 + n.b \\ OP_{2i} = n.c + l_2 . n_2 + n.d \end{cases} \Rightarrow OPD_i = OP_{1i} - OP_{2i} = \left(l_1 n_1 - l_2 . n_2\right) + n.\left(\left(a+b\right) - \left(c+d\right)\right)$$

with $n_1 = 1$. (4-9)

$$\begin{cases} OP_{1f} = n.a + l_1 n_1 + n.b \\ OP_{2f} = n.c + l_2 . n_2 + n.d \end{cases} \Rightarrow OPD_f = OP_{1f} - OP_{2f} = \left(l_1 . n_1 - l_2 . n_2\right) + n.\left(\left(a+b\right) - \left(c+d\right)\right)$$

(4-10)

Where OP stands for optical path, a,b,c,d are the ambient air gaps in both arms of the interferometer and l1, l2 the length of the tubes.

The fringe variations correspond to a variation of the optical path difference:

$$\Delta OPD = OPD_f - OPD_i \quad (4\text{-}11)$$

$$\Delta OPD = l_1 . n_1 - l_2 . n_2 - \left(l_1 - l_2 . n_2\right) = l_1 . \left(n_1 - 1\right) \quad (4\text{-}12)$$

(assuming that $n_2 . l_2$ is constant)

The wavelength of the He-Ne laser is 632.8 nm hence a change in OPD of one fringe corresponds to a displacement of 316.4 nm and the relation with ΔOPD is:

$$\Delta OPD = Fringes \times 316.4 \times 10^{-9} = l_1.(n_1 - 1) \qquad (4\text{-}13)$$

From which we can extract n_1, the refractive index of the humid air.

To evaluate n_1, the values of a, b, c, and d are not required to be accurately known provided they are small compared to l_1 and l_2 so that environmental noise is minimised. Even though n_2 and l_2 aren't present in the formula, it is essential that the gas in tube 2 remains under the same conditions as we require it to act as a reference.

4.2.3 Results of the comparison

As seen in figure 4.4 the experiments resulted in twenty points and were made on several days.

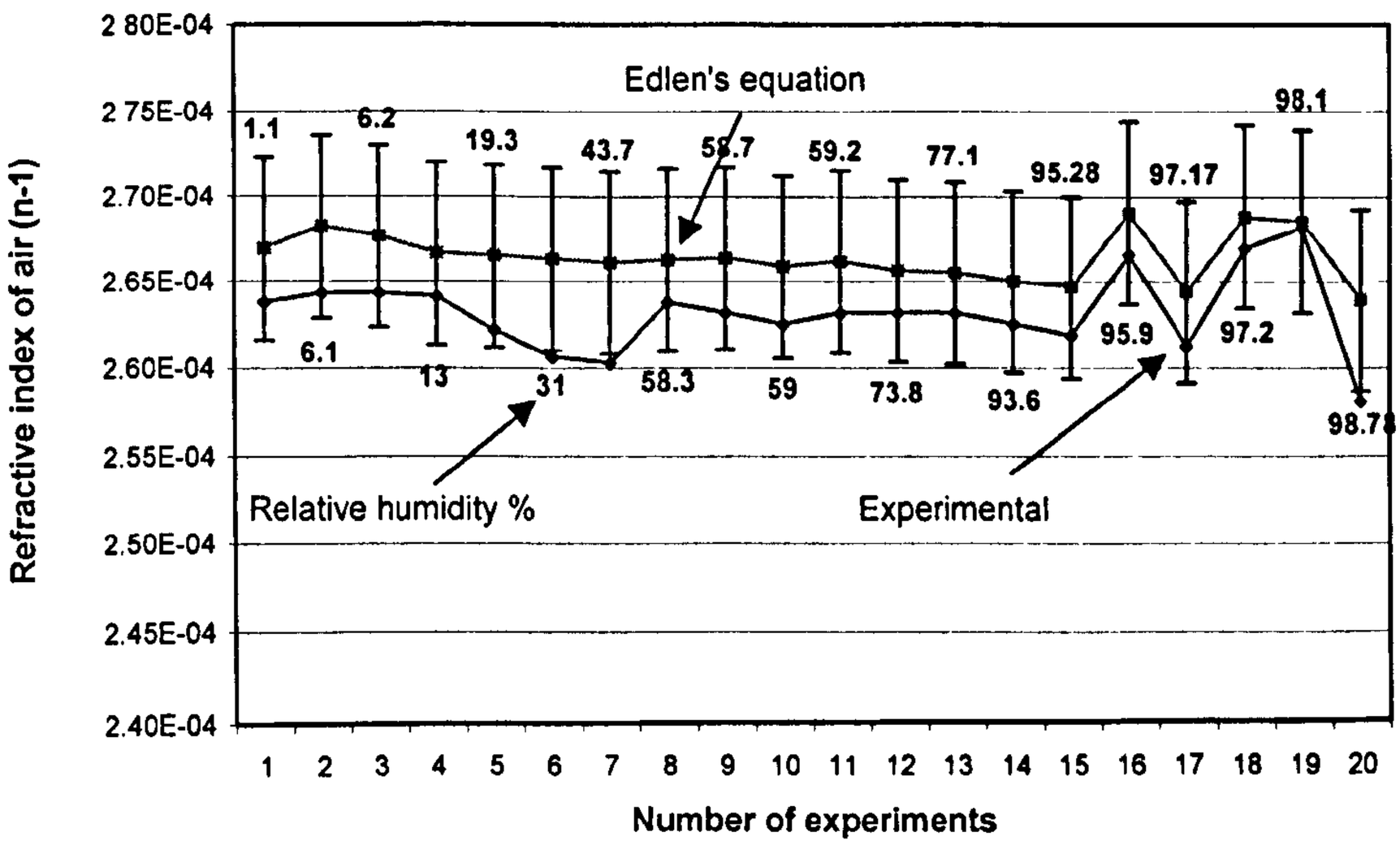

Figure 4.4 shows the comparison between the experimental values of the refractive index of air and the derived values using Edlen's equation

By using the theory described in the previous section, the refractive index of the air was measured. For each experiment the temperature, relative humidity and atmospheric pressure was recorded in order to calculate the refractive index of air by using Edlen's equation. The figure 4.4 shows the refractive index, measured with the optical system compared to the calculated value. The values are very close and the average difference between both curves is 1.21% of the theoretical value. To give an estimation, the error bars on the theoretical curve correspond to 2% of the values.

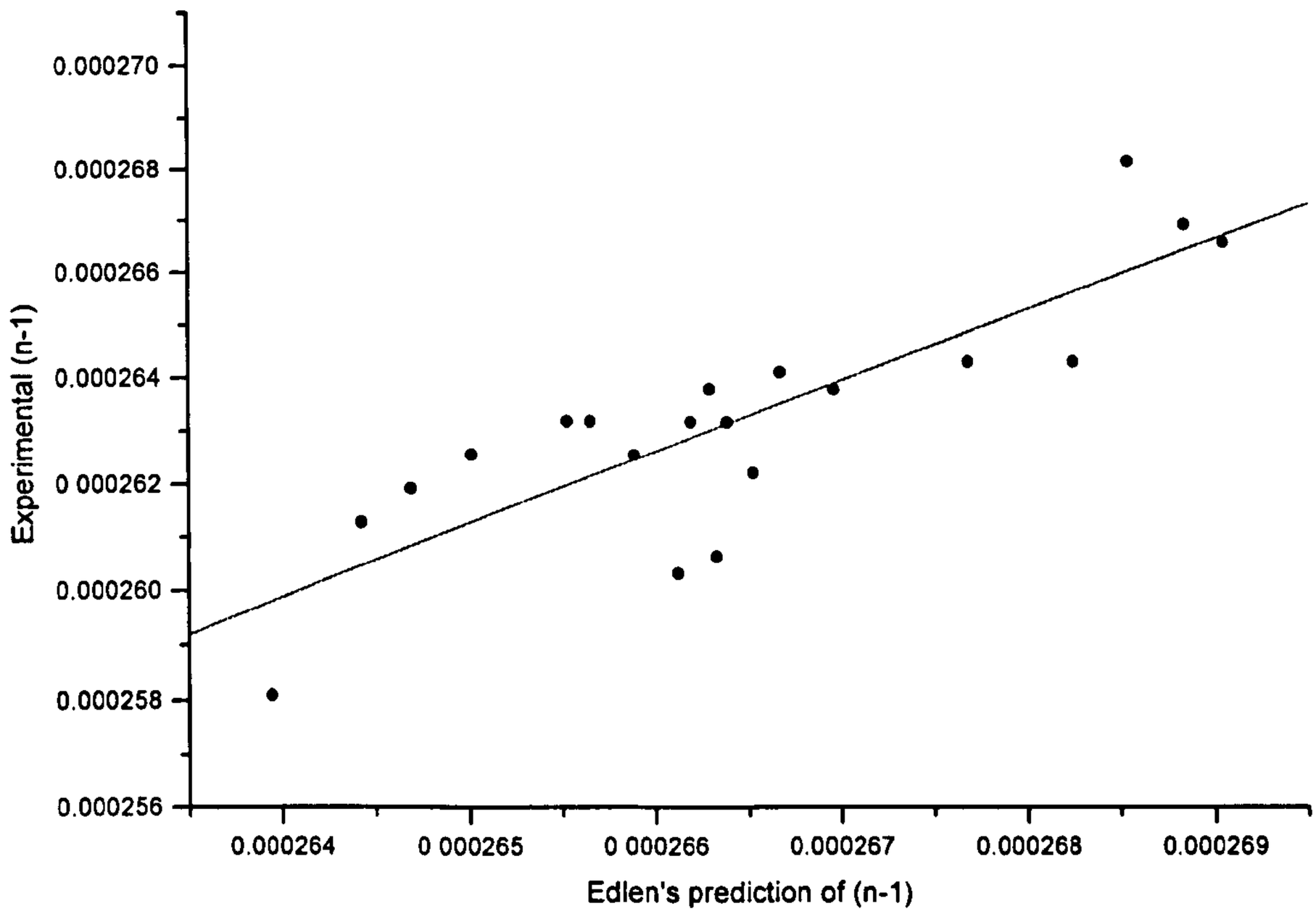

Figure 4.5 shows a linear regression between the experimental values of the refractive index of air and the derived values using Edlen's equation

The coefficient of the regression is R = 0.842 which shows a good correlation of the theoretical and experimental values (0 < R < 1) while the offset of the zero intercept is due to the difference of air composition.

This experiment therefore confirmed the validity of the Edlen's equations and also that the Cauchy's and Lorentz's formulas were not good estimators of the refractivity of air. Edlen's equations were therefore chosen for further work on the refractivity of air.

4.3 Dual tandem interferometry for measuring the refractive index of air

4.3.1 Humidity sensing by measuring the refractive index of air

As described in section 4.1.7 the direct measurement of the humidity of the air by sensing the variation of its refractive index offers several advantages. An optical interferometer was therefore designed and built for this purpose. The system is based on dual interferometry and in this case the sensors head is composed of a Michelson interferometer.

4.3.2 Sensor head design

The dual tandem interferometric configuration allowed remote sensing. The probe was designed to be robust so that frequent handling would not lead to misalignments in the sensor head. A cavity length of 9-10 cm was required, due to the small effect of humidity on the refractive index of air, to allow a good accuracy on the measurement of relative humidity.

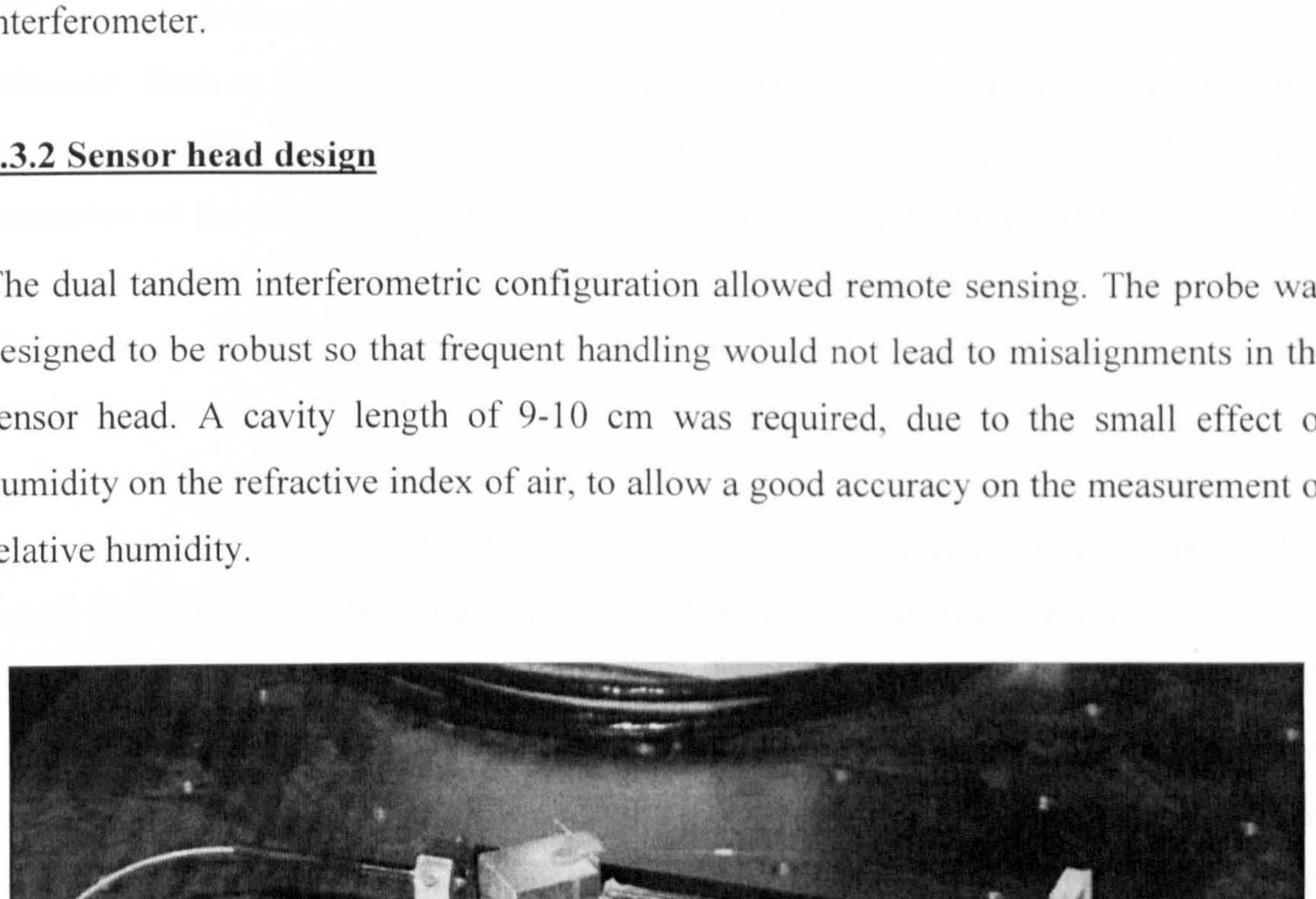

Figure 4.6 shows the Michelson interferometric probe

As the probe was to be used in a remote configuration and may be in specific locations, its size had to be adjusted to its minimum and a larger cavity length was therefore not possible. An important source of error in a cavity of this length can arise from the thermal expansion of the probe. To minimise this problem a Michelson interferometer with two parallel arms with virtually equal path lengths was used to compensate for thermal effects. To ensure that the two arms were of equal length, a common mirror was used at the output of each arm. For the same reasons the alignment of the collimator, the cube beam splitter and the mirror was made with great care to minimise any optical difference on both arms. A sealed tube was inserted into one of the arms to act as a reference. Thus an OPD change resulting from a change in the refractivity of the air was readily detectable. The design is such that the optical path change induced by thermal expansion of the tube in the reference arm was virtually negligible. This is due to the fact that an expansion of the glass tube is equivalent to the replacement of a small slice of reference air with ambient air. To reduce the differential optical path, similar windows were inserted in the sensing arm. An other benefit from placing the windows in the sensing arm was that any dispersion effects induced by the reference tubes windows were compensated. All parts of the probe were glued with cyanoacrylate except the mirror and the collimator. The collimator was inserted into a holder of the right size and was tightened using two screws. The end mirror was first stuck with cyanoacrylate to a three dimensional positioner, and then adjusted to observe interferometric signals. The mirror was then stuck to the metallic base using an epoxy glue and the link to the three dimensional positioner broken. Overall this probe was very robust and could by handled with no particular care. All parts of the probe were either in glass or metal glued together, making it resistant to many aggressive environments such as very high humidities for long periods. This sensor could therefore be used in harsh environments and also when handling of the probe is frequent. Finally this sensor would be perfectly adequate for a meteorological use.

4.3.3 System description

The experimental set-up was based on a dual tandem interferometric system illuminated with a source of limited optical coherence (figure 4.7) [5,6]. Using this arrangement it is possible to simultaneously interrogate four optical sensors.

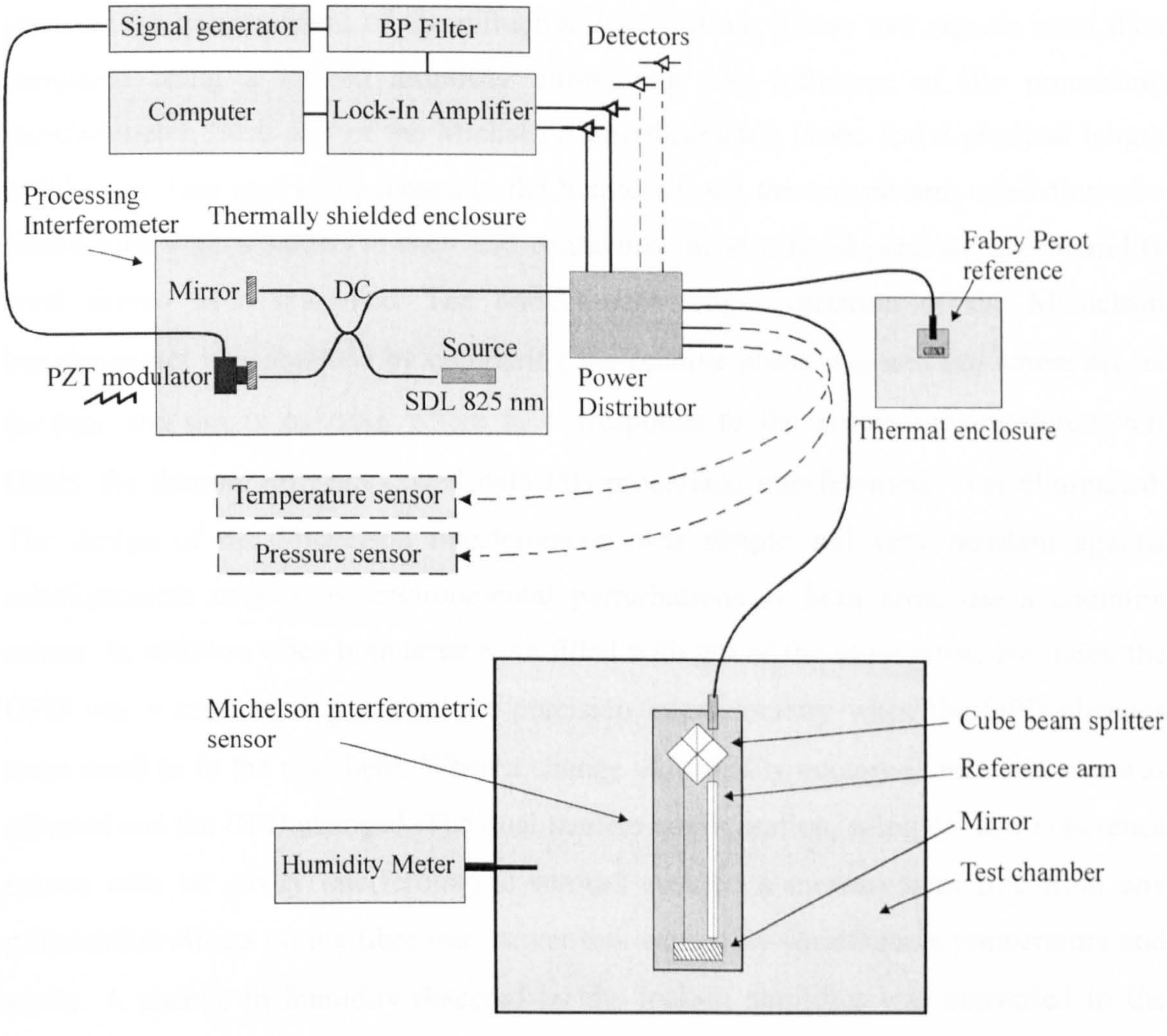

Figure 4.7 Experimental setup of the low coherence interferometric sensor

The processing Michelson interferometer was thermally shielded to minimise any temperature drift during the experiment. This interferometer acted as a modulator for the two remote interferometers conditioning the signal received by the APD detectors. When the optical path differences of the sensors were matched to the processing interferometer within the coherence length of the source interferometric signals were observed. The system was locked on the maximum of the obtained transfer function. The OPD induced by the change of refractivity of air was 171 nm for the full range of humidity and the measurement was thus contained within a fringe. To make precision refractive index measurements it is necessary to compensate for any thermal drift in the system. This was accomplished using a low finesse Fabry-Perot interferometer placed in a temperature controlled environment that was used as a reference cavity. The Fabry-Perot interferometer was addressed via one of the ports of the power distributor. The second interferometer, the remote Michelson interferometric probe described above was

used for the measurement of the refractive index of air. These two signals were then compared using a lock-in amplifier eliminating any influence of the processing interferometer. Each arm of the Michelson interferometric probe had a physical length of 9.75 cm. One arm was exposed to the humid air and the second arm consisting of a sealed tube with windows at each end containing air at a fixed pressure and humidity level served as a reference. The optical path length variation of the Michelson interferometer was obtained by comparing the relative phase ϕ_{FPI} and ϕ_{MI} where ϕ_{FPI} is $\phi_P+\phi_{REF}$ and ϕ_{MI} is $\phi_P+\Delta\phi_{MI}$ where ϕ_P corresponds to the processing interferometer. Hence the thermal drift associated with this processing interferometer was eliminated. The design of the Michelson interferometer was simple and very resistant against misalignments caused by environmental perturbations as both arms use a common mirror. In addition when both arms were filled with gas of the same refractive index the OPD was ≈ zero making it ideal for precision interferometry when the OPD changes were small as in the case here. When a change of humidity occurred, only one arm was affected and the OPD changed. The dual tandem configuration, using the low coherence source with air cavity interferometric sensors ensured a measurement free from any polarisation effects on the fibre transceiver link caused by variations in temperature and strain. A change in humidity detected by the lock-in amplifier was converted to the corresponding OPD variation and recorded by the computer. Then using the temperature and pressure measurements simultaneously recorded with additional sensors, electronic in this case, it was possible to recover the relative humidity using Edlen's equation. As the partial pressure of vapour contained in equation (4-3) of section 4.1.1 is dependent on the temperature a nine degree interpolation was inserted into the Edlen's equation reducing the number of parameters to three. The relative humidity was then recovered using the electronically measured values of pressure, temperature and the optically determined value of the refractive index.

4.3.4 Results using this system

Figure 4.8 shows the experimental transfer function side lobe on which the system was locked to obtain the measurement. This lobe corresponds to the right lobe of figure 2.7 and was obtained by changing the optical path difference of the processing interferometer seen in figure 4.7.

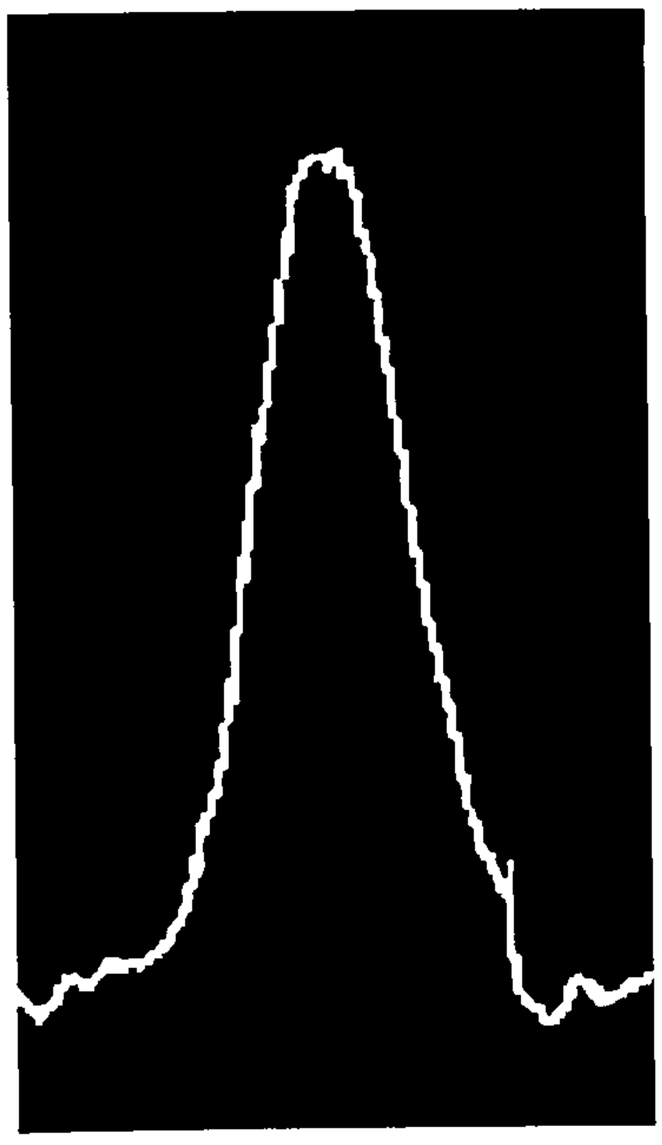

Figure 4.8 Experimental side lobe of the transfer function

The signal was then recorded via an oscilloscope. Figure 4.9 shows the relative humidity obtained experimentally with the system against the values measured with an electronic commercial device. Both curves agree within 5 %RH with an average difference of 1.6 %RH between the two curves and a standard deviation of 1 %RH. As can be seen from figure 4.9 and 4.10, variations in temperature during the experiment did not give rise to any correlated errors in the final relative humidity measurement calculated using Edlen's equations. This is due to the 0.01 °C accuracy with which the temperature measurements were made as shown in figure 4.10.

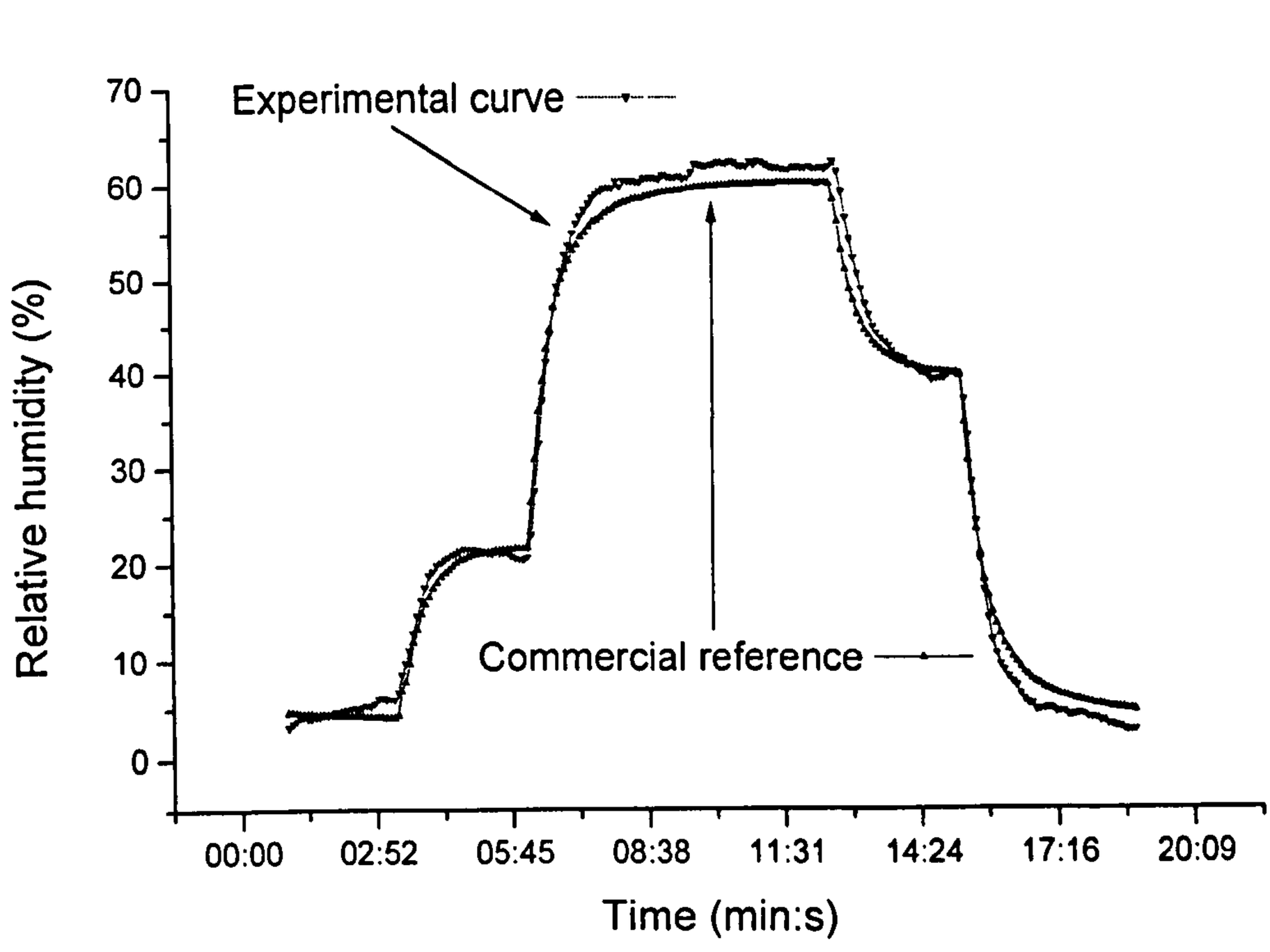

Figure 4.9 shows the experimental and commercial relative humidity response

Analysis of Edlen's equations show that the accuracy is critically dependent on both the accuracy of the temperature and pressure measurements. For example temperature measurements made with only a 0.1 °C accuracy will result in a 10 % error in the relative humidity measurement. Similar errors result from an uncertainty of 30 Pa in the pressure measurement. Optical pressure and temperature sensors with sufficient resolution for this application have already been developed [7]. The system shown in figure 4.6 was designed to allow the multiplexing of several fibre optic sensors. As demonstrated here these sensors can be designed using different types of interferometers, the only constraint being that their OPD's must be similar. It would therefore be possible to implement a fully integrated high accuracy humidity sensor system incorporating optical pressure and temperature sensors at the two unused ports of the optical power distributor. The optical power injected into the humidity sensor is equivalent to this case, i.e. the performance reported here for the sensor corresponds to that achievable with a field deployable system.

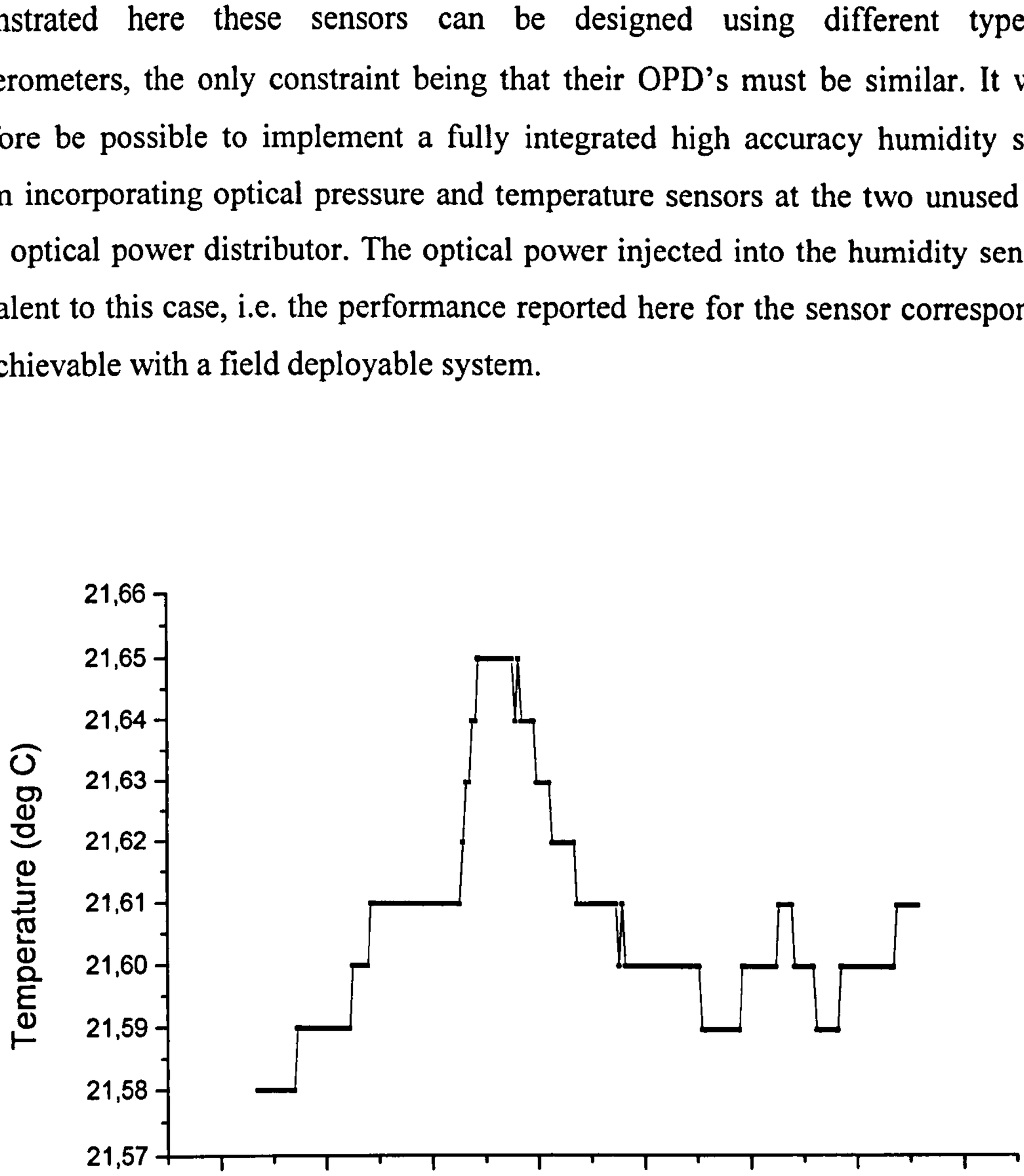

Figure 4.10 shows the temperature change during the experiment

4.4 References

[1] B. Edlen, Metrologia, 2, (1966), 71-80.

[2] K. P. Birch and M. J. Downs, Metrologia, 30, (1993), 155-162.

[3] K. P. Birch and M. J. Downs, Metrologia, 31, (1994), 315-316.

[4] J. C. Owen, Appl. Opt., 6, (1967), 51-59.

[5] Y. Rao, and D. A. Jackson, Meas. Sci. Technol., 7, (1996), 981-999.

[6] Y. Rao, D. J. Webb, and D. A. Jackson, Proc. SPIE 2070, (1993), 35.

[7] Y. Rao, D. A. Jackson, R. Jones, and C. Shannon, J. of lightwave technology, 12, (1994), 1685-1695.

5

Profilometry

5.1 Profilometry for sol-gel monitoring

5.2 References

5.1 Profilometry for sol-gel monitoring

5.1.1 Monitoring of sol-gel swelling using interferometry

The first task of this project was to identify the swelling of TMOS based sol-gel samples when submitted to humid air. The samples were produced by J. D. Wright and designed to be easily inserted into the system. The requirements were sol-gel films having a thickness over 10 μm to allow an easy measurement of its swelling when submitted to humidity and positioned on a glass substrate to permit easy handling. The optical system itself had to be reliable and allow an absolute measurement with the best possible accuracy. Finally the design of the system should allow frequent changing of the sample in order to test different samples. At this stage the response to humidity of the sol-gel samples was not well known and the aim of this first experiment was to obtain the maximum information on the behaviour of TMOS sol-gel when exposed to humidity.

5.1.2 Sample design

To obtain information on the sol-gel material, it was decided to observe simultaneously the physical swelling of the films and its refractive index change when submitted to humidity. This was possible by observing the optical path change induced by the modifications of the material in an interferometer. One part of the sample was therefore composed of a sol-gel layer covered by a deposited silver mirror, while the second was composed of a sol-gel layer over a deposited mirror. The fabrication process was to coat the glass substrate (a microscope cover slide) with silver, the sol-gel film was then deposited over the silver film by spin coating, one third of this film was removed by scraping and finally a thin silver film was deposited over half of the remaining material.

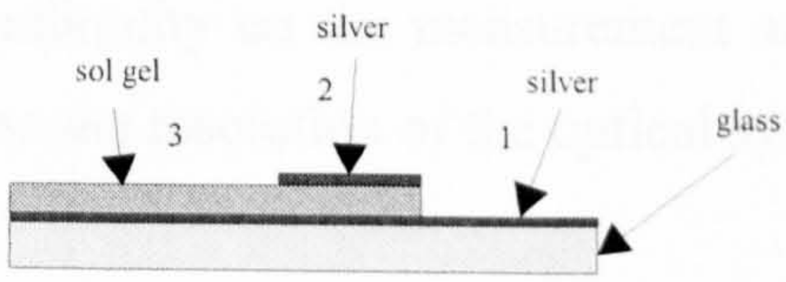

Figure 5.1 shows the structure of the sample

The samples thus offered three testing zones. As seen in figure 5.1 the first zone was only a reference since no material was tested. The second zone allowed the testing of the physical swelling of the sol-gel, while the third zone gave access to the refractive index change of the material when submitted to humidity. Using these samples the scan was planned successively over the three zones.

5.1.3 Description of bulk profilometer

When designing an optical measurement system great care should be taken regarding the type of measurement to be made. If using a Michelson interferometer with a laser, the distance between two fringes is half of the wavelength, this is 316.4 nm in the case of an Helium Neon source. Therefore to eliminate any ambiguity of fringe counting, the optical path change to be measured in the interferometric system should be less than half of the wavelength. In the case of a scanning procedure [1,2] of the previously described sample the optical change includes the step due to the thickness of the film but also its swelling or modification of refractive index when tested. In our case the films were planned to be over 10 μm, i.e. the step between surface 1 and 2 exceeded 10 μm, hence a simple laser illuminated interferometer could not be used, and a system based on low coherence interferometry was developed. When using a Michelson interferometer with a white light source, fringes can only be observed if both arms of the interferometer have the same optical path length. This means that, if one arm of the interferometer is decreased whilst observing interferometric signals, the second arm should be reduced by a similar amount within the coherence length of the source to recover the interferometric pattern. Therefore, if any change occurs in zone two or three of the sample described in section 5.1.2 a compensation in the second arm of the interferometer would be necessary to recover interferometric signals. The displacement of the second arm would therefore indicate any modification of the sample. By using this principle there is no ambiguity on the measurement and any sample can be used provided its size is more than the resolution of the optical system.

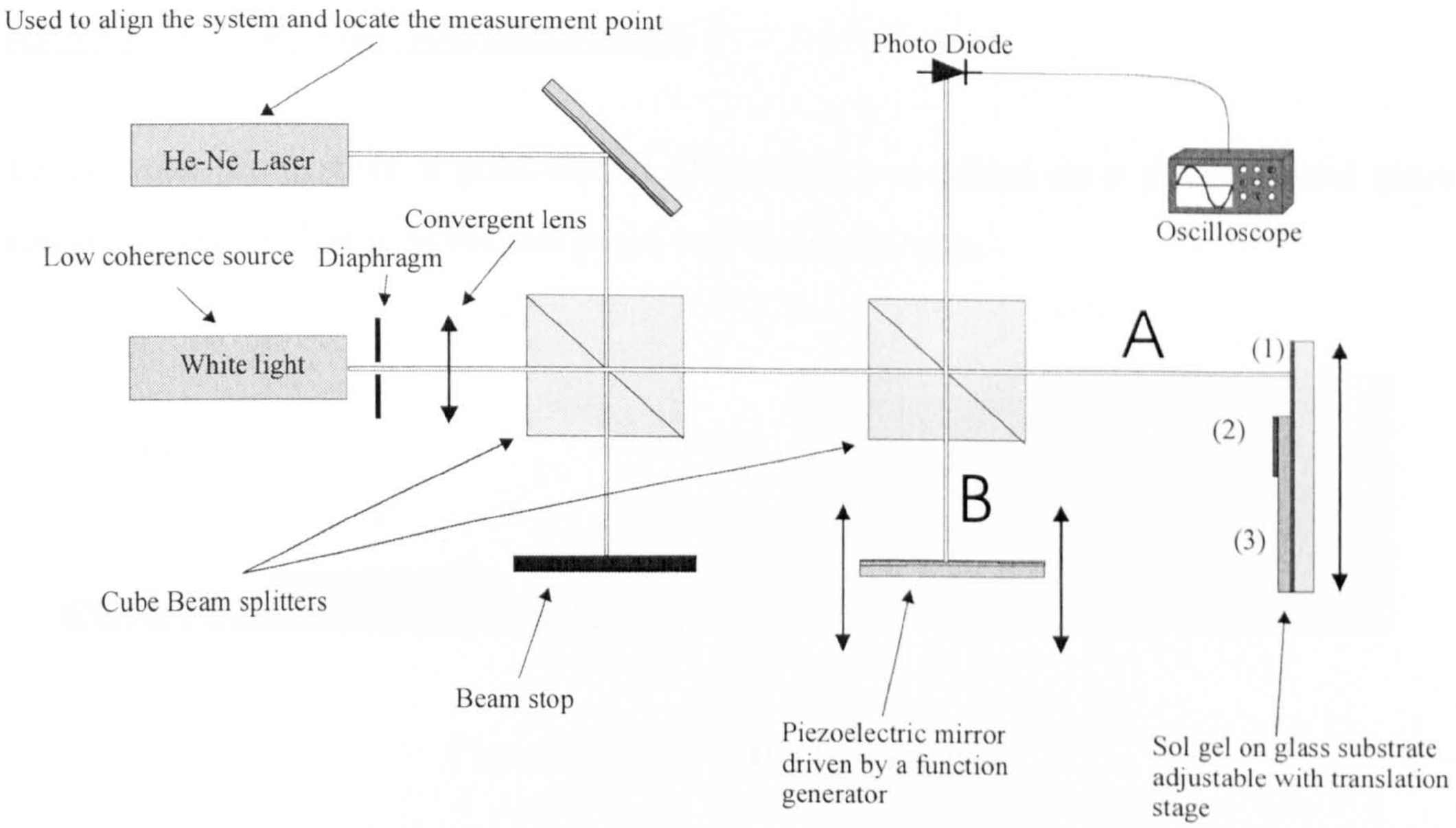

Figure 5.2 shows the bulk interferometric profilemeter

The white light source was a common white bulb and the laser a standard 632.8 nm He-Ne. The laser was used not only for the alignment of the system but also to identify the measurement point at the start of the experiment. The process was first to align the sample using the laser so that to obtain the best interferometric signal. Then the laser beam was blocked and the interferometric signal generated with the white light source was obtained by fine tuning of the translation stage moving the mirror on arm B. As the optical paths of arm A and B of figure 5.2 had to be exactly the same within the coherence length of the source, the white light interferogram could be difficult to obtain. The experiment consisted of reading the position of the translation stage using a micrometric adjuster when the maximum of the white light interferogram was obtained. Then the sample was displaced of a few microns (arm A). Generally the interferometric signal was lost and recovered by moving the mirror of arm B. The mirror of arm B therefore compensated any thickness change while scanning the sample and the values of its position gave the profile of the deposited material. Using this technique, several profiles at different humidities would therefore indicate the optical and physical response of the material.

5.1.4 Evaluation of the scanning system

To evaluate the system, a gold coated glass slide was glued on a silver coated glass substrate. The thickness of the test piece was about 500 μm.

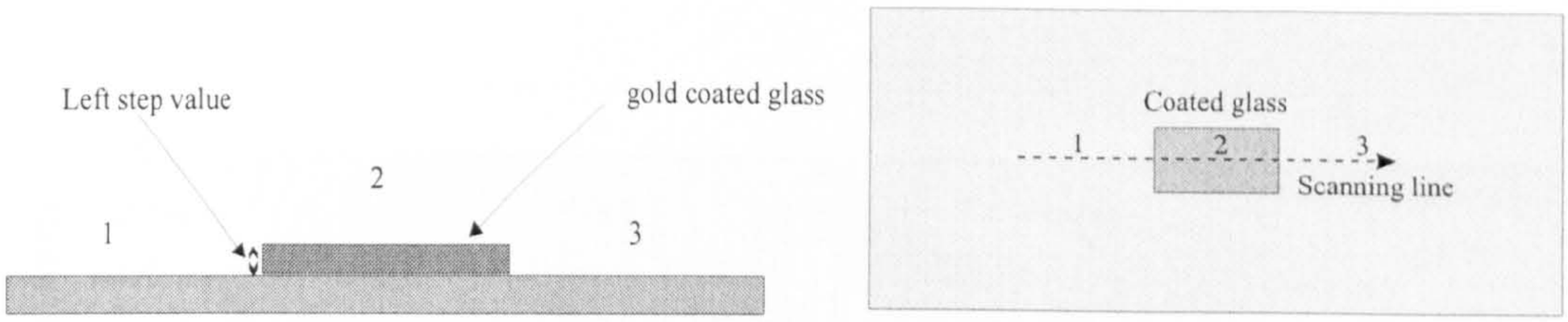

Figure 5.3 shows the test sample

The scan was performed three times on this sample. The results showed that the average left step value was 540 μm while the average right step was 561 μm. The obtained standard deviation on these respective values was found to be 3.43 μm and 2.85μm which leads to the averaged value $\overline{\sigma}_{right,left} = 3.14\mu m$. The resulting scanning was not obtained directly. In fact due to misalignments of the optical system the obtained profile was overall tilted as seen in figure 5.4.

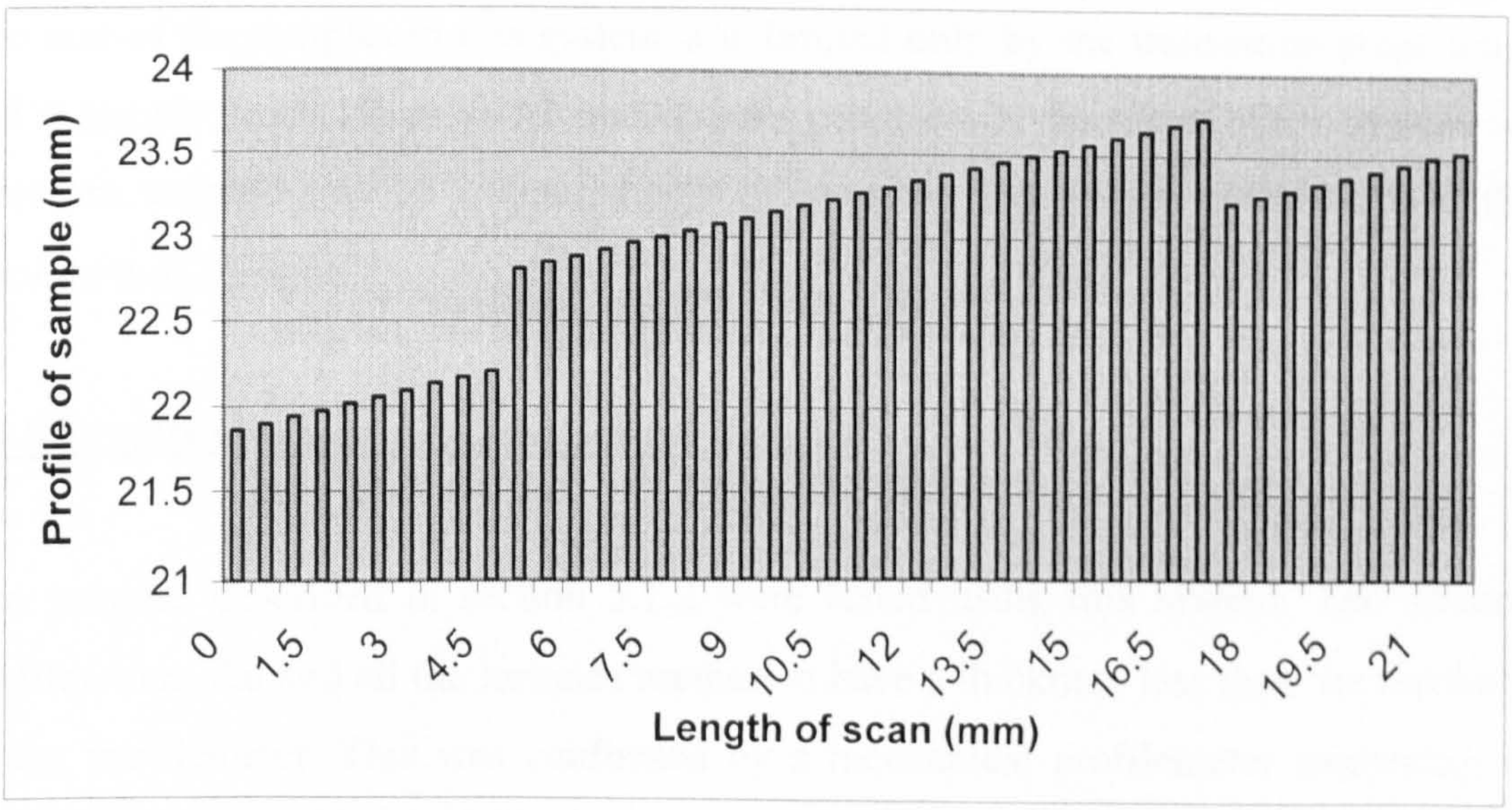

Figure 5.4 shows the obtained profile of the tested sample

This overall tilt on the profile was easily removed by evaluating the slope of the deviation on the 10 first reference points and subtracting the effect on the rest of the chart. Figure 5.5 shows the corrected profile of the same measurement. All samples were subjected to such misalignments but provided a reference area was present (such as the zone 1 in Figure 5.1 section 5.12) the measurement was obtained.

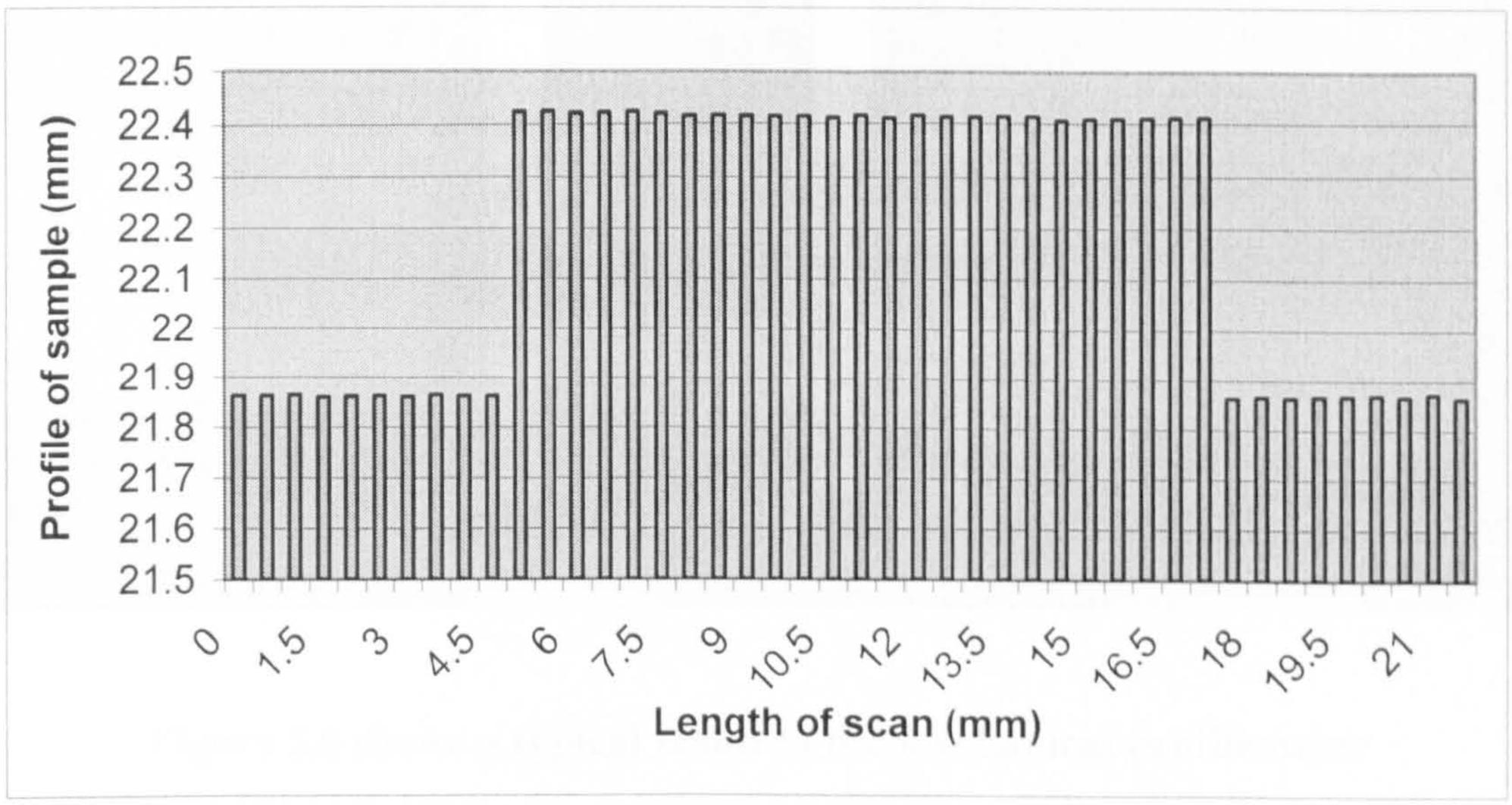

Figure 5.5 shows the corrected profile of the previously tested sample

The size of the samples in this system was limited only by the translation stage length and a sample from 10μm to 10 mm in size could easily be tested. This system was therefore suitable for the measurements of physical and optical thicknesses with a resolution of 3.14 μm.

5.1.5 Results obtained using the sol-gel samples

The samples described in section 5.1.2 were tested using this system. The obtained profiles were flat and all the samples seemed to have a thickness less than the resolution of the profilemeter. This was confirmed by a mechanical profilemeter measuring the physical thickness by contact using a metallic pin. The thicknesses of the provided samples were in fact 120 nm as seen in figure 5.6.

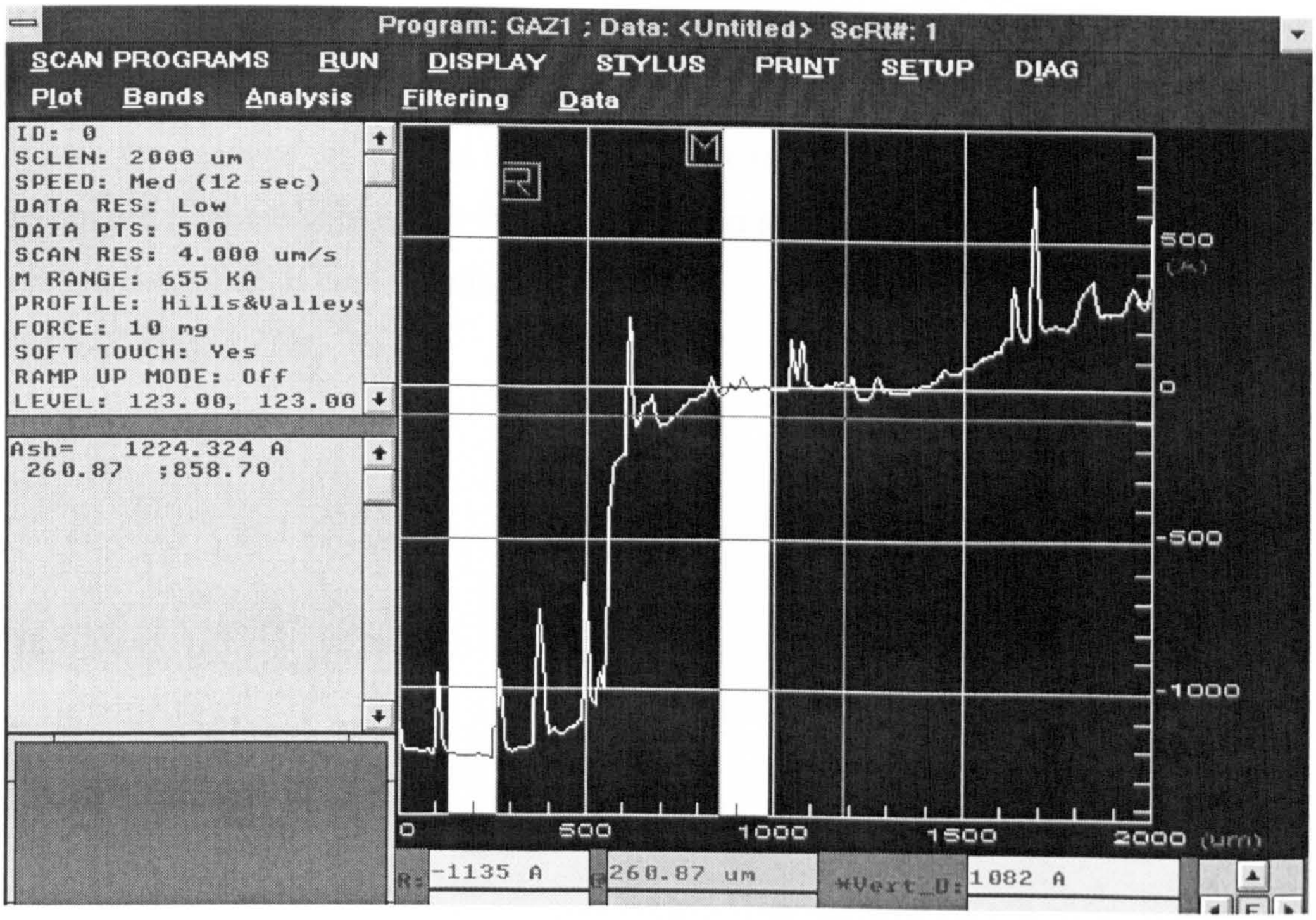

Figure 5.6 shows a typical result of the mechanical profilemeter

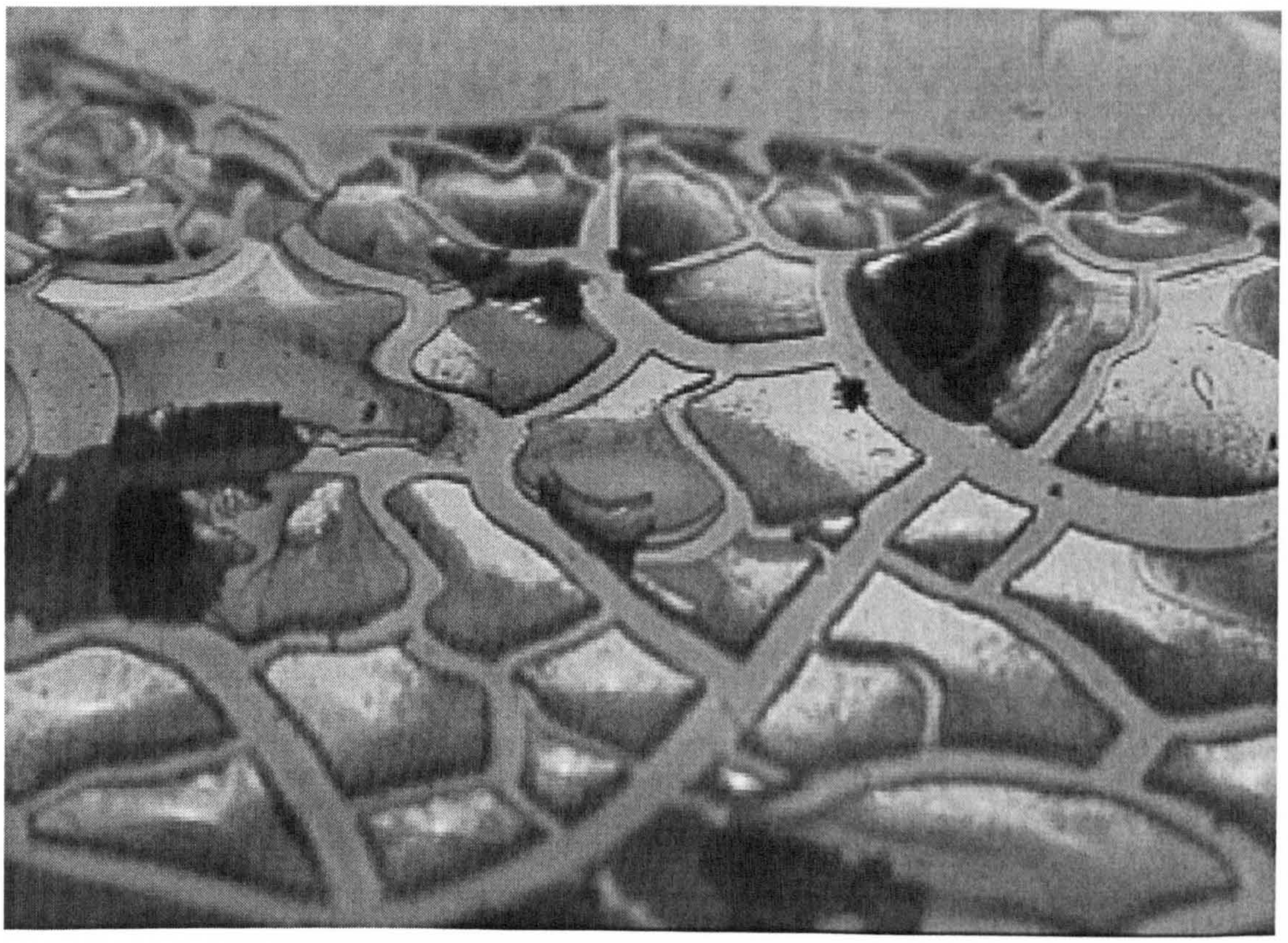

Figure 5.7 shows a cracked sol-gel film

These thin films were far below the resolution of the system but thicker sol-gel films using the spin coating technique were not possible to make due to cracking. Figure 5.7 shows the result of an attempt to produce thick sol-gel films by using the spin coating technique. The sol-gels where therefore made in a different manner and tested with the system described in the following chapter.

5.2 References

[1] P. Sandoz and G. Tribillon, J. of Mod. Optics, 40, (1993) 1691-1700.

[2] P. De Groot and L. Deck, J. of Mod. Optics, 42, (1995) 389-401.

6

Optical humidity sensor based on sol-gels and aerogels

6.1 Dual tandem interferometry for accurate optical path difference variations

6.1.1 Requirement for testing various materials

6.1.2 The design of the system

6.1.3 The Fabry-Perot probe design

6.1.4 Sample mounting

6.1.5 Results using this interferometric system

6.2 Sol-gels

6.2.1 Requirements

6.2.2 Bulk sol-gels

6.2.3 Sol-gel films

6.2.4 Conclusions on the produced sol-gel films

6.2.5 Results using sol-gels

6.3 Aerogels

6.3.1 Sol-gel films for super-critical drying

6.3.2 Super critical drying

6.3.3 Preliminary super critical drying

6.3.4 First experiment

6.3.5 Second experiment

6.1 Dual tandem interferometry for accurate optical path difference variations

6.1.1 Requirements for testing various materials

One part of the project was to find suitable materials for the use as a humidity sensor. Many materials swell with a change in humidity, however it is also possible that a change of refractive index also occur. Thus an optical system allowing the measurement of the film physical thickness and also its optical thickness variations was needed. The requirements of the system were the best accuracy as possible independently of the material type over a large range to cover all possible material thickness changes. In this case the measurement did not need to be absolute, since the aim was to characterise the material rather than making a sensor. Finally, as various samples were to be tested, the probe should allow to change the material films easily and rapidly.

6.1.2 The design of the system

To make precision measurements, it was decided to build an interferometric system. The probe containing the material had to be placed into a test chamber and had therefore to be small and easy to manipulate. This probe had also to have a low sensitivity to temperature to avoid any cross talk with humidity when testing. To allow these properties a dual tandem interferometric system was built. The system was based on a Michelson interferometer coupled with a Fabry-Perot cavity to allow accurate measurements by using low coherence interferometry [1-4]. To measure any change in its thickness, the film material contained in the probe was placed in a test chamber and the humidity levels were varied. The system shown in figure 6.2 is an all fibre dual Michelson, Fabry-Perot interferometer allowing a high accuracy in OPD (optical path difference) change measurements. The sensing interferometer is here localised in the Fabry-Perot cavity resulting in an environmental insensitive communication link as the cavity is air spaced and the samples not birefringent. The two interferometers interact by means of the communication link, which could be of any length. The technique makes use of the fact that when an interferometer is illuminated with a low coherence source, then interference can only be observed when the optical paths differences within the

interferometers are well balanced. The output of the interferometric system is a cosinusoidal function.

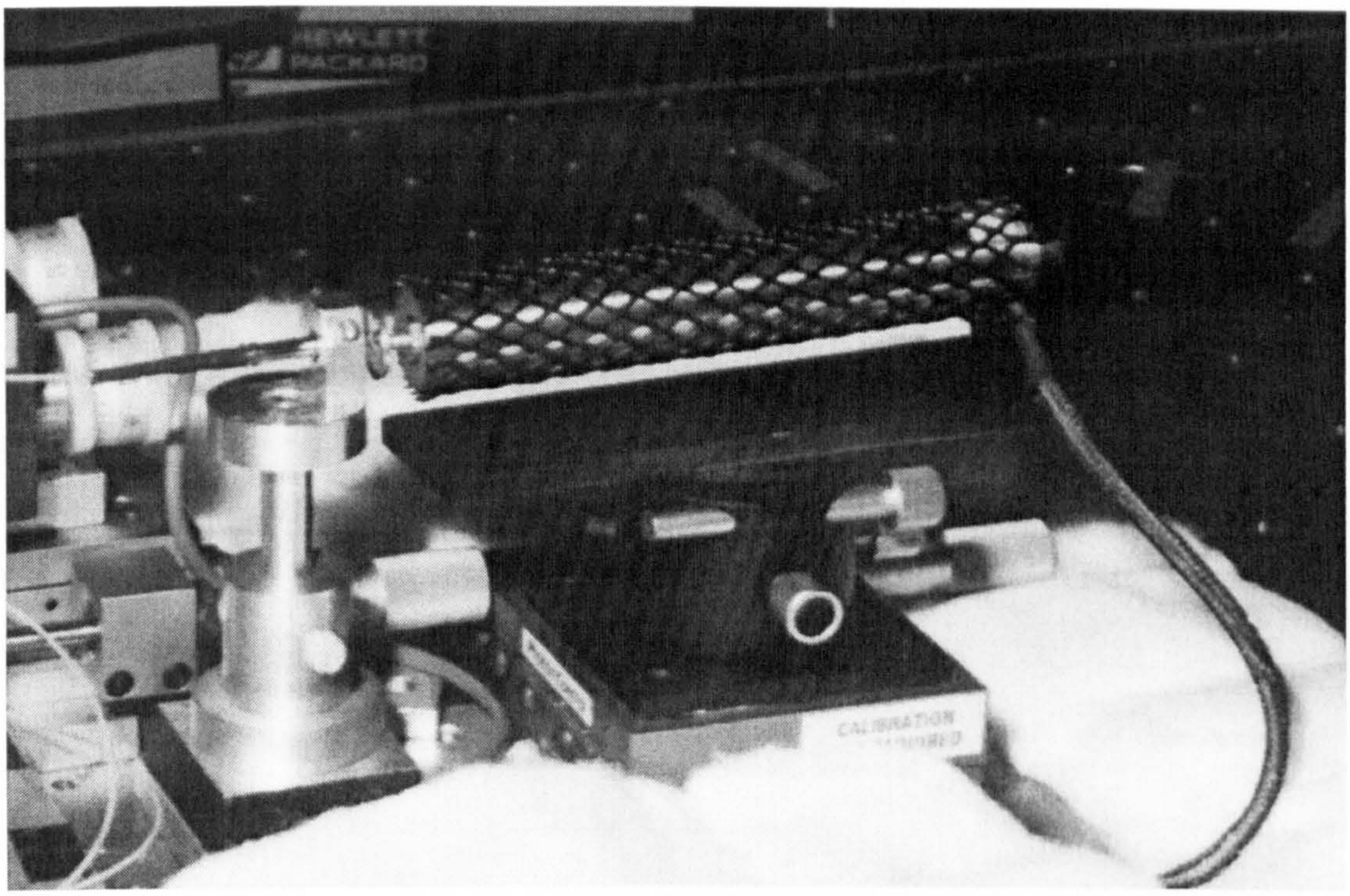

Figure 6.1 shows the PZT compensator in the system

The position of this transfer function will change if the OPD of the Fabry-Perot interferometer changes, resulting in a fringe movement proportional to the displacement. When a change in OPD of the sensor occurs the lock-in analyser detects it by comparing the output from the photodetector with the reference, which is usually, the filtered fundamental of the signal modulating the interferometer. This signal is then analysed by a Labview program that directly drives the PZT compensator. The technique is to program the computer to move this PZT compensator so that any change in the transfer function is cancelled thus keeping the system locked to the original point in the transfer function. The original point was chosen to be the maximum of the transfer function. If sample swelling happened to be faster than the compensation system, the computer would immediately indicate the change of locking point. This is possible as the computer records the phase difference measured between the transfer function and the reference that would increase up to 180° and suddenly drop down to -180° indicating that the locking point has moved of one fringe. Also the amplitude of

the transfer function signal would be less. Practically no sample was found to be fast enough to overcome the compensation system. This technique has the advantage of keeping the interferometer within coherence with a good visibility of the fringes compared to fringe counting techniques, which might result in a significant loss of visibility or even a total loss of the signal if the OPD becomes larger than the coherence length. In this compensating system the accuracy of the PZT is critical as it is the basis of the measurement. The best accuracy (5 nm) was obtained using a Queensgate PZT actuator (as seen in figure 6.1) driven digitally using a computer. This system was used extensively to test various materials by changing the Invar back plate of the Fabry-Perot cavity holding the sample. Typically the tested film was held on the back plate using silicon-gel glue known for its hydrophobicity and total lack of response to humidity, then a small mirror was placed over it to monitor its swelling. The humidity levels were then changed and the reaction of the film recorded.

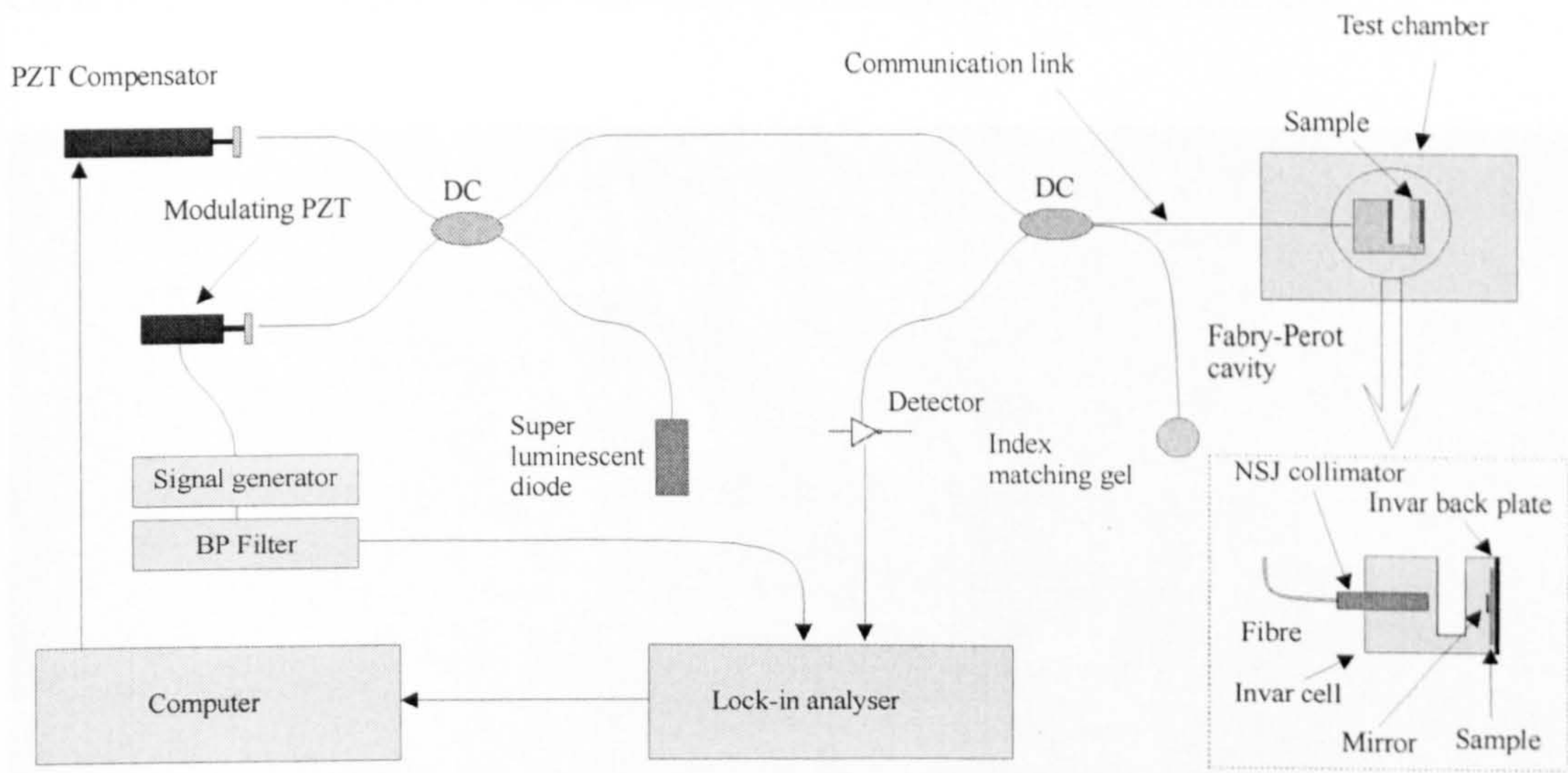

Figure 6.2 shows the experimental setup of the dual tandem interferometer

6.1.3 The Fabry-Perot probe design

The design of the Fabry-Perot probe was critical, as the probe was destined for use in an industrial environment. It had to be robust, small and very resistant to misalignments due to mechanical stress, shocks and thermal variations. The probe was composed of a collimator (from NSJ) and an Invar cavity in which the collimator was fitted and maintained by a screw. The cavity itself was composed of two parts, the main body to which the collimator was attached and an interchangeable back plate on which the

samples were mounted. The optical cavity was formed between the end face of the collimator and a mirror placed over (or under) the sample. To ensure good fringe visibility the face of the collimator was coated with a reflective aluminium coating of 38-40 %. This coating was deposited by a cold evaporation process to avoid any damage on the polymer grin lens composing the collimator. The mirror placed on the sample was a small part of a cover slide coated with gold. In order to observe interferometric signals the two mirrors must be precisely and stabily aligned. The back plate was screwed at the end of the Invar body of the Fabry-Perot sensor and the fine alignment was obtained in two ways depending on the experiment. When the aim of the system set up was only for characterisation of a material, the Fabry-Perot probe did not need to be as robust as for an industrial application. In this case the alignment was made by tightening the two screws of a bracket as seen in figure 6.3, that was fitted on the cavity. The effect of the first screw was to create a tension on the collimator while the second bent the back plate, both inducing a small change in the alignment.

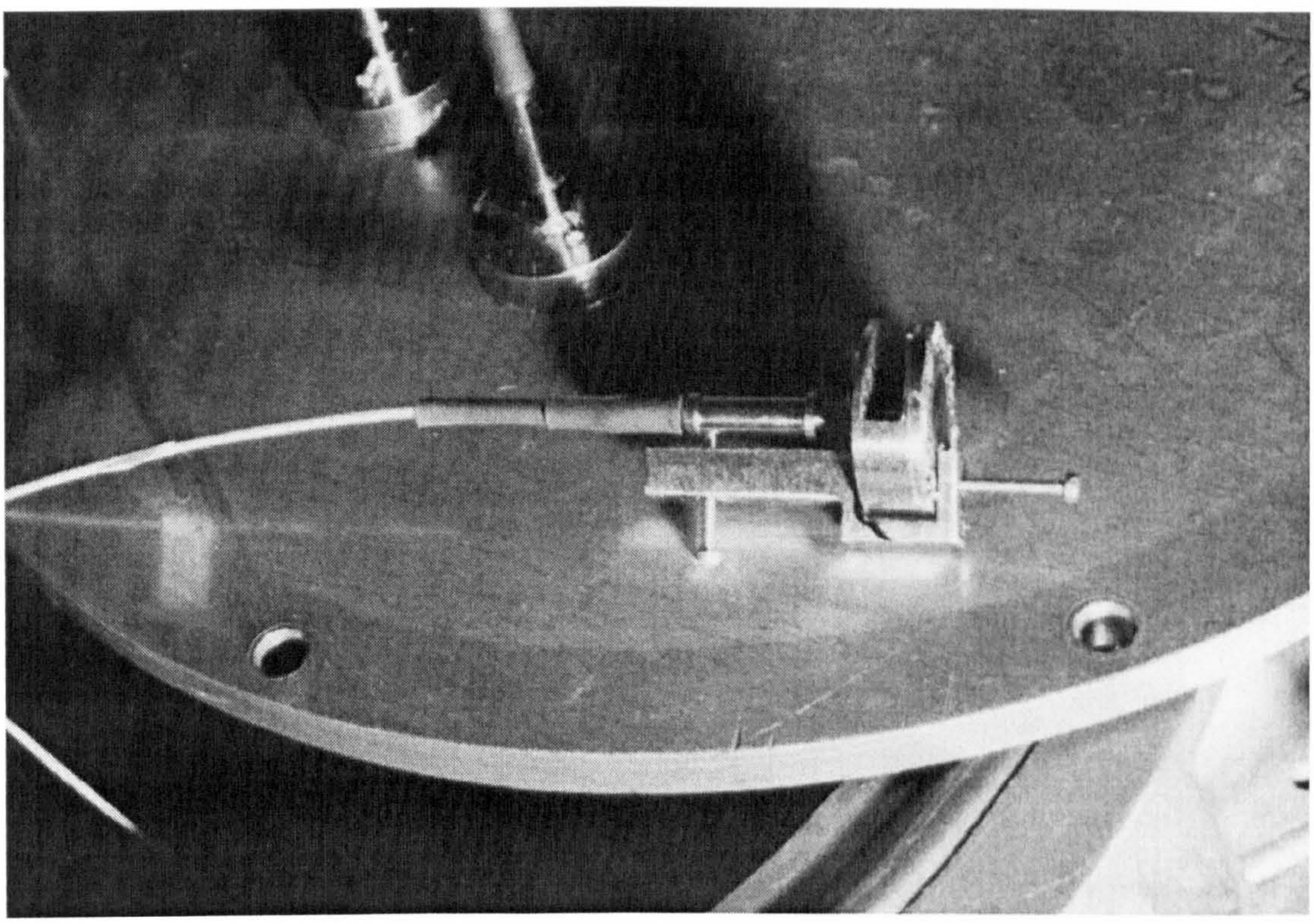

Figure 6.3 shows a Fabry-Perot cavity using the bracket alignment system

However when the purpose of the experiment was to demonstrate a prototype suitable for use in industry, a different mounting technique was used. In this case the sensor had

to be perfectly resistant to any misalignments. To allow this, the back plate was first aligned with the collimator using a three dimensional precision alignment plate and was then glued to the Invar body when the interferometric signal was observed. Several glues such as cyanoacrylate or epoxy were tested. The best results were obtained using Araldite despite its tendency to slightly change the alignment while drying. Despite this small effect very good and robust alignments were obtained using this technique.

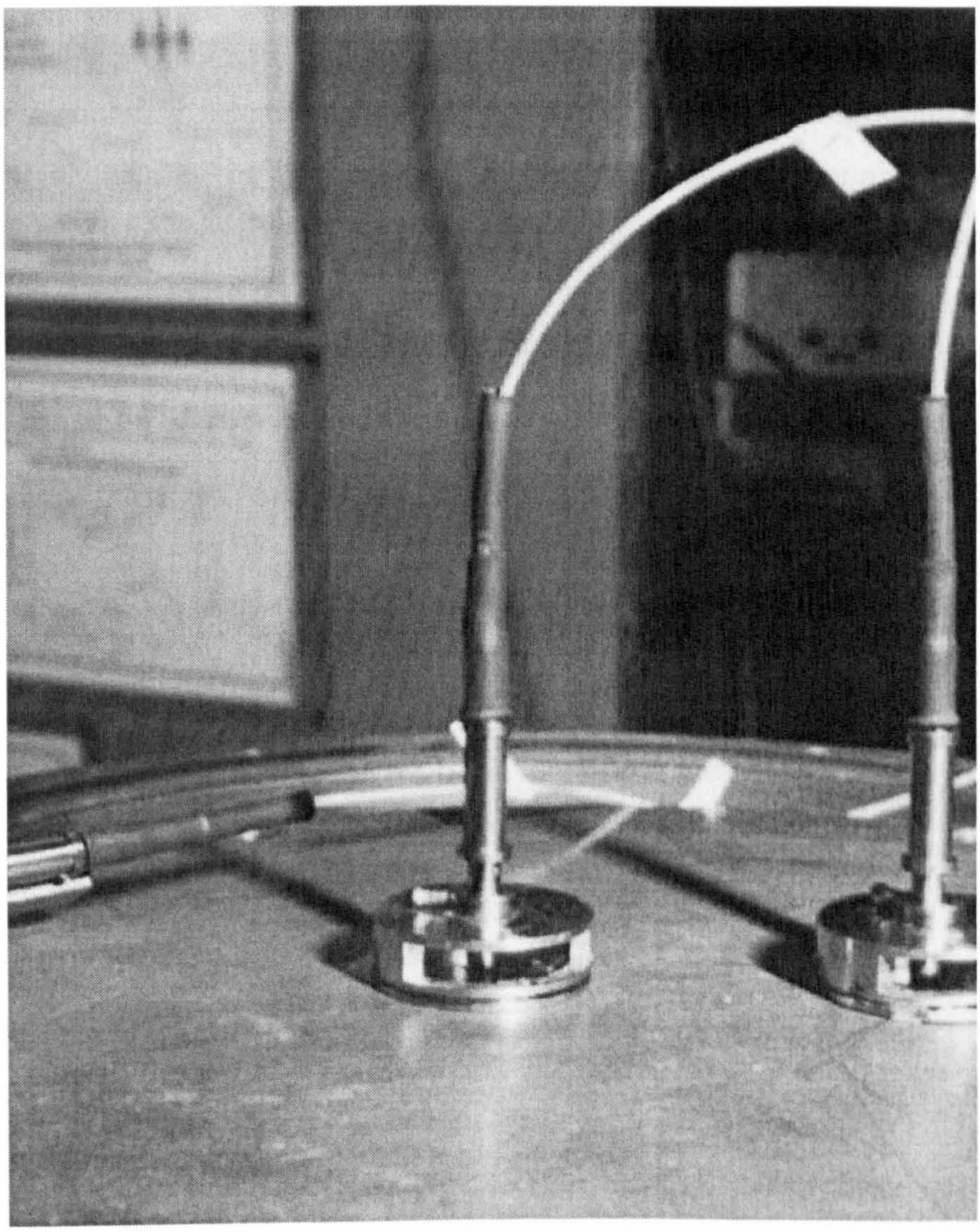

Figure 6.4 shows a Fabry-Perot cavity with a glued back plate

6.1.4 Sample mounting

The mounting of the sample is a critical part of the probe. The samples are usually films that are attached to the Invar back plate to be tested in the interferometric system. It is

important that the sample is fixed to the plate in a permanent way to avoid any drift of the mounting with time. If this happened the response of the tested film would not be repeatable and the evaluation of the properties of the film would be in error. However if the sample is fixed on the back plate too strongly the response might be minimised or a breakage of the sample could happen when swelling with humidity. The ideal mounting would therefore hold the sample always in the same position while leaving it the complete freedom to swell or contract. This was possible by using silicone gel glue. This glue has the property of high elasticity leaving the material free to change its size and is also completely insensitive to humidity as it is totally hydrophobic. Finally the good temporal stability of this silicone gel ensured that the samples were always maintained in the same position. The way the glue was applied was also important. Gluing the sample directly on the plate wasn't the best solution since an excess of glue could reduce the surface contact of the sample with the surrounding atmosphere. The best results using this glue were obtained by using as little as possible.

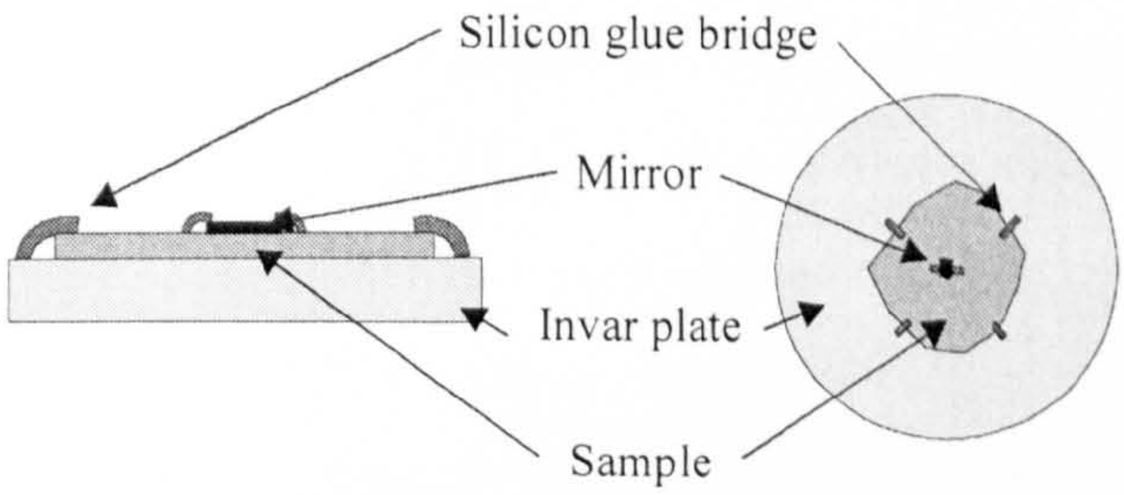

Figure 6.5 shows a typical mounting using silicon gel glue

The samples were therefore fixed to the back plate by small silicon gel glue bridges from the top of the sample to the plate but also from the top of the mirror eventually placed on the top of the sample as shown in figure 6.5.

6.1.5 Results using this interferometric system

The results of this system matched perfectly the need since the accuracy was 5 nm with a range of measurement of 70 μm. The resolution and dynamic range of the system were tested by inserting a piezoelectric actuator at the samples place and by varying the applied voltage. The performance of this system depends mainly on the piezoelectric compensator, better results could be achieved using the latest sub-nanometric resolution

piezoelectric actuators available from Queensgate. One drawback of this system is the sensitivity of the local processing interferometer to temperature. Despite a heavy shielding of this part of the interferometer changes in temperature in the laboratory induced a drift of the system (0-10 nm/min) which was seen in the final response of the tested material. This drift was not critical since only the base line was slightly shifted and the transitions due to the material response were not affected. Therefore many samples including sol-gels and aerogels, were evaluated using this system.

6.2 Sol-gels

6.2.1 Requirements

When using a material in a bulk Fabry-Perot interferometer, the best arrangement is to obtain a film, that can be held on the back reflecting mirror or on which a mirror can be fixed. The difficulty is then to obtain a film of the right size when compared to the interferometric systems performance. Typically the film should be over 10 μm thick and be of a reasonable size so that to be easily manipulated. The diameter of the film is also important since the best sensing film allows a large surface of contact with air. Several techniques used to create these films are described in the following section.

6.2.2 Bulk sol-gels

Three bulk samples were prepared in November 96. The aim was to create large pieces of sol-gel that could be sliced at the required thickness using a microtome. The samples were made to the basic recipe described in the introduction with the adjunction of DMF (dimethylformamide) used as a drying control chemical agent [5]. The two first samples were of 15.5 ml and 100 ml of initial volume respectively. These solutions were poured into bottles and sealed with the supplied plastic lids. As the lids were black, a plastic film was placed between the bottle and the lid, to avoid any contamination due to a potential chemical reaction between the lids and the solutions solvents. The third sample, 120 ml, was made in a beaker and sealed with aluminium foil by using tape. Finally the three samples were left to gel and age in a fume cupboard. The gelation of these gels was seen within two weeks but as the samples were closed tight, the pore liquid could not be evacuated rapidly from the gel. Based on known fragility of the gels, the samples were left sealed. Due to leaks, the liquid of the three samples finally evaporated after two years and clear bulk sol-gel pieces were obtained as seen in figure 6.6. However at the end of the first year the samples were still opaque. The sample in the beaker was dried and removed uncracked, but the smaller bottled sample was partially broken on the surface but uncracked. These three samples were obtained uncracked because of the very slow evaporation process. This resulted in an extremely slow manufacture delay totally incompatible with mass or industrial production.

Furthermore the bulk samples were so brittle that any attempt to obtain a slice of these samples resulted in unusable small fragments. This route was clearly inadequate and more work was accomplished on films.

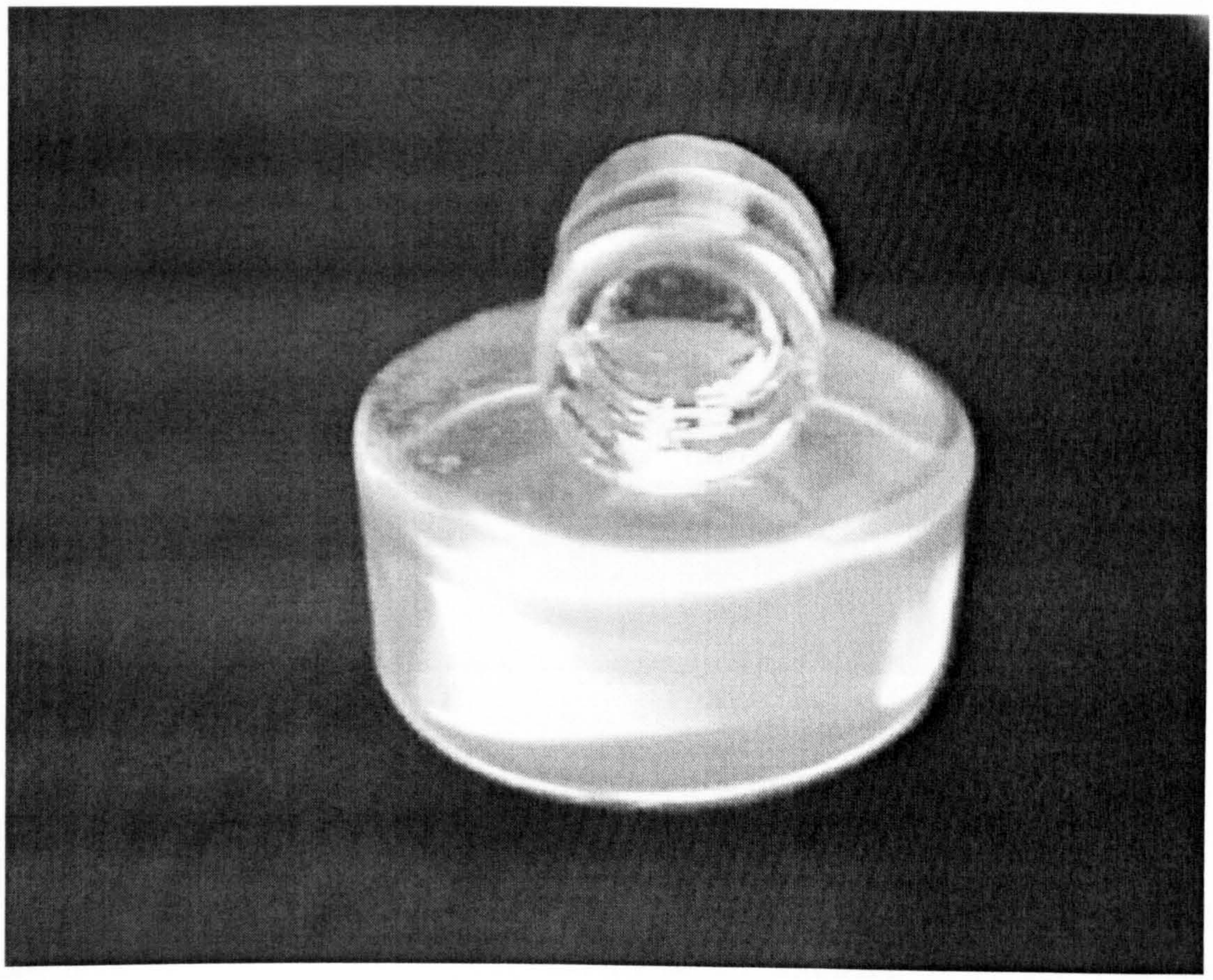

Figure 6.6 shows two produced bulk sol-gel blocks

6.2.3 Sol-gel films

The first set of thin films were obtained using 6 ml of solution. The solution was poured into a petri dish and sealed using aluminium foil and tape, to avoid the solvent escaping. The purpose of the aluminium foil is to confine the solution so that a saturated atmosphere of solvents, corresponding to the pore liquid, remains even after gelation. At this stage the obtained gel does not dry and no stress is applied on its structure. After two weeks when the film had built up sufficient strength, the aluminium foil was pierced with several holes to allow the evaporation of the gaseous solvents, leading to the drying of the gel [6]. The holes in the film were made using a syringe needle, and were as small as possible to ensure extremely slow drying.

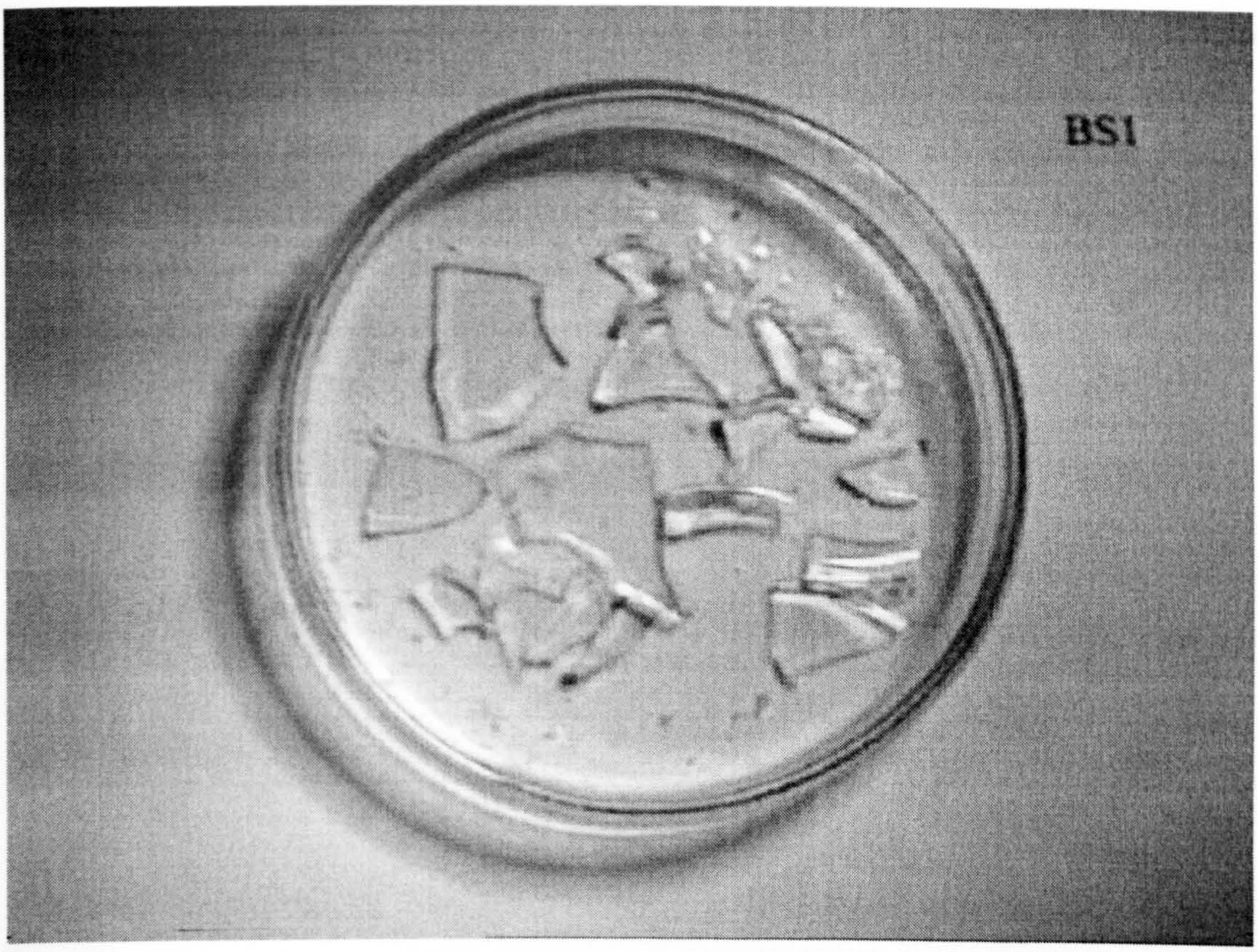

Figure 6.7 shows a sample of the first set of sol-gels

One possible reason for the cracking of the gel, other than the stress due to the drying, is the bonding of the gel to the petri dish during the shrinking of the gel. This can be avoided by treating the petri dish with dichlorodimethylsilane as it reacts with the -OH groups and bonds a silicon to the petri dish surface. The -OH groups are then no longer available for bonding with the sol-gel and any stress of this type is reduced. Despite all precautions the gels broke in small pieces of 2 to 10 mm with a thickness of about a millimetre. The samples obtained using this method and solution quantity, were too thick and were not suitable for use as a sensor.

At the same time a different drying technique was used to produce a second set of samples. The same quantities of solution, using the same petri dishes treated with chlorodimethylsilane were used to produce two samples that were placed into a hermetically closed desiccator rather than covering them with a aluminium foil. Before the desiccator was closed, water and ethanol was added in same proportions. The samples were held over the solution and the desiccator was then placed in an oven at 60°C for two weeks. The purpose of the desiccator is the same than that of the

aluminium foil, that is to maintain a saturated atmosphere of the main solvents used in the recipe reducing any rapid and premature drying. Small evaporation outside the dessicator finally dried the gels slowly. The results using this technique were very similar and no advantages were obtained by its use. This drying technique was therefore abandoned.

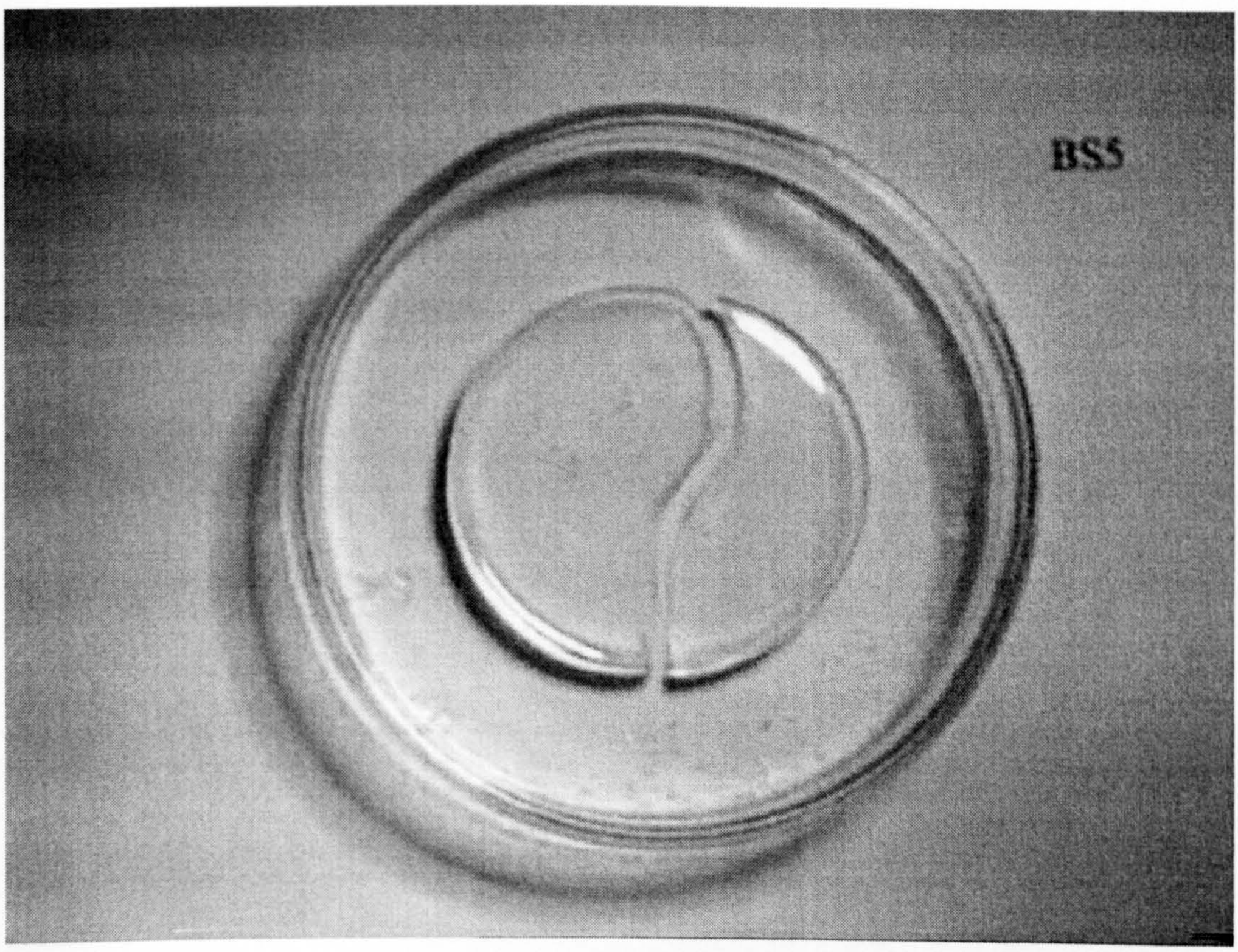

Figure 6.8 shows a sample of the third set of sol-gels

The third set of samples was based on the same recipe and drying technique as set one, except that a DCCA (Drying control chemical agent), DMF (dimethylformamide) was added to the solution. As seen in figure 6.8 the effect of the DCCA was clear since the produced samples were less cracked. Overall the pieces were larger than 2-15 mm and the best sample of the two was broken in two. The DCCA was successful and despite the main pieces being too thick, secondary samples were thin and large enough to allow testing.

The last set of samples were of smaller solution quantity, 1/2/2/2.7 ml respectively for the four samples. The solution remained the same but the petri dish was treated with

Decon 90. The use of a surfactant liberates the OH bonds on the surface of the glass encouraging the sol gel to stick to the glass surface. The aim was to try to give the gel a fixed base, avoiding any movement of the sol-gel lattice thus reducing any cracks due to stress displacements while drying. The samples did not stick to the surface and cracked in small pieces except the last sample of 2.7 ml that cracked in larger pieces but were still too thick.

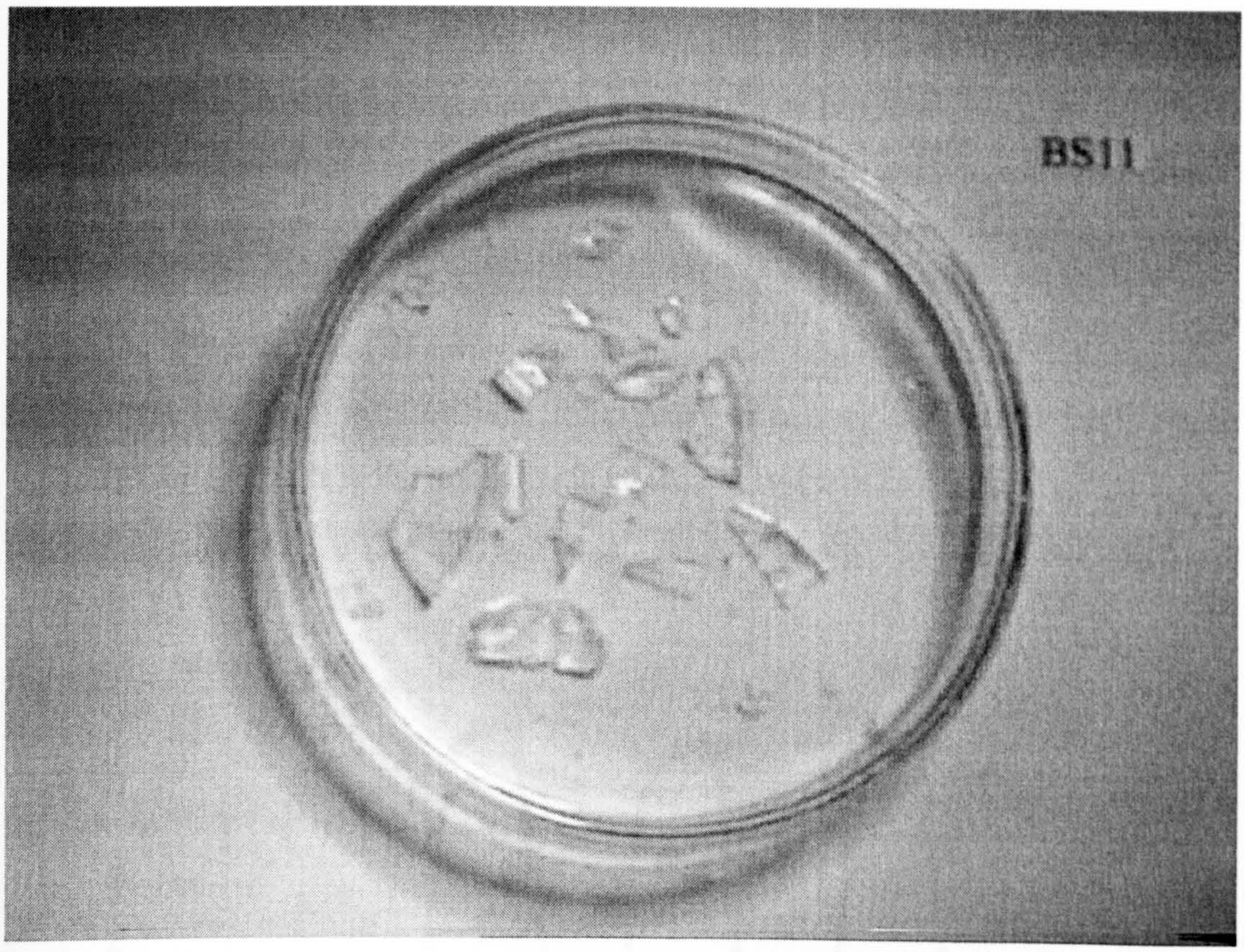

Figure 6.9 shows a sample of the last set of sol-gels

6.2.4 Conclusions on the produced sol-gel films

Using the first series of sol-gels, several parameters were tested. The volume of the solution, the use of DMF, the used of Decon 90 or dichlorodimethylsilane, and finally the drying technique using petri dishes or a desiccator. Concerning the volume of the solution, it is clear that, if using two inches in diameter petri dishes, the solution should be around 1ml considering the shrinkage of the gel. The use of dichlorodimethylsilane allowed the gel to 'slide' on the glass when shrinking and avoided further stress on the

sol-gel lattice. The benefit of Decon 90 in preventing cracking was doubtful. The drying technique using petri dishes gave better results than using a desiccator, but more important, it was clear that the drying procedure had far more influence on the gels than any of the other parameters. Ideally the drying technique would allow the removal of all the pore liquid without causing any stress to the sol-gel structure.

6.2.5 Results using sol-gels

As described in section 6.2.3, secondary pieces of 100 μm thick were recovered from a sol-gel made from 6 ml of initial solution. The sample was stuck to the Invar plate using silicon gel glue and a mirror was also attached to the sol-gel using this glue. This sample was placed in the optical system described in section 6.1 and the physical thickness of the gel was monitored as a function of humidity level. Unfortunately the sample was too small to allow any direct measurement of the optical thickness of the sol-gel by including it in the optical path of the Fabry-Perot cavity.

Figure 6.10 shows the reaction of a sol-gel film with humidity

As seen in figure 6.10, the response to humidity was clear and repeatable. The maximum deviation obtained using this gel was 900 nm. This corresponds to 0.9 % of

its physical thickness. This small expansion can be explained by a reduced amount of -OH bonds inside the sol-gel structure due to an incomplete drying and a large amount of pore liquid in the structure. This can lead to a possible ageing of the gel resulting in an increase of its strength due to cross-linking and reducing its swelling properties. However despite this small expansion of the gel the response was repeatable over the different humidity cycles shown in figure 6.11. The time response of this film was about 10 minutes when increasing the humidity and similar when drying. By comparing figure 6.10 to figure 6.11 we can see that the physical thickness of the sol-gel film was not modified by the temperature fluctuations during the experiment but only by the humidity variations. Finally an artefact appears at the beginning of the response to humidity. This might be due to a response to humidity in two modes. The first mode being a temporary contraction of the lattice with humidity while the second, of a greater order of magnitude, is an expansion of the gel due to the penetration of the water molecules into the sol-gel structure.

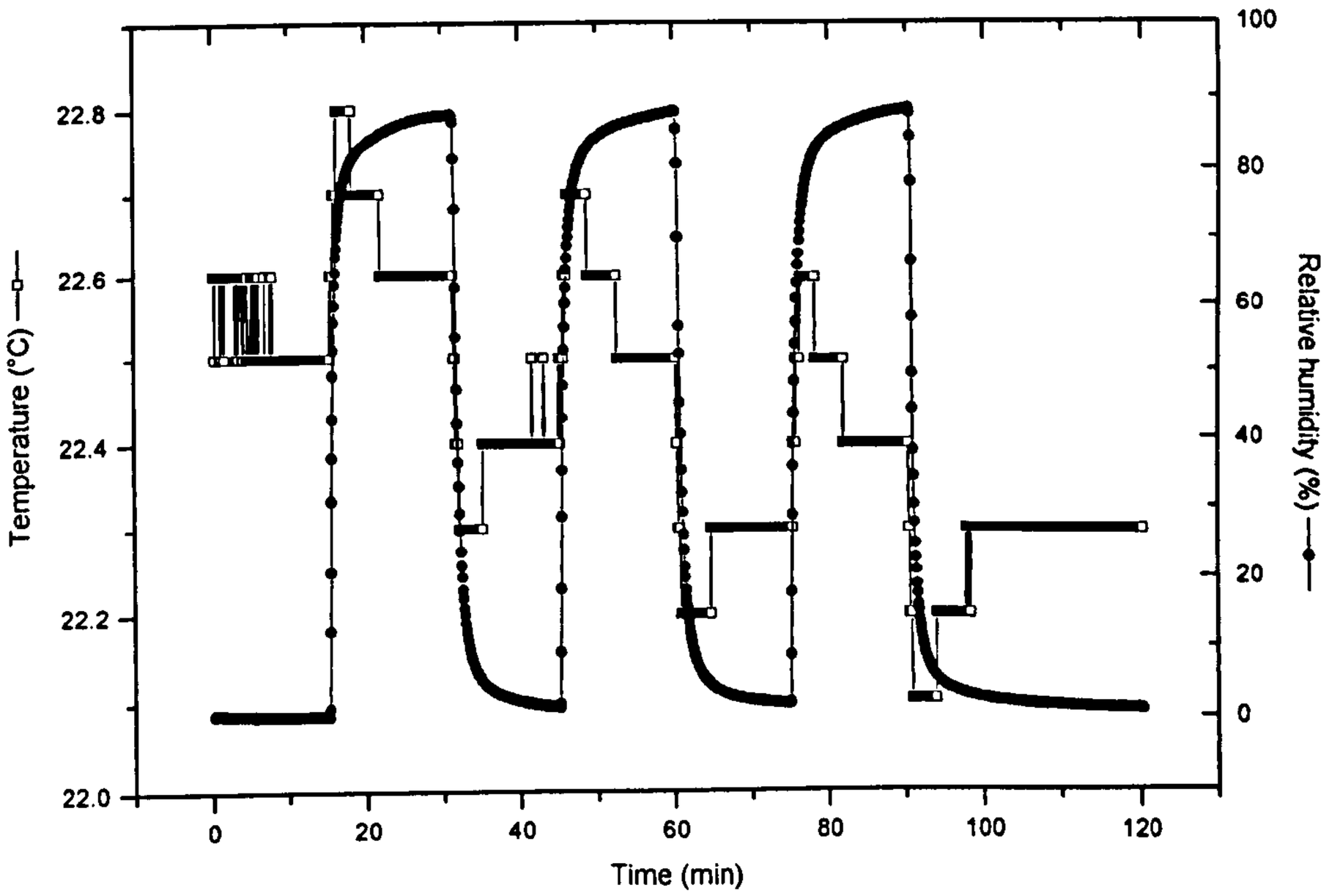

Figure 6.11 shows the humidity and temperature variations

Several tests were performed on this sample over several months. Despite the shape and the repeatability of the response to humidity remaining the same, a loss of amplitude

was observed. As seen in figure 6.12 the initial response of 900 nn was reduced to 200 nm after 240 days. This is explained by the cross linking in the pores and ageing mainly due to the presence of pore liquid in the structure.

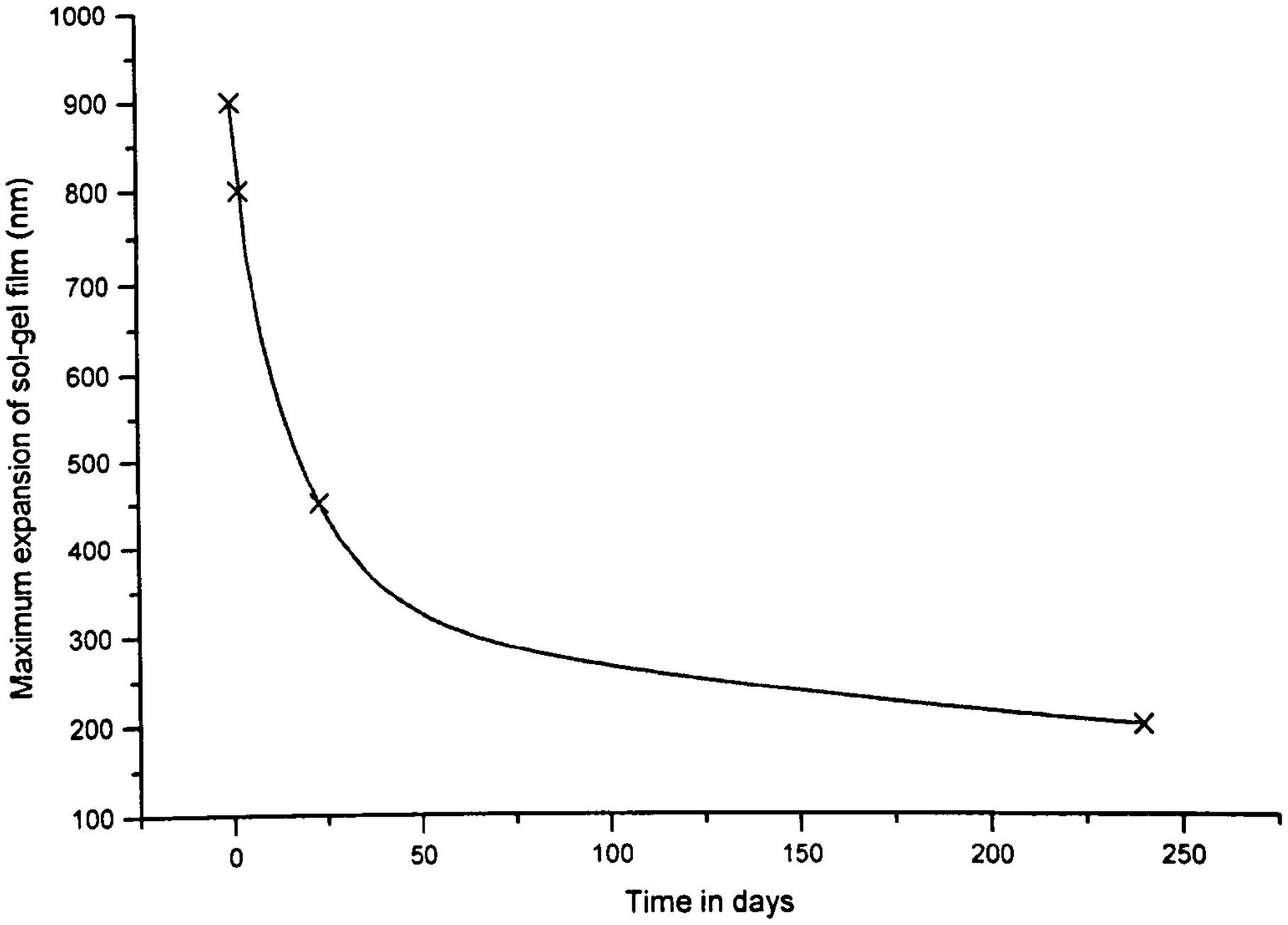

Figure 6.12 shows the decay of response of the sol-gel film over a long period

This film showed that optical sensing of humidity using sol-gel films was possible. The main problem of this film is its continuous ageing in time making the gel difficult to use as a sensor on a long term scale. To solve this problem, the super critical drying technique was the best solution, since the gel does not crack when drying, allowing large pieces to be produced. It also removes the pore liquid responsible for early ageing and low sensitivity after long periods.

6.3 Aerogels

6.3.1 Sol-gel films for super-critical drying

It was clear that at this stage the best way to obtain uncracked sol-gel samples was to super-critically dry them. The procedure was to produce sol-gel films by the same method used for the previous series of sol-gels without drying them. The super-critical technique would then be used to dry the samples into aerogels. A new series of samples was made but with volumes from 0.5 ml to 6 ml. The samples were sealed with tape using the provided glass cover of the petri dish rather than aluminium foil. All 21 samples were kept unopened prior to the supercritical drying procedure

6.3.2 Super critical drying

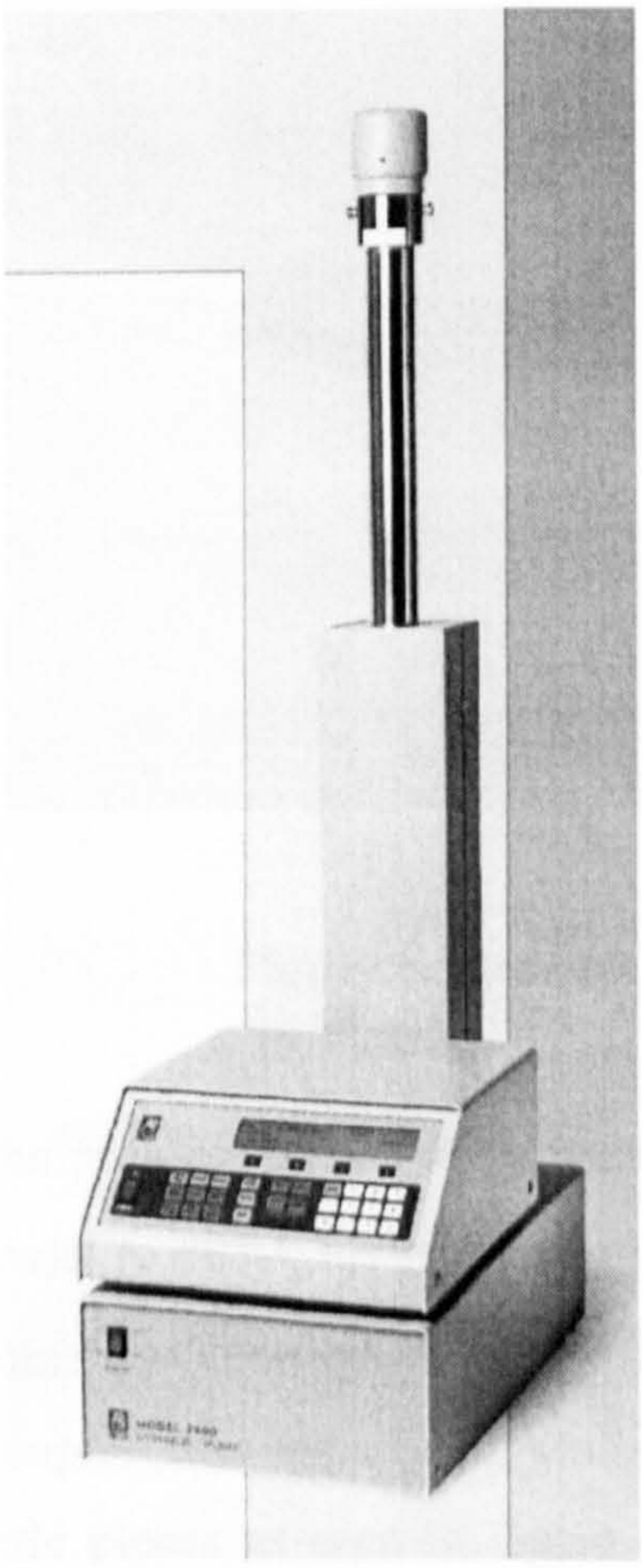

Figure 6.13 shows the syringe pump used during the experiment

The super critical drying [7-13] took place at Preston UK in the BNFL laboratories. The super critical drier was composed of an Isco syringe pump model 260 d (figure 6.13) capable of reaching pressures up to 51.7 MPa with a flow from 1.0 μl/min to 100 ml/min of liquid CO_2. The pump was connected to a supercritical fluid extraction vessel in which the samples were placed. This vessel was inserted into a programmable thermostatic enclosure to control the vessel's temperature during the experiment. The flowing CO_2 was compressed by the syringe pump, and passed through the vessel at a pre-set flow and was finally released in the fume cupboard. The controlled parameters were the type of gas used, the flow in the vessel, the pressure in the vessel, and finally its temperature. Overall five experiments were performed.

6.3.3 Preliminary super critical drying

The first sample to be tested was a 6 ml solution prepared as described in section 6.3.1. The film was of about 1 mm thick and was dried for testing purpose only. The aim of this experiment was to determine what protocol would be suitable in order to obtain uncracked aerogels from the prepared sol-gel samples. The experiment was performed by Dr. S. Port from BNFL.

Figure 6.14 shows the result of the first super critical drying

The protocol used was to insert the sol-gel piece into the vessel, then slowly heat the vessel to 40°C, the pressure was then increased over three hours until the supercritical point was reached. Then the fluid was drained and the vessel opened to collect the sample. This experiment was repeated twice and produced a gel cracked in multiple little pieces as seen in figure 6.14. The breakage of the gel can be explained by the increase of the meniscus curvature at the liquid-gas interface inside the pores of the sol-gel creating a great stress on its lattice, due to the increase of the evaporation rate of the

pore liquid when heating. It was therefore clear that to avoid this phenomenon, the sample had to be kept in conditions were no evaporation could occur before the super critical drying. This was achieved by first increasing the pressure favouring condensation rather than evaporation but also by constantly maintaining the sample in ethanol.

6.3.4 First experiment

A sample, resulting from the 2 ml recipe (TM2D) was chosen as large as possible and placed in the vessel containing 1.25 ml of ethanol corresponding to half of the inner vessels volume. When the sample was transferred from the petri dish to the vessel the sample was exposed to air for a short period and the onset of evaporation could be seen on the sample surface. It is therefore likely that air penetrated into the sol-gel structure. This justifies the importance of the pressure increase before the temperature raise in the protocol. It was therefore decided to increase the pressure up to 100 bars slowly within an hour and then to increase the temperature from ambient to 40°C also within an hour. The syringe pump was programmed to reach 70 bars rapidly and then to increase the pressure slowly to 100 bars. Once the super critical point was reached, the apparatus was left in this state for twenty minutes. This allowed the pore liquid to diffuse out of the sol-gel structure and thus to be diluted in the super critical CO_2. The second phase was also a twenty minute period during which a flow of 0.7 ml/min was applied. This had the effect of draining out of the vessel all the pore liquid by washing the sample with super critical CO_2. Finally the third step was a 20 min diffusion process similar to step one. The pressure was then released during one hour while keeping the temperature to 40 °C. The vessel was finally opened and the sample collected. This experiment was a success since the recovered aerogel was uncracked and had a translucent bluish tint due to the scattering of the light in the empty pores of the gel.

6.3.5 Second experiment

The second super critical drying was done using three pieces of the same sol-gel as in the previous experiment. The protocol was typically the same except that the heating period was reduced to 25 minutes rather than 1 hour. The result was also a success and

three aerogels were obtained despite several technical problems during the experiment. A pressure drop, that was recovered within seconds, down to 45 bars when close to 100 bars occurred, due to a syringe pump misfunction. This irregularity in the protocol showed that the sample was not prone to stress during the pressure rise period.

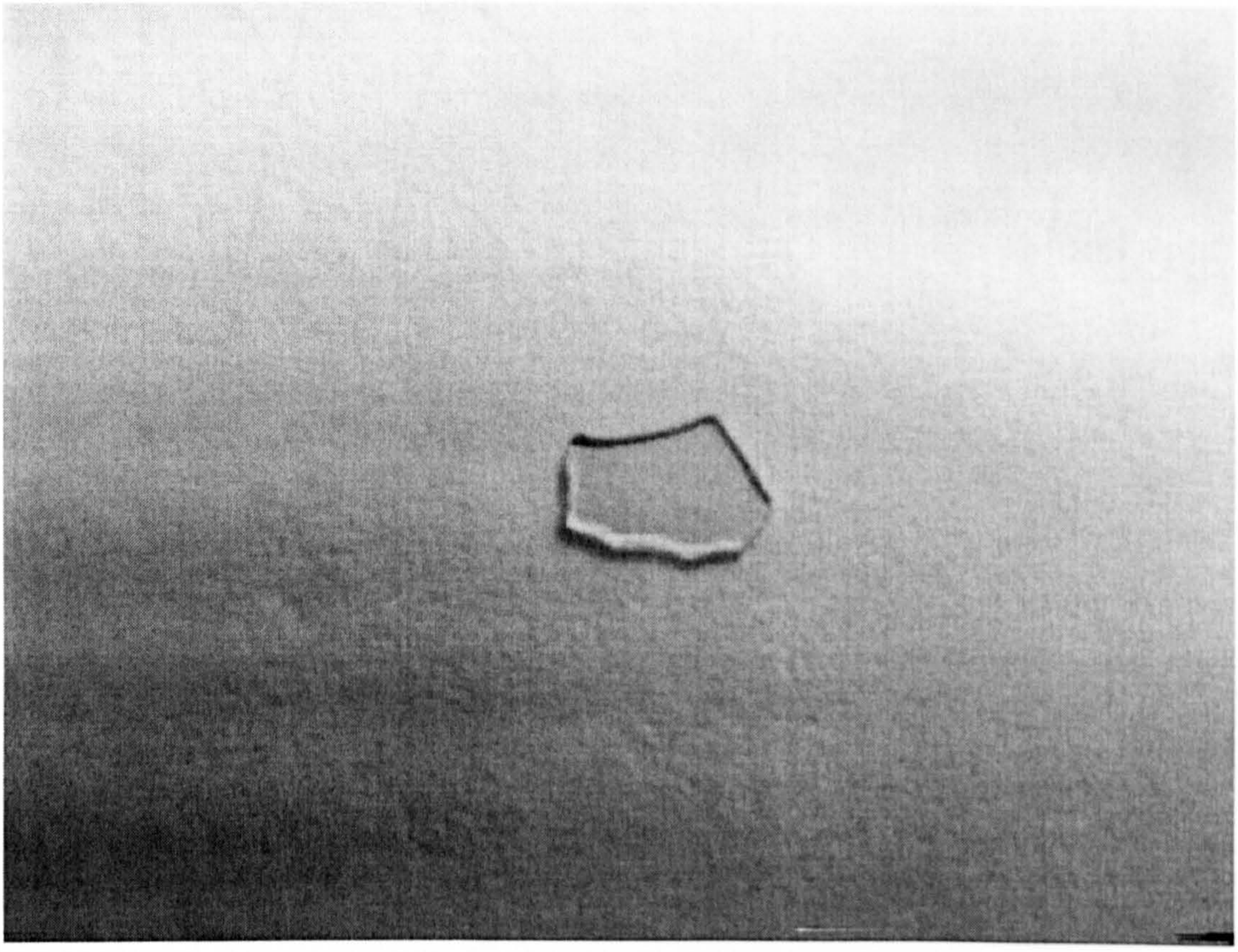

Figure 6.15 shows an aerogel resulting of the second experiment

6.3.6 Third and fourth experiment

As a result of the second experiment, a shorter protocol was adopted to dry several pieces resulting from the 1 ml recipe. The pressure was raised to 100 bars within 30 min rather than 1 hour followed by the 30 min rise of the temperature up to 40 °C as seen in figure 6.16. Despite similar pressure drops as in experiment 2 the aerogels were obtained perfectly dried and uncracked.

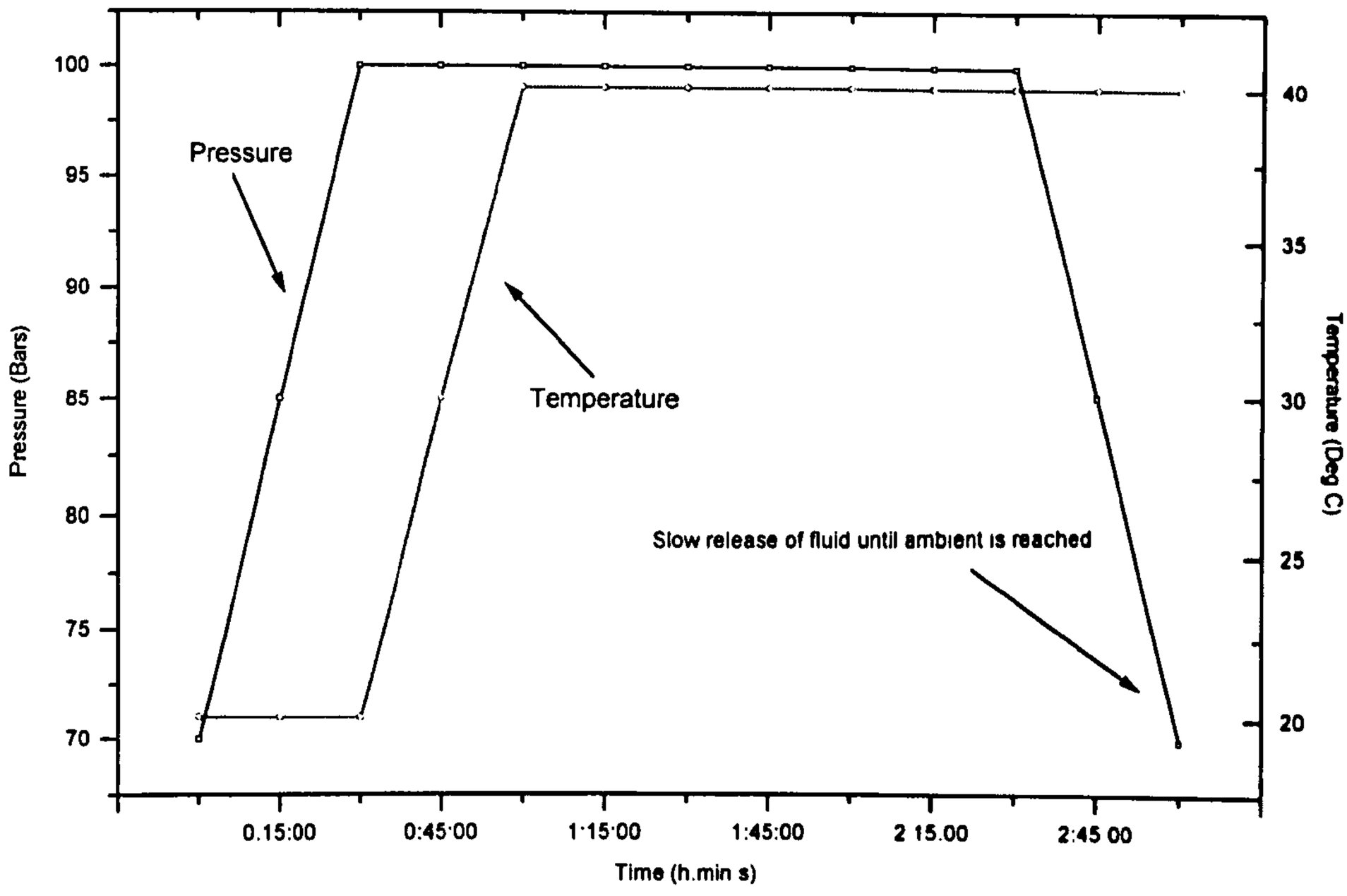

Figure 6.16 shows the final super critical drying protocol

6.3.7 Conclusions on the supercritical drying

Despite several minor problems, all the sol-gel pieces were correctly dried and suitable for testing. The technique of inserting ethanol in the vessel with the samples was successful and avoided any damage on the gels when pressure drops occurred. This drying technique was very reliable and produced many samples that were light, transparent and large enough to be used for humidity sensing.

6.3.8 Results using aerogel samples

The aerogels recovered from the four super critical drying experiments were tested using the optical system described in section 6.1. Fortunately the samples were clear and flat enough to allow the light beam to pass through the aerogel and permit the measurement of the optical thickness of the material. This was coupled with the measurement of the physical thickness of the aerogels when submitted to humidity.

6.3.8.1 Measurement of the physical thickness of aerogels

To measure the physical thickness variation of the aerogel with humidity a mirror was placed over the sample by using the bridge technique described in section 6.14. The sample was then aligned with the optical system (6.1) and the physical thickness was monitored while the humidity levels were varied inside the test chamber.

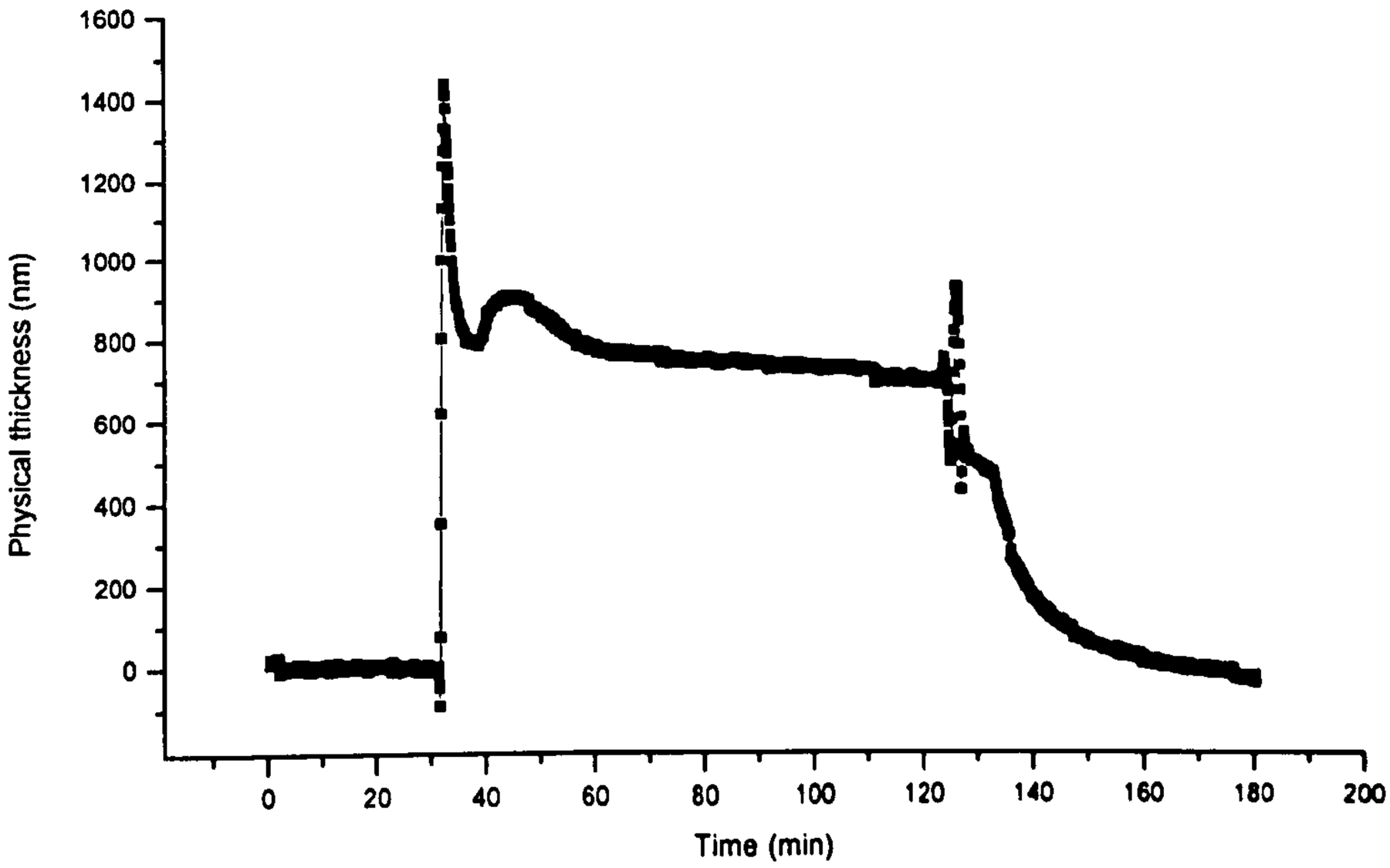

Figure 6.17 shows the physical thickness change with humidity

As seen in figure 6.17 the response to humidity was fast with an amplitude of 750 nm in the middle of the curve, and figure 6.18 shows the corresponding humidity and temperature variation during the experiment. The aerogel sample was 156 μm thick and the response to humidity was therefore 0.5 % of its thickness up to 80 %RH. This small value was not suitable for use in a precision multiplexed humidity sensor. Also artefacts at each change of humidity level could lead to an incorrect interpretation at the sensor output. Therefore this configuration was not considered as a potential sensor. These artefacts were noticed when testing other aerogels in the same configuration. This could be due to a non uniform swelling of the aerogel. If the aerogel swells first on top and on the sides where in direct contact with air, the aerogel will slightly bend increasing the apparent physical thickness. When the equilibrium is reached the bending stops and the

true physical thickness is reached. This would also happen when drying if the mirror is not perfectly centred onto the aerogel.

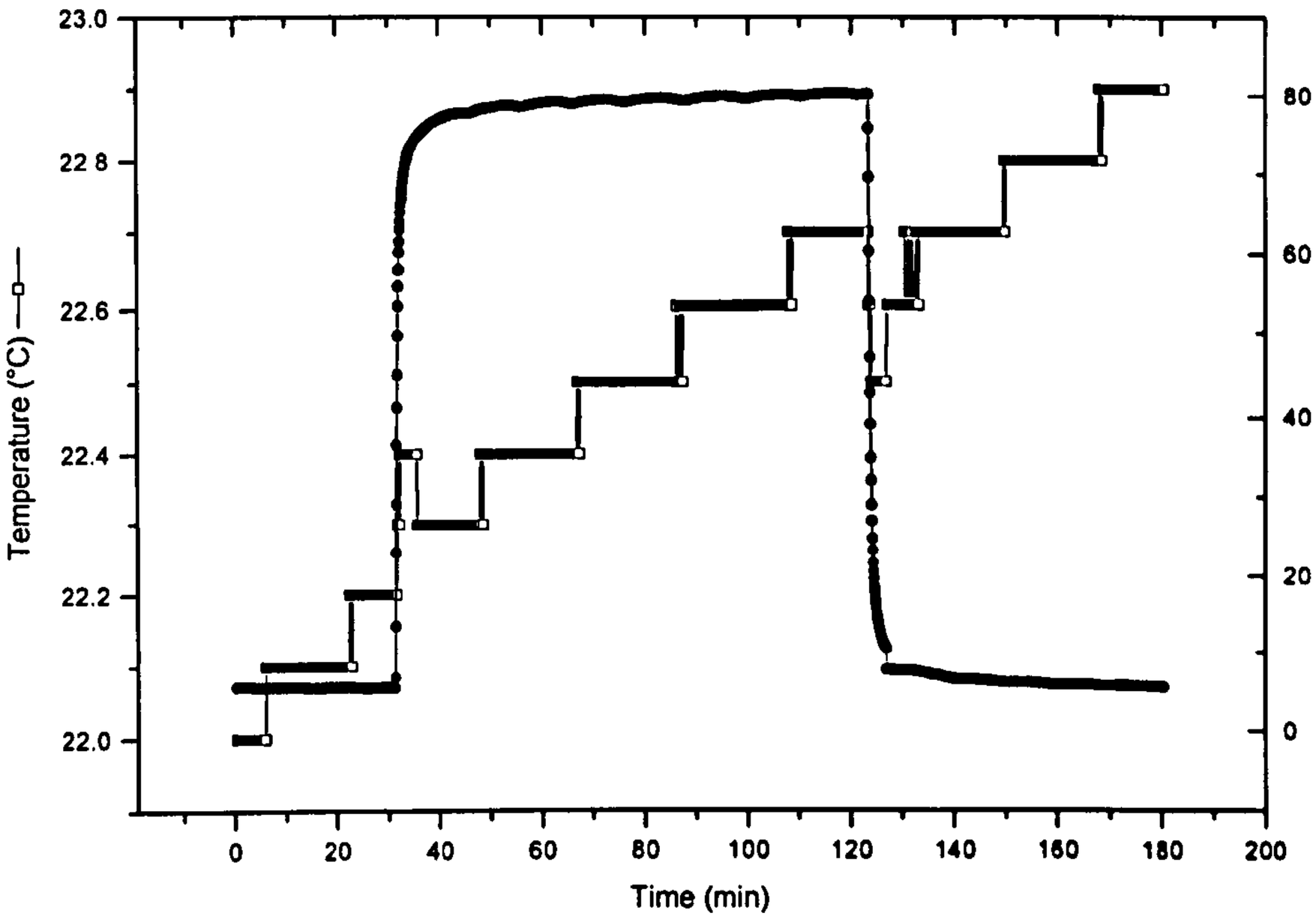

Figure 6.18 shows the temperature and relative humidity during the experiment

To avoid any bending of the aerogel a different method of mounting the sample was tested. Instead of mounting the aerogel using bridges, the whole bottom was glued to the substrate, with a mirror placed in a similar fashion on top. The results, as seen in figure 6.20, showed that the artefacts were no longer present but the response time increased to one hour. The relative humidity and temperature variations during the experiment are seen in figure 6.21. The result of this mounting was not successful since the sample cracked in four pieces during the experiment. The increase in amplitude is possibly due to a larger thickness despite the fact that the sample was dried at the same time than the previous sample and came from the same sol-gel sample. This is possible since the initial sol-gel film was not perfectly uniform and small differences in the thickness of the film were noticed. The result of this experiment showed that the mounting technique was important and that maximum freedom of movement had to be given to the sample to avoid any stress leading to breakage. Finally, the overall performance of the aerogel when measuring its physical thickness was not sufficient for consideration as a sensor. Therefore several tests were performed to evaluate the variation of the optical path,

induced by the refractive index change, in the interferometric system while varying humidity.

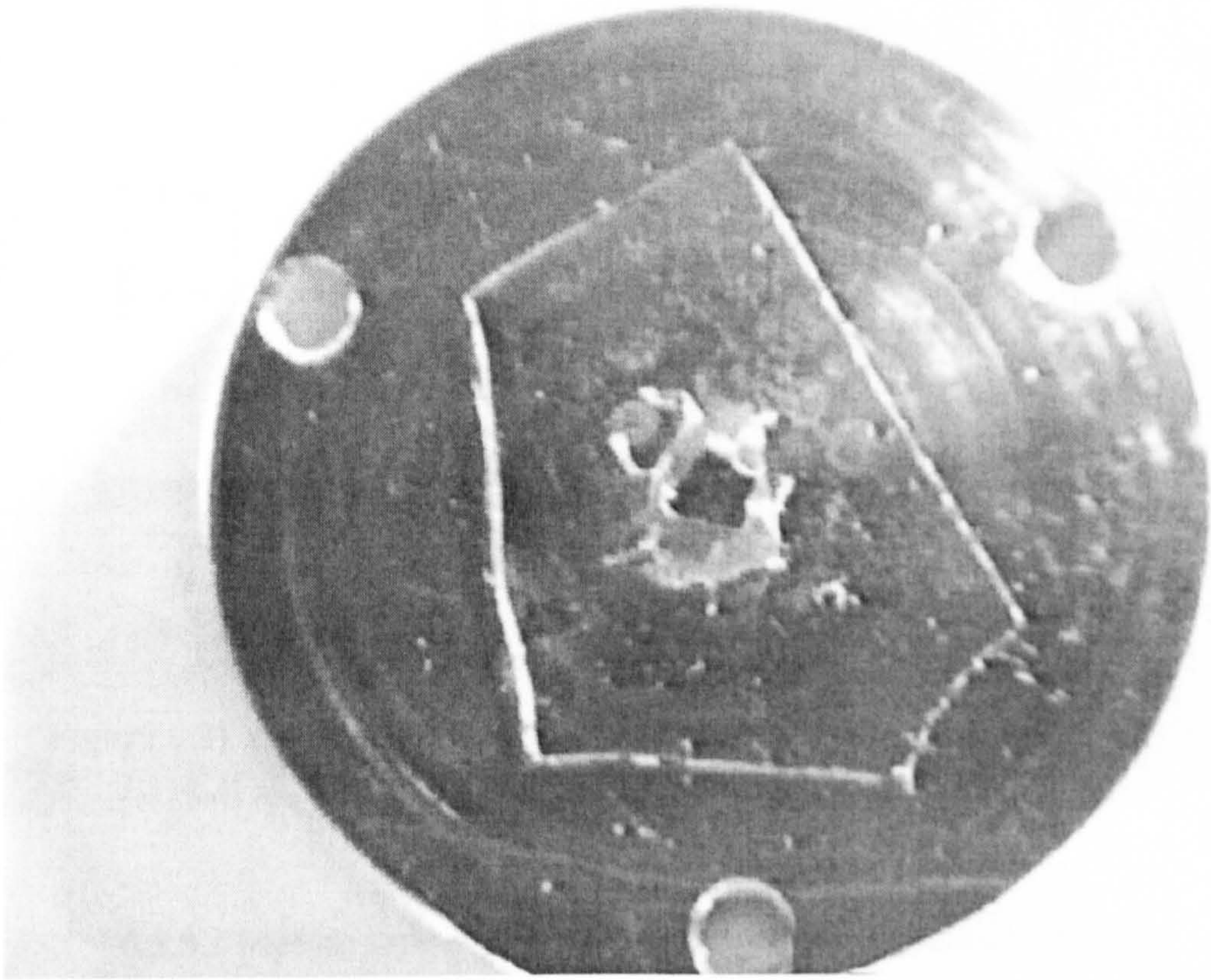

Figure 6.19 shows the sample mounted corresponding to figure 6.17

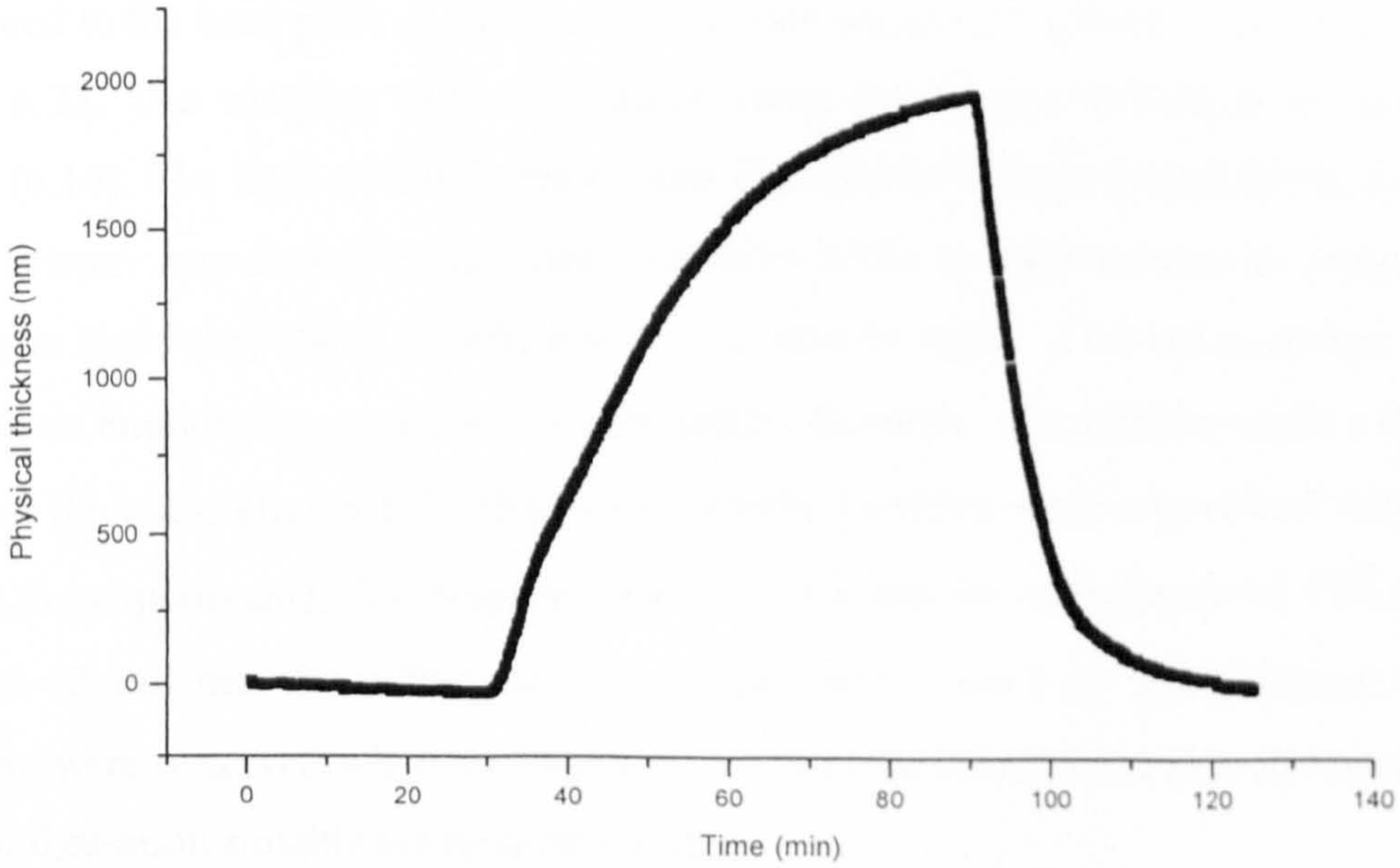

Figure 6.20 shows the physical thickness change of the aerogel with humidity

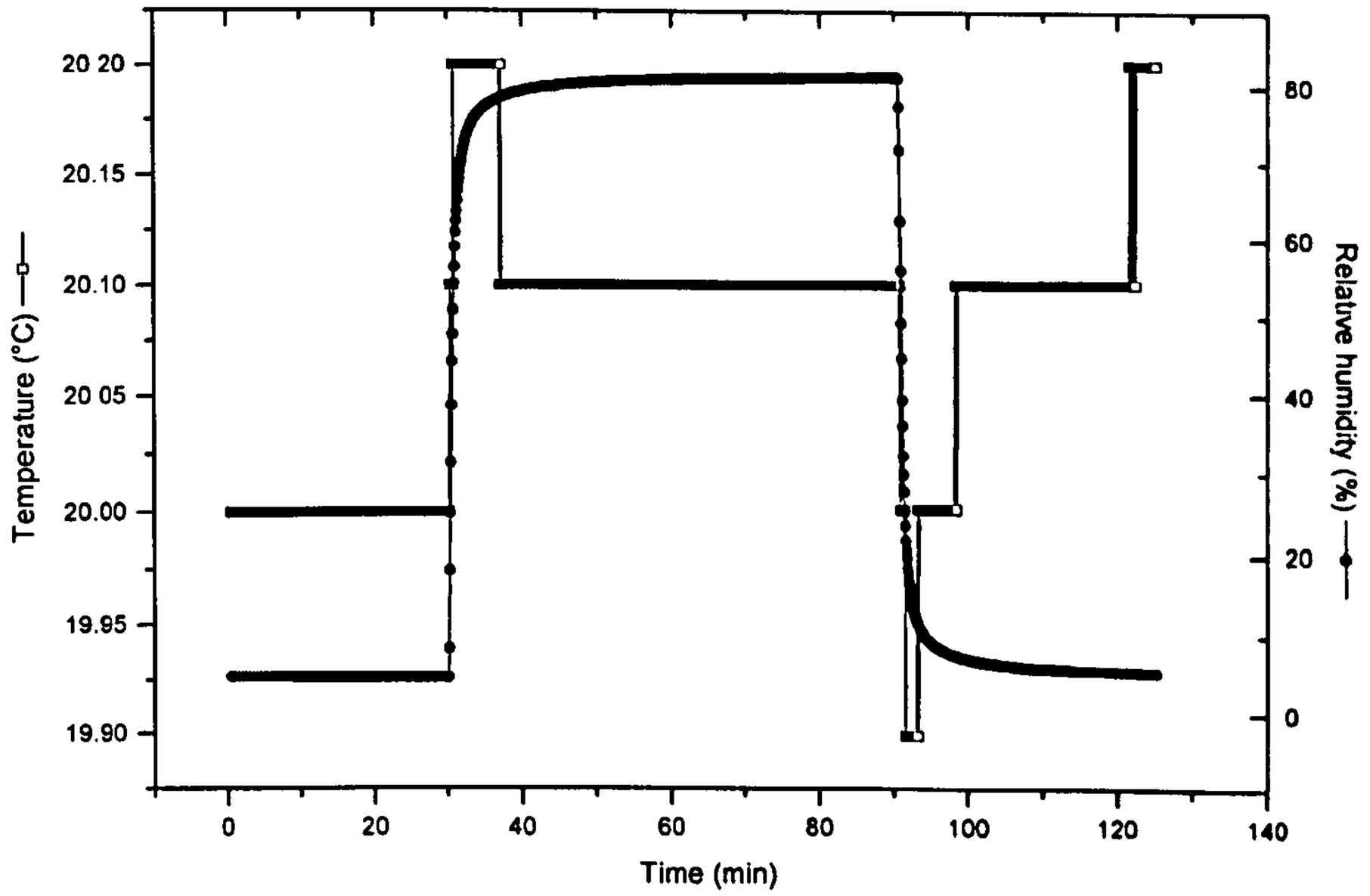

Figure 6.21 shows the temperature and relative humidity variation during the experiment

6.3.8.2 Measurement of the optical thickness change of aerogels

To measure the optical thickness change of the aerogels with humidity, the samples were placed in the Fabry-Perot cavity of the system described in section 6.1. A mirror was glued to the back plate of the Invar cavity and the aerogels placed over it as seen in figure 6.22. The samples were maintained using the bridge technique as described earlier (6.14). The light would therefore pass through the aerogel before being reflected by the mirror. Any change in the refractive index of the sample induced an optical path change in the Fabry-Perot interferometer. As seen in figure 6.23 the response of the aerogels to humidity is greater when their optical thickness is considered rather than the physical thickness (figure 6.24 shows the relative humidity and temperature variations during the experiment). The response was over 8.6 μm for a thickness of 156 μm but reached 12 μm near 90 %RH. Several samples were tested by transmission and no artefacts were observed when the humidity levels were changed making the samples in this configuration suitable for humidity sensing.

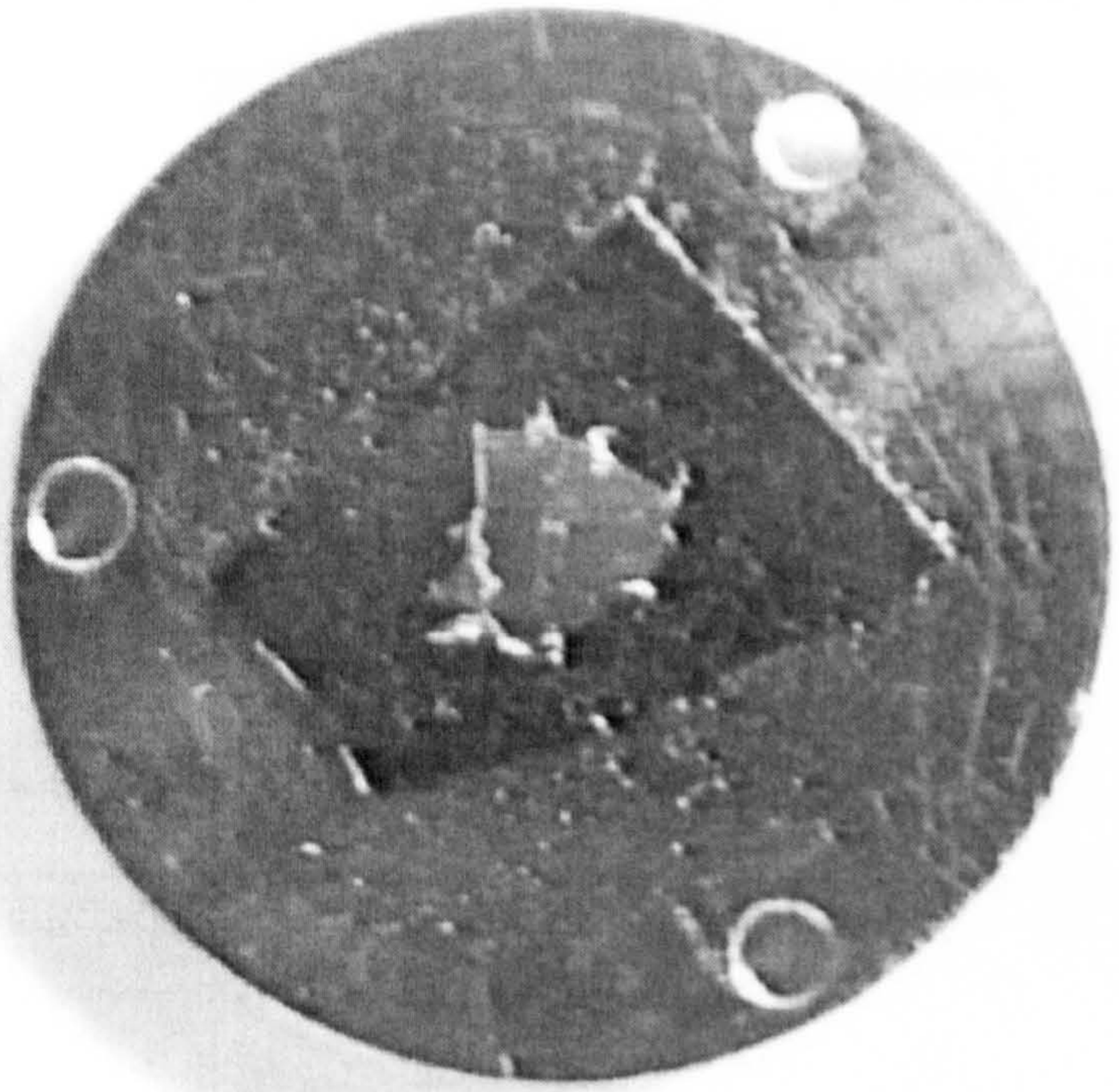

Figure 6.22 shows the tested aerogel mounted on the Invar back plate of the interferometer

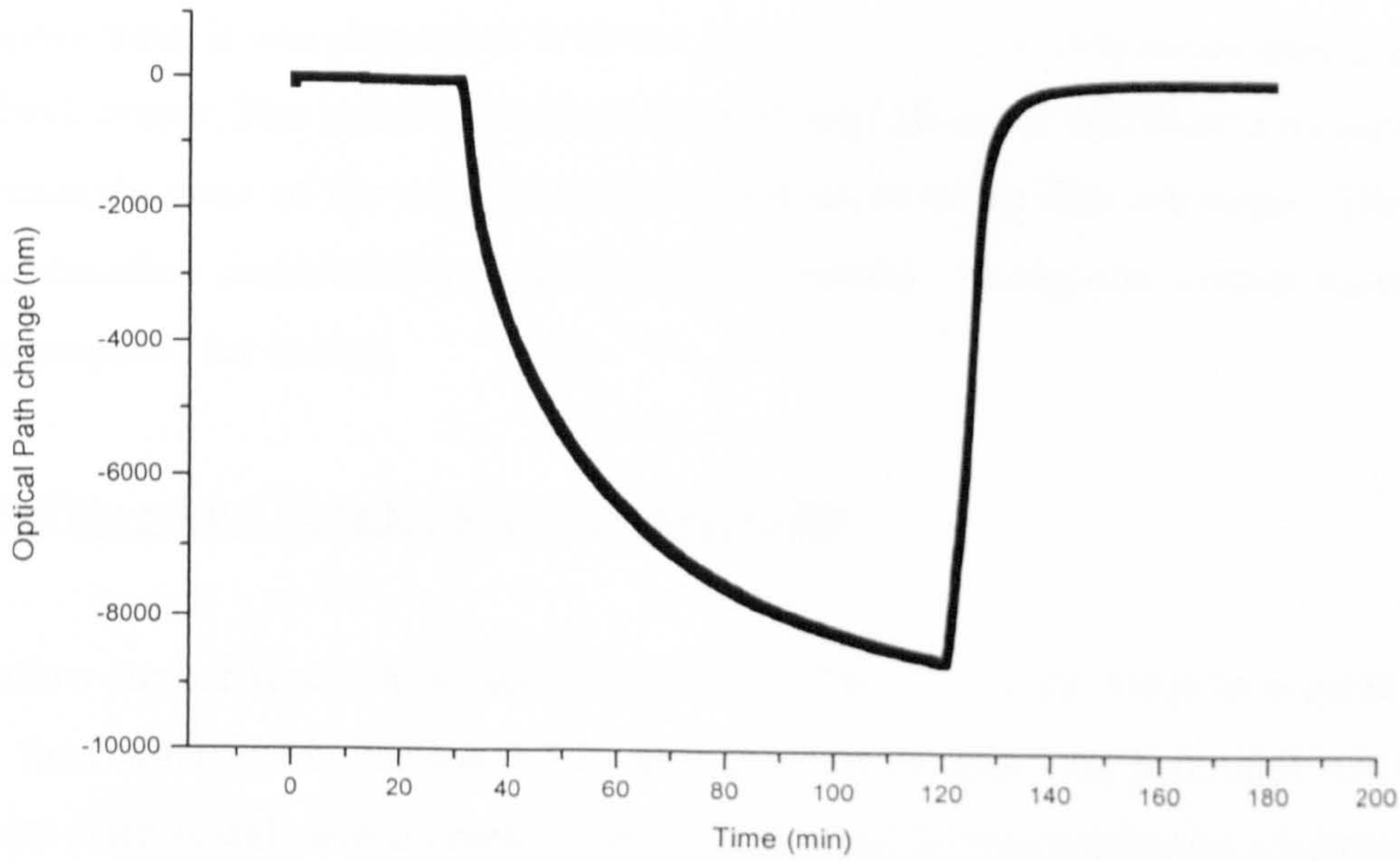

Figure 6.23 shows the optical path change induced by an aerogel sample when submitted to humidity

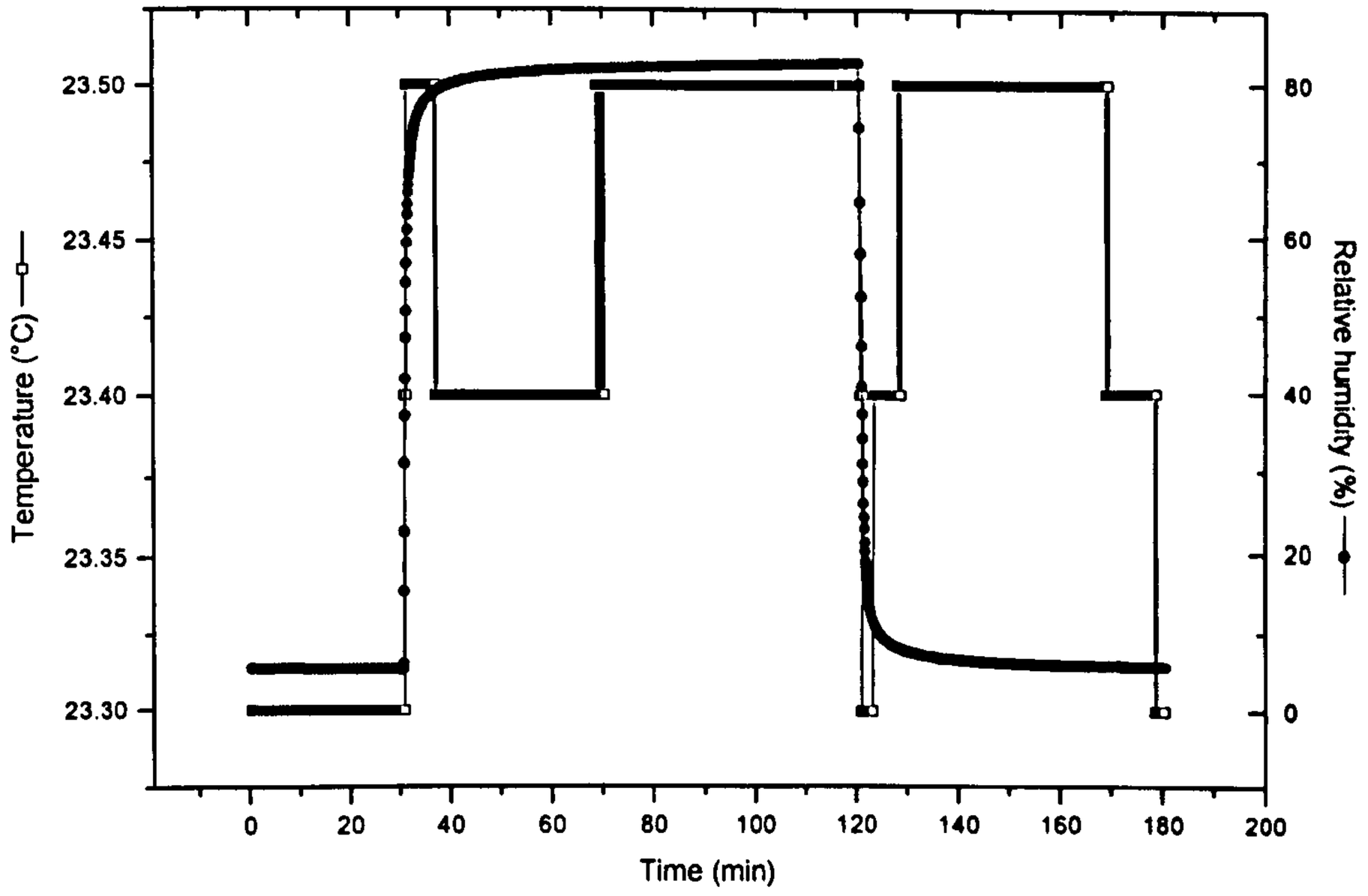

Figure 6.24 shows the temperature and relative humidity change during the experiment

The time response in this experiment was about 120 minutes. This time could be reduced by using thinner films as the response time is a function of the aerogels thickness. Also, to increase the contact area of the film with air and therefore its response time, it was planned to hold the sample in the light path rather than gluing it to the back mirror. The gels were extremely brittle and therefore difficult to manipulate but surprisingly none of the samples were broken when using this technique. The aerogel films therefore constituted a novel route for humidity sensing and several thinner films were prepared for testing.

6.3.9 Thin sol-gel films for super critical drying

To allow further research on aerogels, thinner films had to be made in a more reliable way than described in section 6.3.1. Also the transfer from the petri dish to the super critical drier vessel caused cracks in the samples and did not constitute a reliable way to obtain aerogels. The various super critical dryings showed that the best results were obtained by inserting the samples in ethanol, previously poured into the vessel. It was

therefore clear that the samples had to be produced in an environment saturated in solvent not to crack but also conserved in this solvent to be finally poured into the super critical drier vessel. This would allow no contact with air and therefore no premature drying. The technique used to produce such samples was to use a crystallisation dish in which were placed a series of cover slides held together two by two by using paper clips. The cover slides, previously treated with dichlorodimethylsilane to avoid any adhesion of the gels, were separated by using an appropriate number of layers of cling film at each end so as to separate the cover slides by the desired distance. The gaps between the two slides were set at 25, 45, 60, 75μm. Finally the two slides were held together using standard paper clips. The delicate part of the procedure was to insert the solution into the gap between the slides. The solution previously prepared in a beaker, was inserted in the interspace by using a syringe. The needle of the syringe was placed in the middle of the cover slides gap and a small amount of solution was dispensed. The solution naturally filled the whole interstitial space by capillary action. All samples produced this way were placed in the crystallisation dish. Before closing, the dish was filled with a sufficient amount of ethanol to reach the first cover slide without touching it. If the ethanol reached the first entrapped liquid film, the immediate effect would be to dissolve it. Finally the dish was hermetically closed using Nesco film (a plastic extendable film that allows to seal petri dishes). During all the gelation and ageing process it was important to maintain the ethanol level in the crystallisation dish. The first films were obtained in one week. The second delicate part was to produce from these very thin films round samples of three millimetres in diameter to be inserted into the super critical drying vessel. To do this, the paper clips were removed and the film and cover slides placed in a large petri dish full of ethanol. The two slides were then very carefully separated liberating a extremely thin film floating in the solvent. As the films were difficult to see with the naked eye a binocular microscope was used to create small discs. The discs were punched out the film and were sucked up in a tube of a larger diameter than the discs. Finally the discs were placed into small sample storage jars (10 ml) filled with ethanol and closed. A large number of samples were made this way. The technique is very reliable and does not need any special apparatus. The thickness of the films can be chosen and once the discs are enclosed in the small sample storage jars, they can be conserved for long periods with no degradation.

6.4 Conclusion on sol-gels and aerogels

The results obtained with aerogels showed that this material was suitable for humidity sensing. A way of producing thin sol-gel films, in a reliable way, for super critical drying was developed. Unfortunately, despite the promising results from the produced thin sol-gels films, the super critical drying apparatus became unavailable, due to a change in location of the BNFL laboratories, and further testing on aerogels was no longer possible.

6.5 References

[1] Y. J. Rao, and D. A. Jackson, Meas. Sci. Technol., 7, (1996), 981-999.

[2] Y. J. Rao, D. J. Webb and D. A. Jackson, Proc. SPIE 2070, (1993), 35.

[3] J. L. Brooks, IEEE J Lightwave Technol., 3, (1985), 1062-72.

[4] F. Farahi, T. P. Newson, J. D. C Jones and D. A. Jackson, Opt. Commun., 65, (1988), 319-21.

[5] T. Adachi and S. Sakka, J.Mat. Sci., 22, (1987), 4407.

[6] G. W. Scherer, J. Non-Cryst. Solids, 100, (1988), 77.

[7] F. Lu, S. Chen, and S. Peng, Cat. Today, 30, (1996), 183-188.

[8] B. Novak, D.Auerbach, and C. Verrier, Chem. Mater., 6, (1994), 282-286.

[9] K-H Lee, S-Y Kim and K-P Yoo J. Non-Cryst. Solids, 186, (1995), 18-22.

[10] H. Yokogawa, M. Yokoyama, J. Non-Cryst. Solids, 186, (1995), 23-29.

[11] G. Rogacki and P. Wawrzyniak, J. Non-Cryst. Solids, 186, (1995), 73-77.

[12] M. J. Bommel, A. B. de Haan, J. Non-Cryst. Solids, 186, (1995), 78-82.

[13] J. Fricke and A. Emmerling, J. Sol-gel Science and Tech., 13, (1998), 299-303.

7

Optical humidity sensor based on polymers

7.1 Multiplexed dual tandem interferometry

7.1.1 Requirements for multiplexed system

7.1.2 System description

7.2 Polymers

7.2.1 Introduction

7.2.2 Polyvinyl acetate

7.2.3 Cellulose acetate

7.2.4 Polyamide nylon

7.2.5 Polyvinyl alcohol

7.2.6 PMMA (poly(methyl methacrylate))

7.2.7 Results using the previously described polymers

7.2.8 The PMMA-PMTGA-PMMA polymer

7.2.9 The PMMA-PMTGA-PMMA polymer result

7.3 References

7.1 Multiplexed dual tandem interferometry

7.1.1 Requirements for multiplexed system

The requirements defined by British Nuclear Fuels at the beginning of the project were the following. The sensing should be over the full range of humidity, at normal temperatures and under atmospheric pressures. The sensor itself should be small enough to be used in all configurations and also robust to be used in industry. The final system was to be composed of a central unit with various sensors placed remotely at the end of optical fibre links to sense humidity. Ideally the system could support the multiplexing of a large number of sensors. Also the final prototype was to have the facility to display the measurements on a computer screen.

7.1.2 System description

The measurement system is based on low coherence tandem interferometry [1-4] (figure 7.1). The optical processing unit is a fibre optic Michelson interferometer illuminated by a low coherence superluminescent source at 825 nm with a 22.2 nm bandwidth as seen in figure 7.2. At the end of each fibre arm of the interferometer were placed bulk mirrors driven by two piezoelectric actuators. The optical path difference of one of the arms was driven sinusoidally over a small range at 80 Hz via a PZT, (1) of figure 7.1, to produce a periodic modulation of the transfer function. The OPD of the second arm was linearly varied by a PZT actuator, (2) of figure 7.1, manufactured by Queensgate Ltd as shown in figure 6.1 of section 6.12. This digitally driven actuator was used to simultaneously scan the transfer functions of the four independent sensors in order to establish their respective coherence matched positions and hence the change of optical path in each sensor as a function of humidity. The Queensgate PZT unit has an accuracy of 5 nm and can scan over a range of 70 μm. Here it was driven in steps of 20 nm over 20 μm.

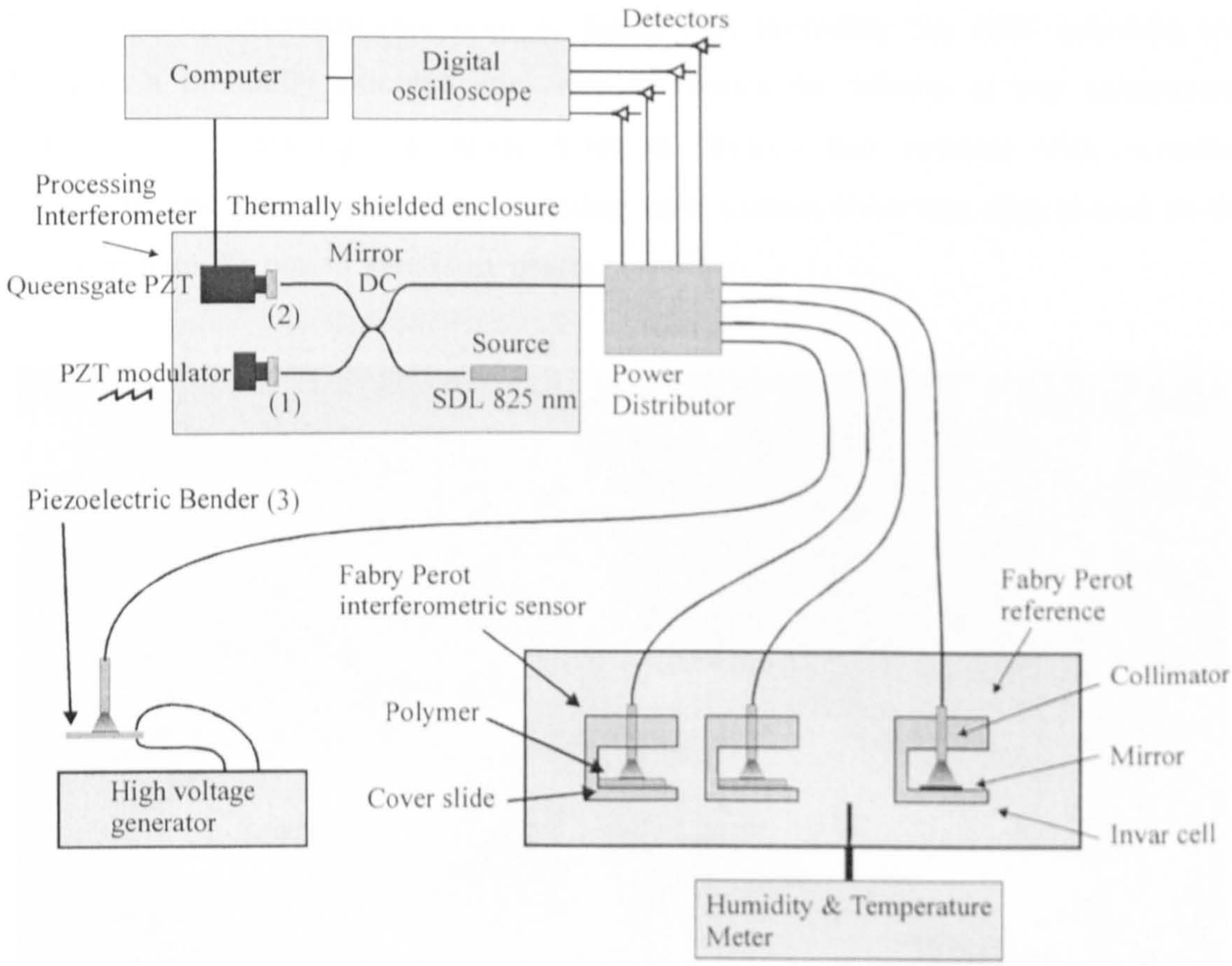

Figure 7.1 shows the experimental set-up of the interferometric system

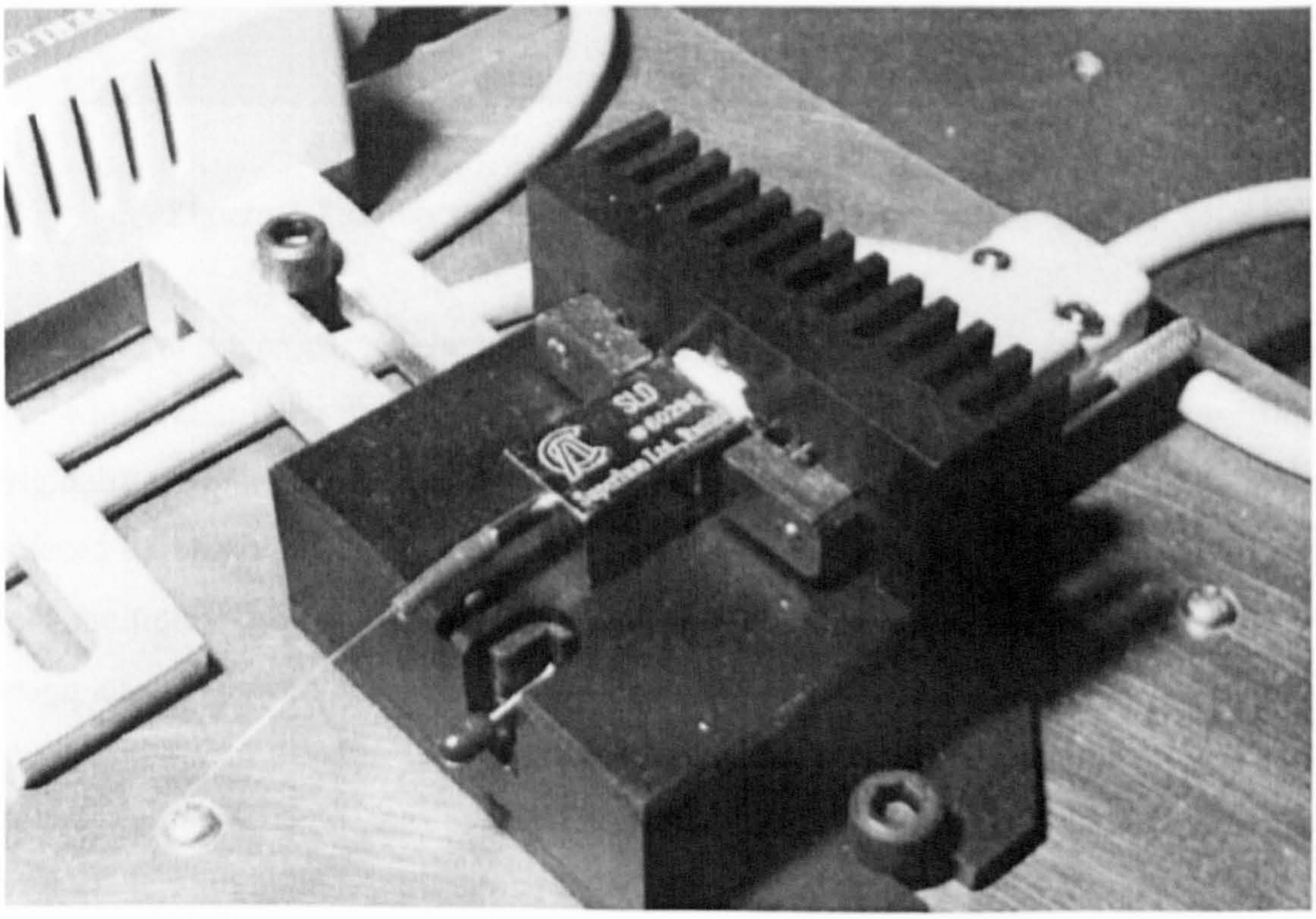

Figure 7.2 shows the super luminescent source used in the system

The processing interferometer seen in figure 7.3, including the PZT actuators was placed in a thermally shielded enclosure to reduce the effects of any temperature gradients. The shielding was made from an Perspex box covered with expanded polystyrene and placed over the processing unit. Cotton wool was also placed on the optical table in the box to avoid any drafts.

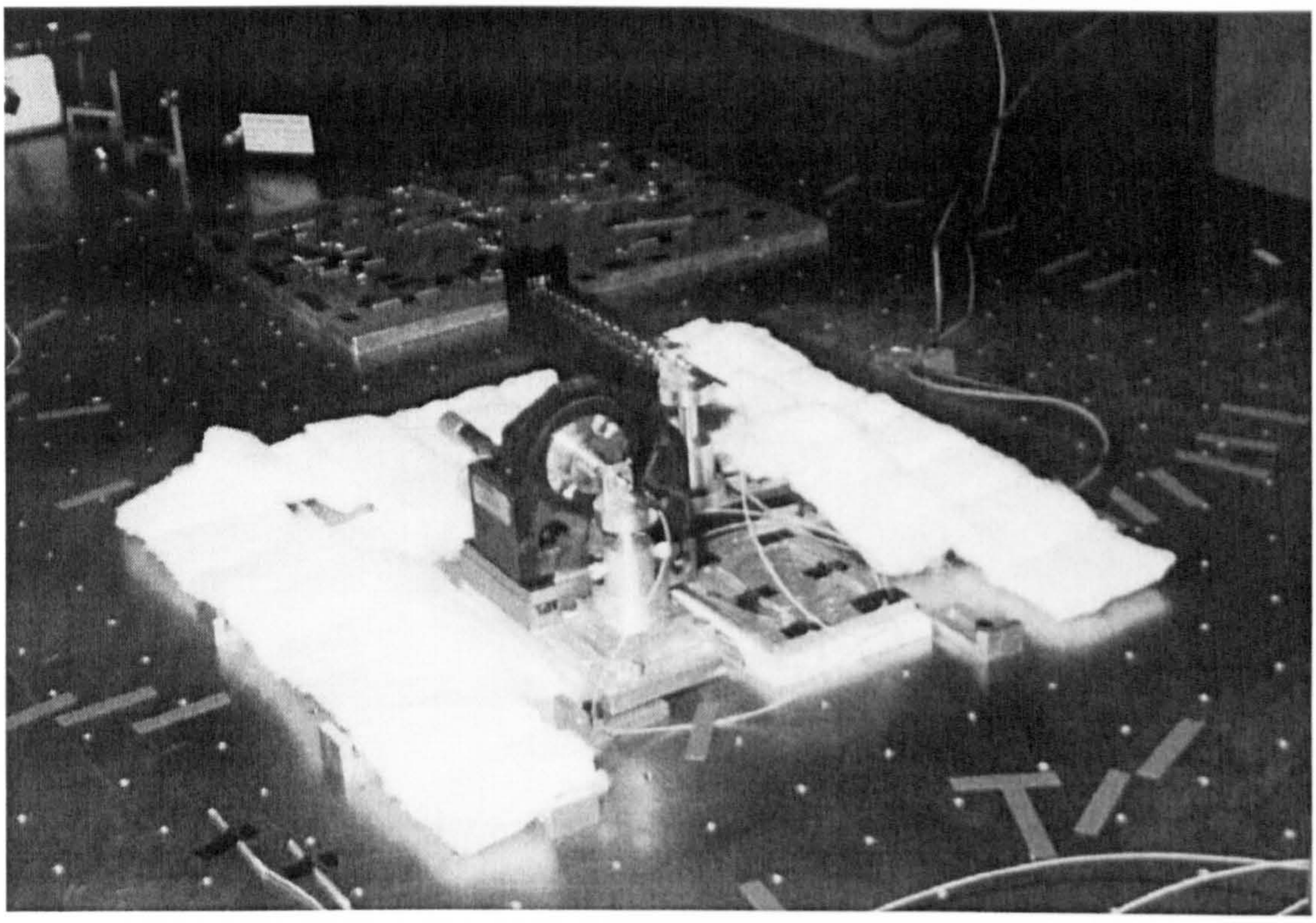

Figure 7.3 shows the processing interferometer of the system

The output of the processing interferometer is connected to an all fibre power distributor tree, which distributes the power uniformly between the four fibre transceiver fibres. Originally a commercial power distributor was used but due to power losses, it was replaced by seven 3-dB couplers spliced together forming a tree. This tree could allow eight multiplexed lines and had the advantage that it could be expanded further. The design of the power distributor [5] allowed all the four sensors to be interrogated simultaneously in parallel. A sensor was mounted at the distal end of each transceiver link. A separate detector was required for each sensor. On the four available lines were mounted two humidity sensors, one displacement sensor and one reference sensor, all four sensors being based on low finesse Fabry-Perot interferometers. The two final humidity sensors were based on a (PMMA-PMTGA-PMMA) polymer but could be

composed of any material that modified its size or optical thickness with humidity. All polymer films were tested using this system.

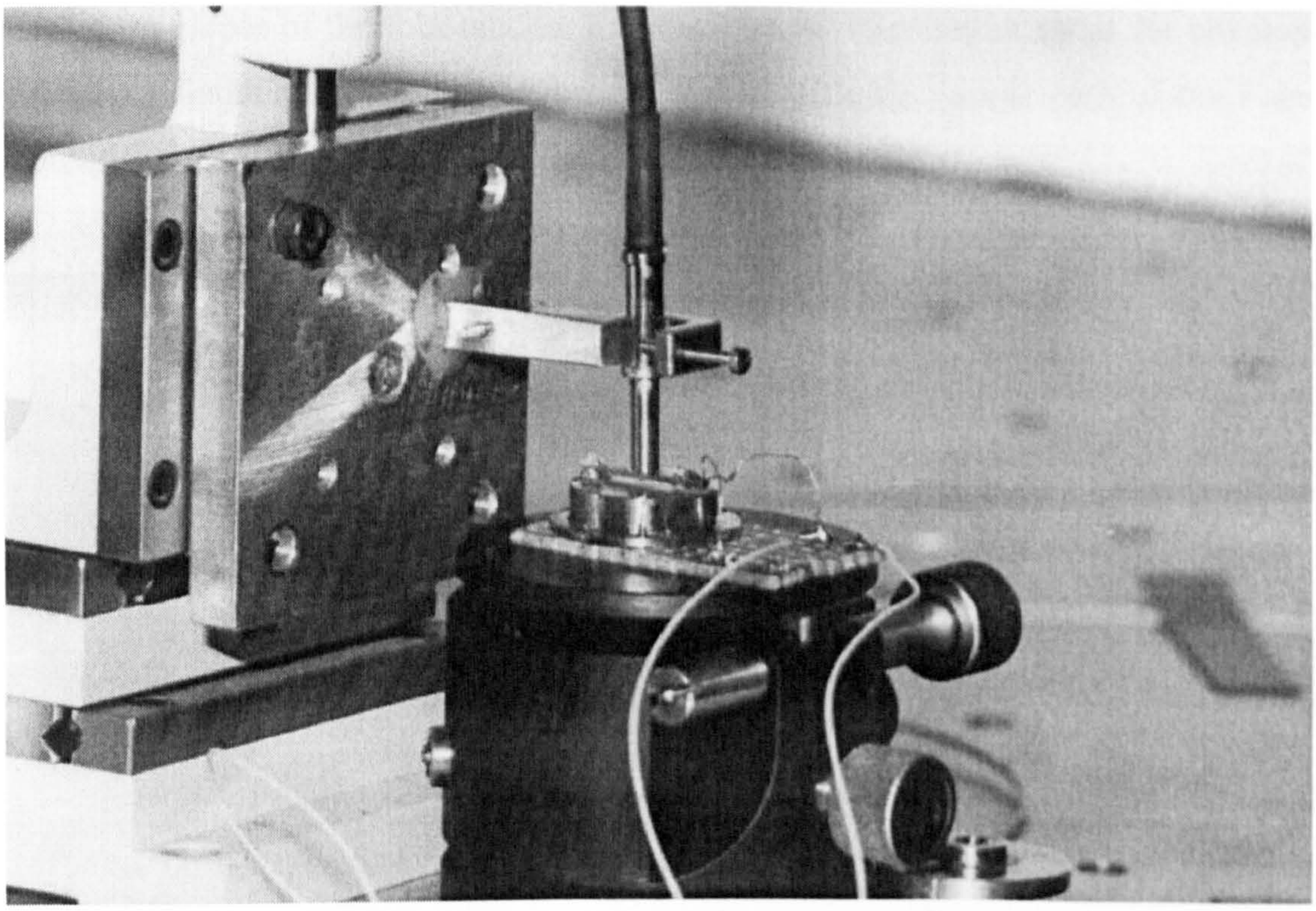

Figure 7.4 shows the piezo-electric bender simulating a sensing material

The polymer was deposited on a cover slide glued to the bottom of an invar cell. A mirror was then glued on the free face of the polymer as described in section 6.1.4, so as to act as one of the mirrors of the Fabry-Perot, the end of the fibre collimator being the other mirror of the Fabry-Perot cavity. The displacement sensor configuration was similar with a piezoelectric disc, (3) of figure 7.1, replacing the polymer. As can be seen in figure 7.4 the purpose of the displacement sensor was to demonstrate the response of the optical system to fast changes in OPD independently of the effects of the polymer. An OPD change of 10 μm could be resolved with an accuracy of 50 nm in a 4 minute scan. The reference sensor was similar to the two polymer based sensors except no humidity sensing polymer material was inserted in the cavity. The reference therefore sensed any drift in the interferometric system due to temperature gradients allowing the three other sensors to be compensated for such effects. Each of the four transceiver links had a return path connected to a highly sensitive detector and the resulting AC signals of the four optical lines were measured simultaneously on a four input digital

oscilloscope. The signal amplitudes where then transferred to a computer via an IEEE link for subsequent processing. Each scan of the Queensgate actuator produced four data sets which included a series of points corresponding to the maxima of the transfer function envelopes of the four tandem interferometers. The maximum of the envelopes (typically a Gaussian profile) were directly linked with the optical path of the Fabry-Perot sensor and were located with a Labview program.

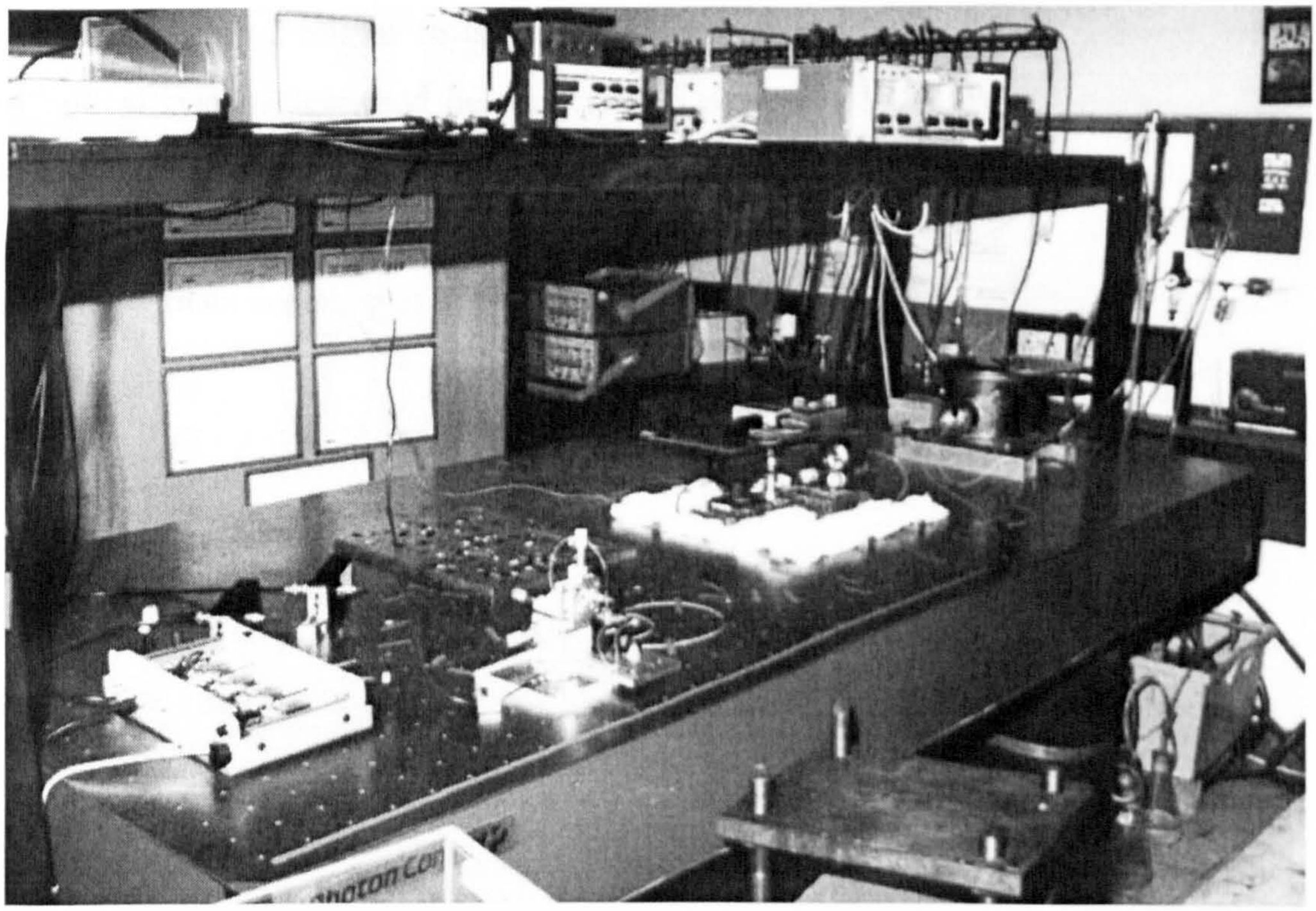

Figure 7.5 shows an overview of the optical system

Therefore, any optical change due to the swelling of the polymer with humidity resulted in a proportional movement of the maximum of the transfer function envelope. To increase the accuracy of the measurement a simple averaging procedure was performed. The best results were obtained by averaging over 200 points corresponding to 20% of the whole scan area, this resulted in a smooth curve free from noise, allowing a resolution of 50 nm over the full range scan (70μm) with the minimum step of 5 nm. Other techniques such centroid fitting were investigated with similar results. In this case only four sensors were multiplexed but the number could be easily extended to eight, as there are two output ports at each power distributor output. For example this could be achieved by producing, four additional sensors with the same cavity lengths where the

OPDs are greater by at least the OPDs of the first set of sensor plus the anticipated length change of the polymers. One of the factors that limits the number of sensors which can be multiplexed is the optical power available. In the present system the power was set to 2.5 mw although the maximum source power is 10 mw. Thus the same performance regarding S/N ratio could be maintained if the number of output ports of the power distributor were increased by 4 to 16. This would allow 32 sensors to be multiplexed via 32 independent transceiver lines, provided the OPDs of the sensors were divided into 2 sets of 16 with the OPD requirements as indicated above. Overall, *the optical system described here is capable of* optical path measurements of 70 μm with a resolution of 50 nm allowing many possibilities for general sensing. In the application of humidity sensing, PMMA-PMTGA-PMMA films allowed to sense humidity with an accuracy of 1.21 % RH.

7.2 Polymers

7.2.1 Introduction

Although it was interesting to explore the properties of the aerogels in their own right, the loss of the super critical drying facilities made it imperative to explore other materials, hence various polymers were tested to find a suitable material for humidity sensing. Polymers have already been used in resistive or capacitive humidity sensors and are the base of most modern electronic humidity sensors. Overall six different polymers, mounted on glass substrates, were tested to assess their capacity to be integrated into a multiplexed interferometric system (7.1), as described earlier in this chapter. The requirements concerning these films are a good resistance to humidity usually leading to little ageing but also a good reproducibility with no hysteresis. The following polymers were selected for their known uptake of water when submitted to humidity as described in the literature [6]. Various mounting techniques were explored as the polymers were supplied in different forms. The experimental procedures to obtain these films and the obtained results are described in the following sections.

7.2.2 Polyvinyl acetate

The polyvinyl acetate polymer, supplied as a powder, had to be dissolved in order to deposit it as a film on a substrate. The powder was dissolved using chloroform transforming the polymer to a viscous transparent liquid. A drop of this polymer was then spin coated on a glass substrate at 200 rpm twice, creating a 42 μm thin film. The film was deposited on a cover slide substrate previously coated with gold. This had the benefit of allowing the measurement of the optical thickness change of the polymer when submitted to humidity. Unfortunately, in this case, the sample did not allow this measurement to be made because the film was non homogeneous resulting in a poor optical signal. The swelling of the film was therefore tested by placing a mirror over the polymer. The sample was then placed in the optical system and tested.

7.2.3 Cellulose acetate

This polymer was supplied by Goodfellow Ltd as a thin 0.035 mm film. To stick the film to the substrate the film was dissolved using acetone. The film was placed over the substrate and a drop of acetone was placed on the film. This dissolved the polymer sufficiently to bond the polymer to the substrate. Both configurations were tested, measuring the optical thickness change of the film and also measuring its physical swelling when submitted to humidity. Depending on the configuration one or two layers were applied. Finally the samples were mounted in the optical system and tested.

7.2.4 Polyamide nylon

The polyamide nylon films also came from Goodfellow Ltd and had a thickness of 0.1mm. The film was opaque and did not permit measurement of its optical thickness variation when humidity levels were changed. The film was found to be difficult to dissolve on a substrate. Thus a special mounting avoiding sticking the polymer on the substrate was used. The polymer was held against the Fabry-Perot back plate by a washer maintained in position by a spring. This has the advantage that the back plate could have holes giving the polymer maximum contact with the air. However this system was not reliable and was used only on specific occasions.

7.2.5 Polyvinyl alcohol

This polymer was supplied by Aldrich as a powder. The best dissolution was obtained by water. The water was heated (70-80°C) and the powder slowly incorporated. The result was a viscous liquid that hardened into a film when cooled. The film was clear and measuring the optical thickness change with humidity possible. The obtained 35 μm sample was therefore tested in both configurations using the optical system.

7.2.6 PMMA (poly(methyl methacrylate))

This polymer supplied as a powder was dissolved using chloroform. The resulting viscous polymer was then spin coated on a substrate in a similar way to the polyvinyl

acetate samples. The obtained film was 45 μm for one layer spread at 1000 rpm. The film was transparent and both the optical thickness change and physical thickness were monitored using the optical system, as a function of humidity.

7.2.7 Results using the previously described polymers

This section describes the results obtained with each of the previously described polymer films by observing the physical thickness change with humidity of the film, and when possible its optical thickness change. Figure 7.6 shows the responses of the different tested polymers over the 0-90 %RH range at ambient temperature (22°C) and atmospheric pressure. The measurement of the thickness change of the polymers with humidity was measured when a plateau was reached. As the polymers had different thicknesses, the relative increase of thickness $\Delta n\Delta l/l$ and $\Delta l/l$ were plotted respectively as seen in figure 7.6. Most of these films were transparent and as with the aerogel sample, either the optical path change could be measured or the change in film thickness by appropriate placing of the mirror. The first and second column, over which the response times are indicated, corresponds respectively to these two measurements. The values of the optical path change for polyvinyl acetate and polyamide nylon, as a function of humidity, could not be measured due to their poor optical properties.

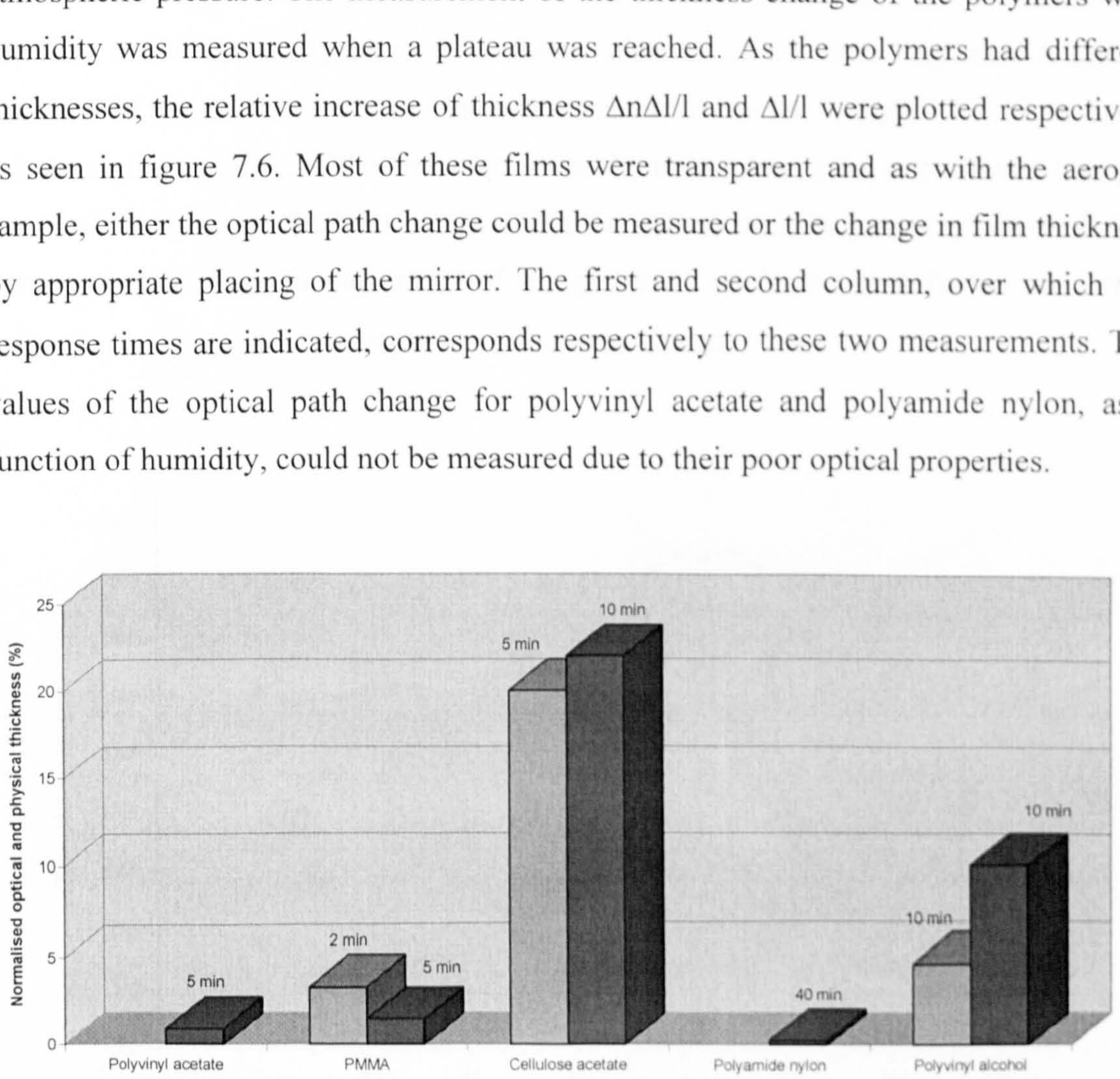

Figure 7.6 shows the response of different polymers to humidity

As seen in figure 7.6 the polyvinyl acetate, PMMA, and polyamide nylon had a very low response to humidity. The first two films had amplitudes less than 1500 nm while the polyamide nylon responded up to 14 μm for a thickness of 0.1mm resulting in a swelling of 1.4%. Furthermore the polyvinyl acetate sample had an artefact when humidity was increased. These three polymers where therefore discarded for any use in optical humidity sensing.

The best response was obtained with the cellulose acetate film with 20% and 22% respectively but also showed an artefact when the physical thickness was measured and a tendency to reduce its amplitude at fixed humidities when measuring its optical thickness. Finally the polyvinyl alcohol films had a response of 1.6 μm and 3.7 μm for a thickness of 35 μm and response times of about 10 min. An increase of the thickness of the film would inevitably result in a drastic increase in the time response. A typical variation of the thickness of the film with humidity is shown in figure 7.7 while figure 7.8 shows the variation of the temperature and humidity during the experiment. Overall, the best results were obtained by the cellulose acetate and the polyvinyl alcohol. The polyvinyl alcohol had the advantage of being clear of artefacts and drifts but had a long response time compared to its physical thickness change.

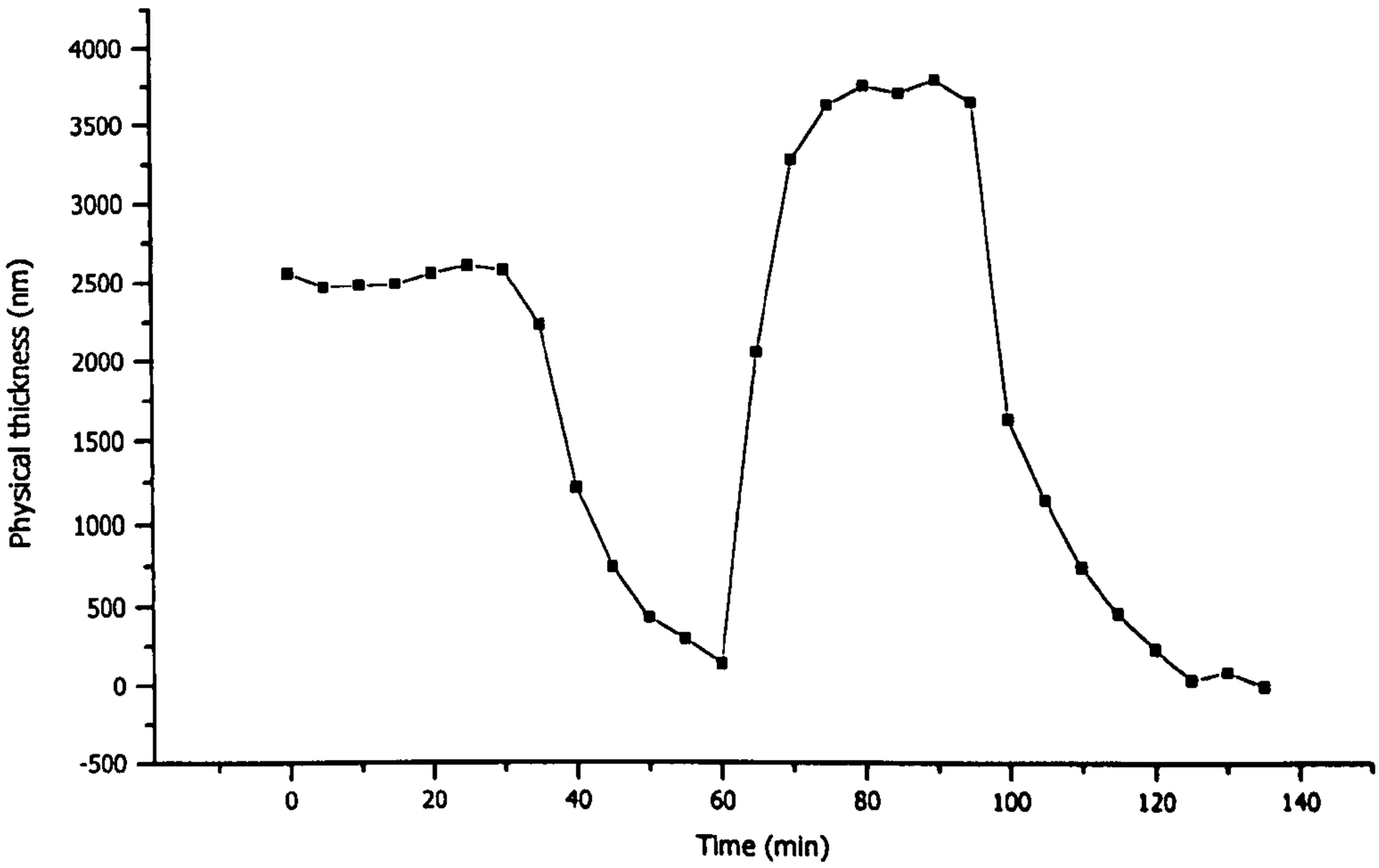

Figure 7.7 Shows the physical thickness change of polyvinyl alcohol when submitted to humidity variations

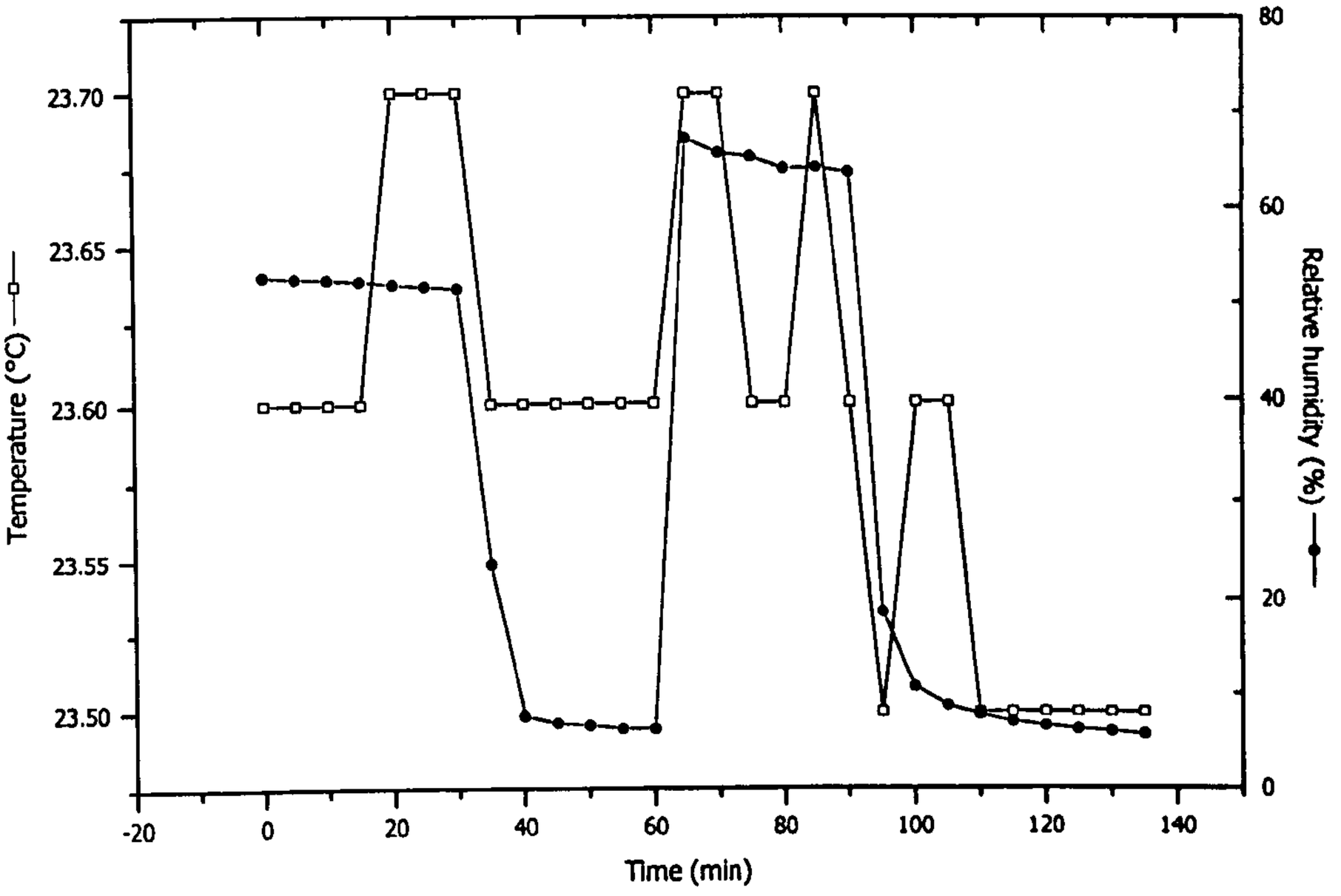

Figure 7.8 shows the temperature and relative humidity change during the experiment

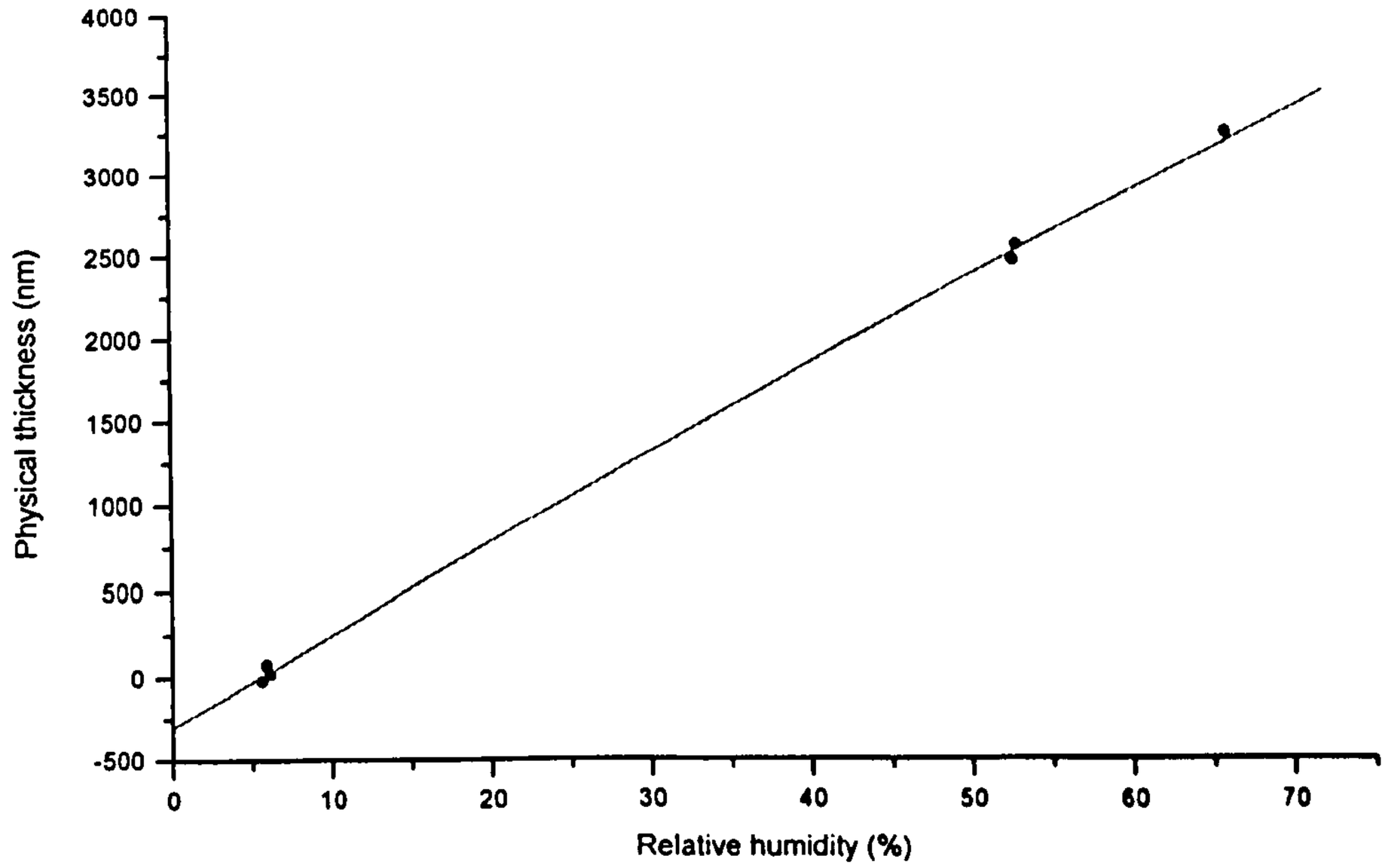

Figure 7.9 shows the linearity of the polyvinyl alcohol film when submitted to humidity

7.2.8 The PMMA-PMTGA-PMMA polymer

This last tested polymer was supplied by J.Keddie from the University of Surrey. The tested polymer film is composed of a triblock copolymer having PMMA endblocks and a hydrophilic midblock composed of poly(methoxytriethylene glycol acrylate) (PMTGA). The PMTGA block copolymer was made by transesterification of poly(tert-butyl acrylate) [7] obtained via anionic polymerization, as described by Chen et al [8,9]. The degree of polymerization of the PMMA end blocks and the PMTGA midblock was determined to be 220 and 664, respectively. The polydispersity index of the copolymer is 1.27 which refers to the molecular weight distribution in the polymer structure. To deposit the film to be tested as a humidity sensor the copolymer was first dissolved in a mixture of ethanol and toluene at 80 °C to make a 1.2 wt.% solution. This solution was cooled to ambient and then spread on the surface of an evaporated gold film that had been deposited onto a glass substrate to allow measurements of OPD changes through the polymer. The solvent was left to evaporate for several minutes. The resulting viscous, concentrated solution was further smoothed under shear stress by spinning at 2000 rpm for 30s on a commercial spin-coater. Sufficient solution was used to obtain a final polymer coating thickness of 12 μm. The obtained film was transparent and both tests could be made.

7.2.9 The PMMA-PMTGA-PMMA polymer result

The polymer is a tri-block molecule in which the center block is a hydrophilic acrylate and in which the end blocks are poly(methyl methacrylate) (PMMA). The hydrophilic midblock has side chains that contain short poly(ethylene glycol) segments that impart hydrophilicity [8]. Previous thermal analysis [9] and investigations of the swelling behaviour [8] of the copolymer suggest that the PMMA end blocks form a separate microscopic phase. The PMMA domains create physical crosslinks that prevent dissolution of the copolymer in water but do not decrease the hydrophilicity of the midblock. Measurements with a microbalance revealed that a thin film of this polymer absorbs up to about 30 % of its mass when exposed to 90% relative humidity. The absorption reaches an equilibrium level within a few minutes after the exposure to humidity. The absorption is reversible, such that when the polymer is in a lower

humidity environment, the water is desorbed. These water uptake characteristics are described in detail elsewhere [8].

7.2.9.1 Evaluation of the optical thickness change of the polymer when submitted to humidity

The sample was inserted in the optical system (7.1) and tested. The mirror was placed behind the polymer material and the optical path changes induced by the refractive index variations were monitored while varying the humidity levels. The result is seen in figure 7.10 while figure 7.11 shows the temperature and relative humidity changes during the experiment. The maximum deviation of recorded in figure 7.10 was 3 μm which is respectable compared to the 12 μm thickness of the polymer. However the optical path change was not stable when humidity levels were maintained at a constant value as seen in figure 7.10 and as was already observed for the cellulose acetate samples. Even if the response was far better than the previously tested polymers this configuration was therefore not considered for the final sensing configuration when compared to the measurements of the physical thickness of the film described in the following section.

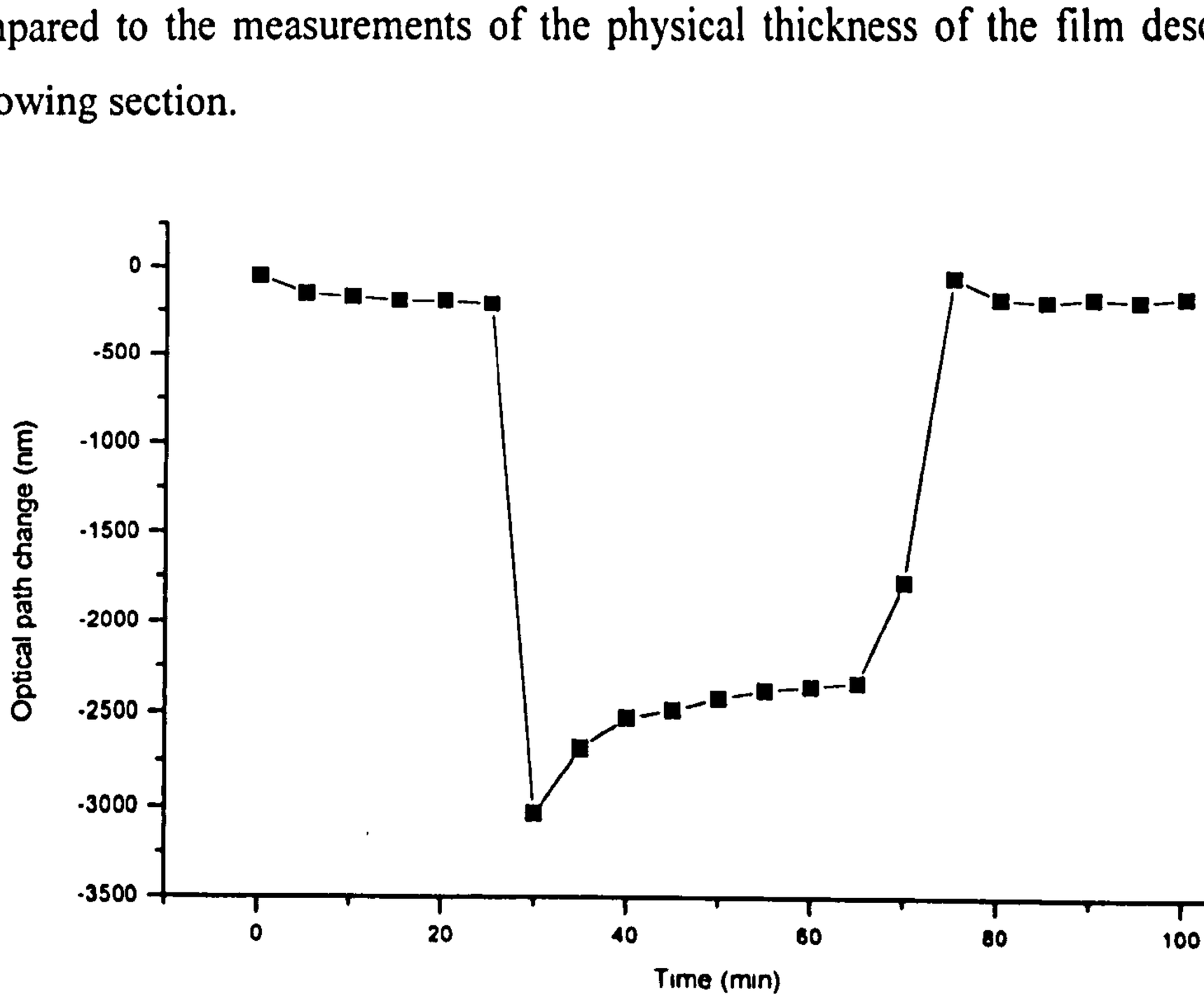

Figure 7.10 shows the response of the PMMA-PMTGA-PMMA sample when varying humidity

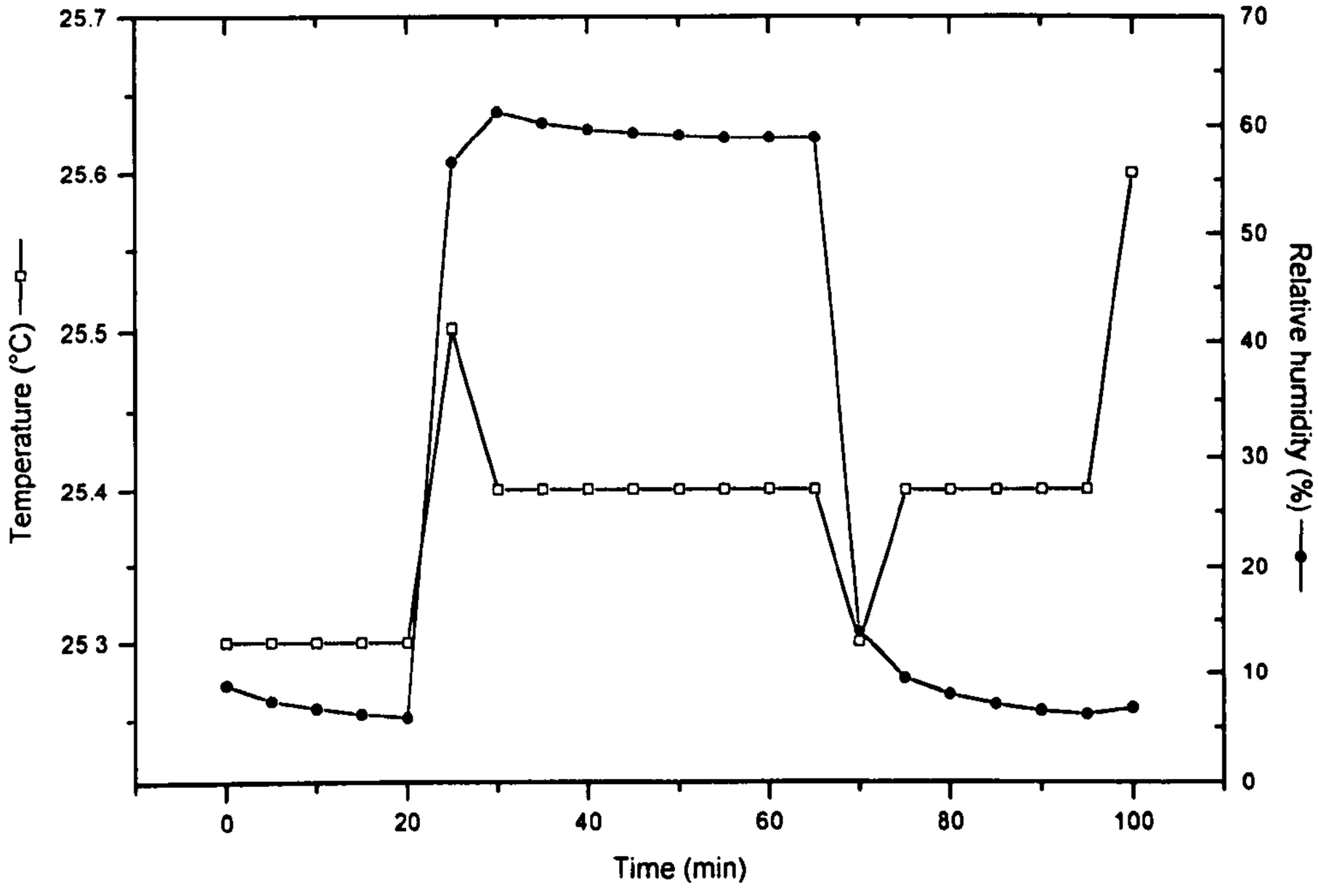

Figure 7.11 shows the temperature and humidity changes during the experiment

7.2.9.2 Evaluation of the physical thickness change of the polymer when submitted to humidity

As in the previous experiment the polymer was placed in the optical system described in section 7.1 on two lines. As seen in figure 7.12 the response of the physical thickness of the polymer was clear and closely followed the electronic commercial reference. This polymer being the best material obtained for humidity sensing a calibration was made converting the physical path change to relative humidity allowing a direct comparison with the commercial probe as seen in figure 7.12. The amplitude response of the polymer increased to 6 μm between 4 and 85 % RH. This corresponds to 51% of the thickness of the film. This high value compared to the previously tested polymers was coupled to a perfect repeatability and no ageing over long periods.

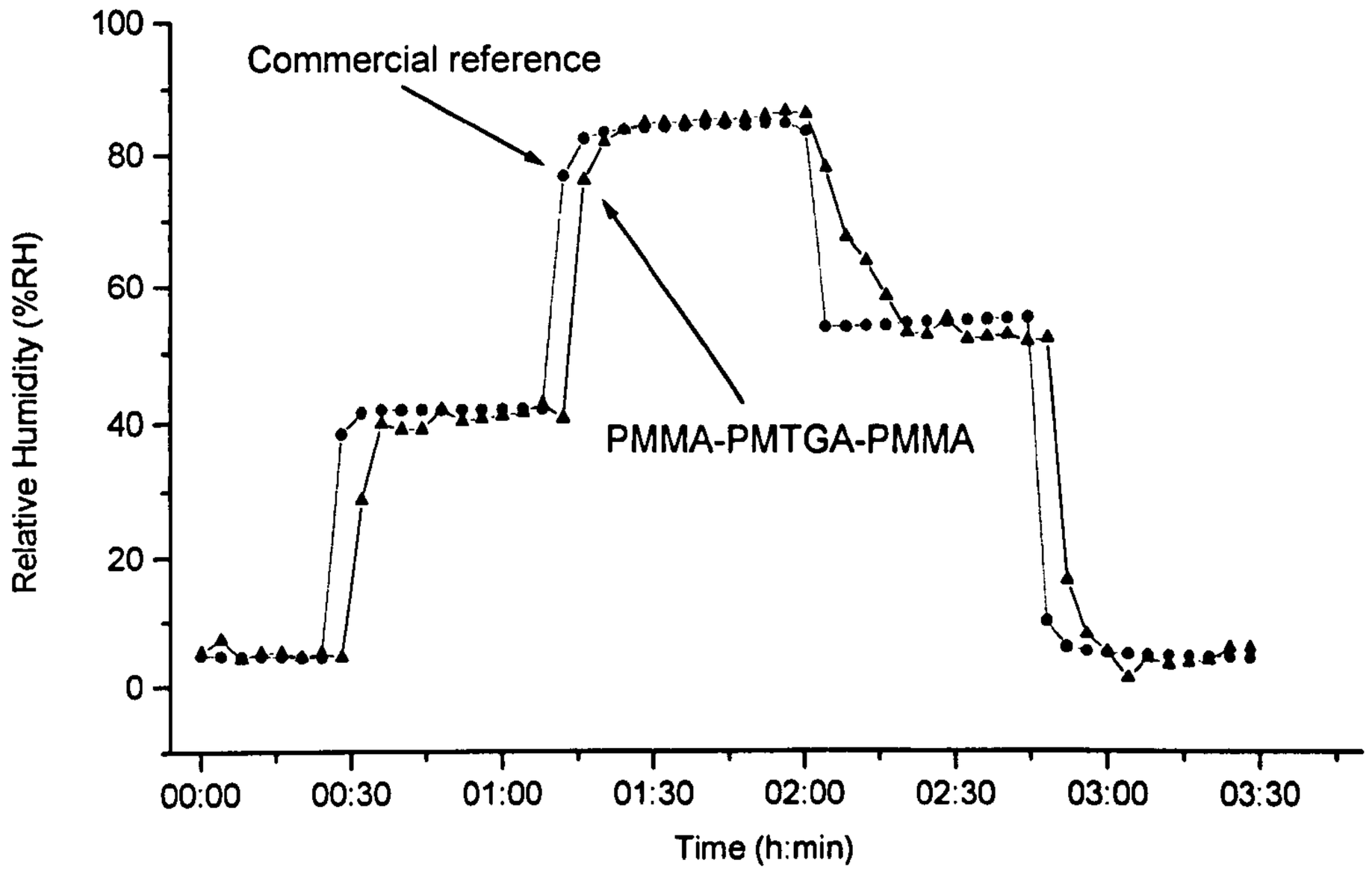

Figure 7.12 shows the response of the PMMA-PMTGA-PMMA polymer when submitted to humidity

This polymer was therefore used in the final prototype for demonstration in the optical system described in 7.1. The humidity could be cycled several times without any alteration of the response of the polymer.

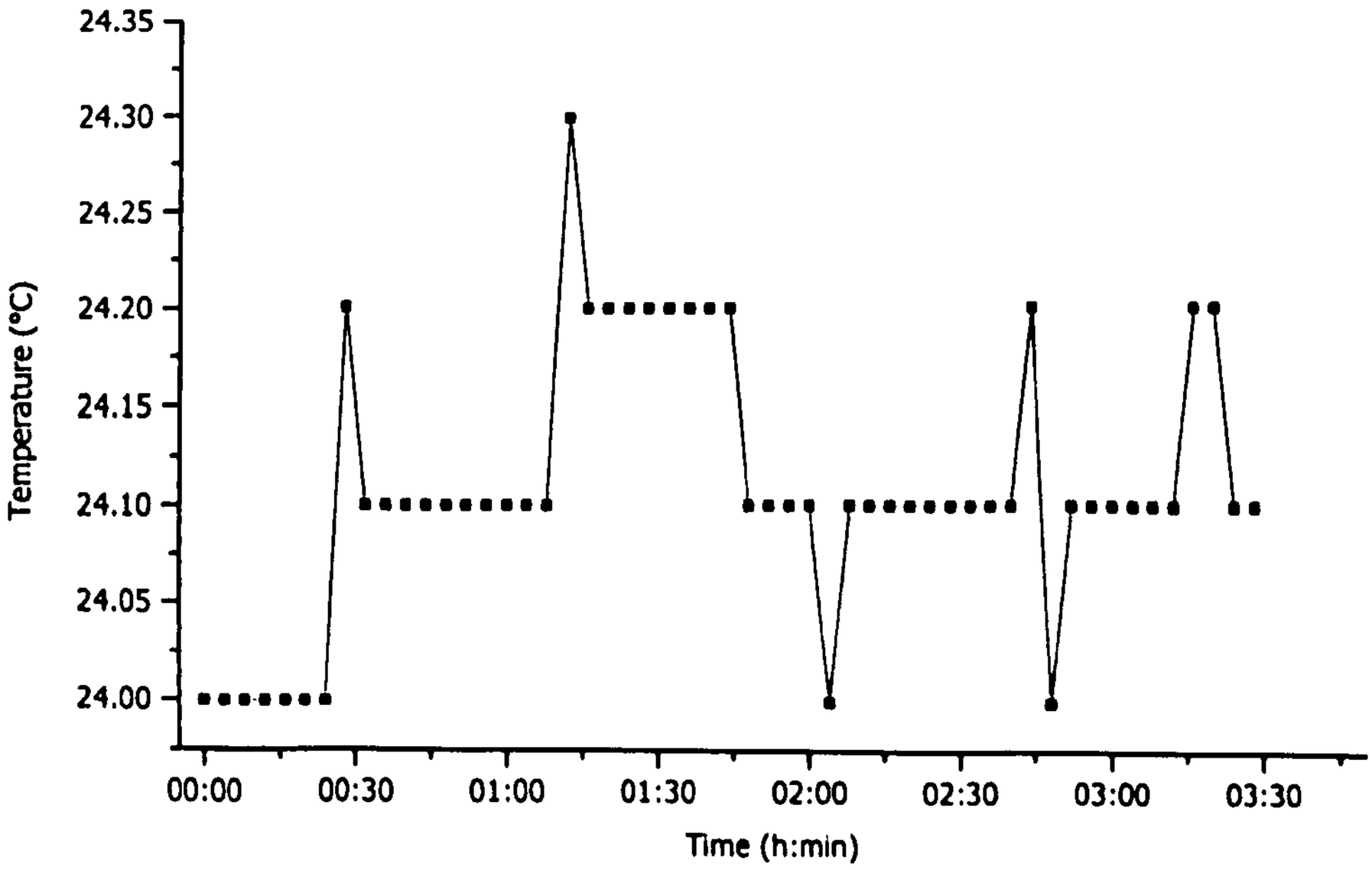

Figure 7.13 shows the temperature variation during the experiment

The overall response to humidity of the optical system using this polymer is accurate down to 1.21 % with a standard deviation of 0.9% at equilibrium. Figure 7.13 shows that the temperature variations (measured electronically in the test chamber) during the experiment remained small. Also, temperature fluctuations were found to have no influence on the relative humidity measurement. The final demonstrated prototype was multiplexed over four lines as described in section 7.1.2, two sensors were based on this polymer measuring relative humidity independently, the third line was coupled to a piezoelectric bender to demonstrate the optical performance of the system independently of the polymer, and finally the last line was used as a reference. As described in section 7.1.2, minor modifications to this system could allow the multiplexing of 32 independent optical humidity sensors.

7.3 References

[1] Y. J. Rao, and D. A. Jackson, Meas. Sci. Technol., 7, (1996), 981-999.

[2] Y. J. Rao, D. J. Webb and D. A. Jackson, Proc. SPIE 2070, (1993), 35.

[3] J. L. Brooks, IEEE J Lightwave Technol., 3, (1985), 1062-1072.

[4] F. Farahi, T. P. Newson, J. D. C Jones and D. A. Jackson, Opt. Commun., 65, (1988), 319-321.

[5] Y. J. Rao, A. B. Lobo Ribeiro, and D. A. Jackson, Opt. Commun., 125, (1996), 53-58.

[6] W. J. Roff and J. R. Scott, "Fibres, Films, Plastics and Rubbers - a handbook of common polymers", (1971), Butterworths.

[7] S. K. Varshney, C. Jacobs, J. P. Hautekeer, P. Bayard, R. Jerome, R. Fayt and P. Teyssi, Macromolecules, 24, (1991), 4997.

[8] W-L. Chen, K. R. Shull, T. Papatheodorou, D. A. Styrkas and J. L. Keddie Macromolecules, 32, (1999), 136-144.

[9] W.-L. Chen and K. R. Shull, Macromolecules, 32, (1999), 6298-6306.

8

Conclusion

8.1 Introduction

8.2 Materials

8.2.1 Sol-gels

8.2.2 Aerogels

8.2.3 Polymers

8.3 Interferometry

8.3.1 Sensing humidity by measuring the refractive index of air

8.3.2.Profilemeter

8.3.3 Dual tandem interferometry for accurate optical path difference variations

8.3.4 Final prototype using dual tandem interferometry

8.4 Further possibilities for humidity sensing

8.5 Overall conclusion

8.1 Introduction

During this project several tasks were accomplished. The first task was to find a suitable material for optical humidity sensing. The three main routes explored were, sol-gels, aerogels, and polymers. The second task was to create an optical system capable of testing the materials with potential for use as humidity sensors. This was accomplished by an optical profilemeter and an interferometric system based on dual tandem interferometry. Finally, the last task was to demonstrate a fully working prototype system, based on a processing interferometer connected to interferometric Fabry-Perot type sensors multiplexed spatially on separate monomode fibre transceiver links, for sensing humidity by using the adequate material and suitable for demonstration.

8.2 Materials

8.2.1 Sol-gels

The first samples evaluated as humidity sensors were sol-gels. The fabrication of sol-gels proved to be difficult when made in thick films (over 10μm). The main problem was to control the drying process to avoid any cracking of the gel. The use of a DCCA such as dimethylformamide was useful but not sufficient to create uncracked sol-gel samples in a repeatable way. However small samples were recovered and tested. The results showed that the sol-gel material responded to humidity but not in a repeatable way as ageing effects occurred over long periods. Also as the amplitude of the response was not sufficient, it was not possible to reduce the response time by decreasing the thickness of the sol-gel film. The sol-gel material was therefore a possible material but the ageing, and the reliability of the fabrication had to be solved. As the ageing phenomena in the sol-gel structure is due to the continuation of the sol-gel reactions creating further cross-links in the structure, a possible solution was to remove the remaining pore liquid. This was achieved by super-critical drying the samples leading to aerogels.

8.2.2 Aerogels

Using the same type of samples as for sol-gels, aerogels were made in BNFL's laboratories. The super critical drying was done using liquid CO_2. The process was time consuming (three hours) but several samples could be produced each time. Several samples were produced and their reaction was recorded when submitted to humidity. Using the same sample it was possible not only to measure its physical thickness change but also its optical thickness as the samples were transparent. The results showed that measuring the physical thickness was a possible solution for humidity sensing despite apparent random fluctuations (artefacts) during humidity level variations. However the optical thickness response of the aerogels was found to have a greater amplitude without any artefacts. The sensitivity of the aerogels was higher than that of the sol-gels but the samples tested had a long response time. It was therefore planned to reduce the thickness of the samples. Also the samples were to be held in the light path of the

Fabry-Perot interferometer rather than to be stuck to the back reflecting mirror of the cavity to allow the maximum contact with air. Unfortunately, due to a change of location of the BNFL laboratories, it was no longer possible to use the super critical drying apparatus, although a highly reliable technique for producing thin sol-gel films was developed, leading to many undried samples. Finally the experiments on the produced samples showed that aerogels offered a potential route for a novel type of humidity sensor. Unfortunately, for reasons beyond our control, the research direction had to move to different types of material such as polymers.

8.2.3 Polymers

Polymers were the last type of materials tested. All tested polymers reacted favourably to humidity. However several problems occurred such as a low amplitude of response, artefacts, long response time, often coupled with a loss of response amplitude with time. This loss of amplitude response is due to the modification of the polymer when water molecules penetrate the structure. It is thus important to find the right balance between the strength of the structure and its hydrophilicity. This was the case for the cross linked PMMA-PMTGA-PMMA polymer that showed a good sensitivity, and virtually no ageing. Also, this sample obtained the best results since the response of the film was identical, even after many humidity cycles, and over long periods. This polymer was therefore implemented as the final material in the optical humidity sensor prototype.

8.3 Interferometry

8.3.1 Sensing humidity by measuring the refractive index of air

The Edlen's equation showed that the effect of humidity on the refractive index of air was not negligible. In fact the optical path difference of 171 nm corresponding to the full range of humidity is easily measurable using an interferometric system. The experiment showed that, provided the values of pressure and temperature were known with sufficient accuracy, it was possible to accurately sense humidity by measuring the refractive index of air. The accuracy achieved by this approach being comparable to the best electronic humidity sensors. This novel method has obvious advantages. As there is no sensing material the sensor does not suffer from ageing, high response time, hysteresis or other drawbacks of solid state materials. The probe is made of materials perfectly resistant to very high humidity levels and all parts were glued to allow handling. Obviously the probe could be far thinner, the only limitation being the cavity length. The optical system described shows only one probe, but a multiplexed system could be easily achieved. As discussed previously the effect of CO_2 is not an important issue since in most case, as for a meteorological use, the CO_2 levels remain constant making this probe suitable for most situations. Furthermore, by detecting any sudden changes in amplitude of the returned signal, this sensor could be used to detect any suspicious smoke. This sensor could also be used to check the calibration of other coupled sensors. In the case of a meteorological station, temperature, pressure, and relative humidity are recorded periodically. The calibration of these three sensors is done regularly to avoid any false measurement and can become costly if many sensors are involved. When coupled to other sensors this probe could be used to check the calibration of each sensor by sensing the refractive index and comparing this value with the calculated value derived from Edlen's equation. Therefore, this novel system has many possibilities, either as a complementary probe to check calibrations or as an accurate and maintenance free humidity sensor

8.3.2.Profilemeter

This bulk optical system was built to test sol-gel samples planned to be 10 μm or thicker. The system was able to measure physical and optical thicknesses and had the ability to track step changes during the scanning. The samples were prepared to enable the measurement of any change in the optical or physical thicknesses to be observed in one scan. The system was tested and a resolution of 3.14 μm was observed. Unfortunately, the sol-gel material cracked when thick layers were deposited and all uncracked samples provided by J. D. Wright had a physical and optical thickness less than the resolution of the profilemeter. This device is a powerful instrument since, both physical and optical thickness can be measured at the same time during one scan. Also, this system had the advantage of allowing the testing of samples thick from 10μm to 10 cm. Simple modifications could improve the performance, such as an automated coherence finding routine using a precision translation stage driven by a computer. This would increase the resolution of the system but also its scanning speed. (Commercial stages are available with a resolution better than 1 nm).

8.3.3 Dual tandem interferometry for accurate optical path difference variations

This system was built to allow the measurement of physical and optical thicknesses with the maximum of accuracy (5 nm) over a maximum range (70 μm). This system was extremely useful enabling many materials to be tested for their response to humidity. The system was convenient to use as the back plate of the sensor's head could be replaced very easily by removing three screws. Also the samples could be of different sizes as the collimator could be easily adjusted. The speed of the piezoelectric compensator was found to be sufficient as no material exceeded the compensation speed while swelling or by changing its optical thickness. Globally this system was perfectly adequate for measuring small or large optical path changes.

8.3.4 Final prototype using dual tandem interferometry

The final prototype was suitable for demonstration. A computer using a Labview program controlled the full system. The computer recovered the interferometric signals from a digital oscilloscope via an IEEE communication link, controlled the scanning piezoelectric actuator by using a digital card, and finally imported the values of the relative humidity and temperature in the test chamber sensed with the electronic Vaisala transmitter using an RS 232 serial interface.

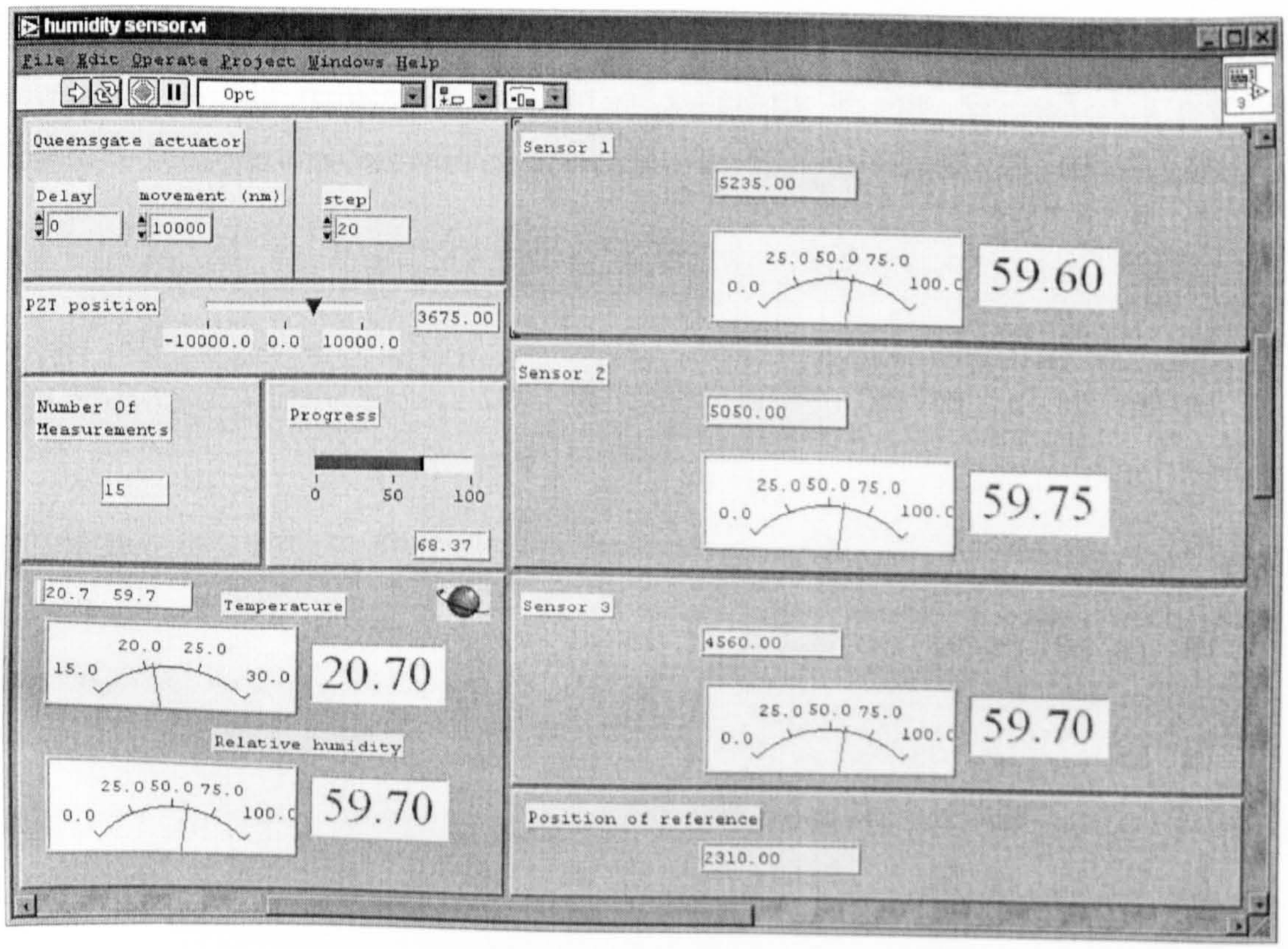

Figure 8.1 shows the graphical interface of the Labview program used to drive the prototype

As the optical system was illuminated with a low coherence source, the location of the maximum of the transfer function of each line allowed an absolute measurement on each sensor. Therefore the system could be switched on and off without any calibration or tuning to be made, as for a commercial device. The system was placed on an optical table but all parts of the system could be easily packaged allowing transportation and easy deployment in virtually any location. The prototype allowed measurements on four

separate lines, however, as mentioned earlier, the number of multiplexed lines depends only on the available power. This multiplexing scheme could allow 32 sensing lines using the same 10 mw super luminescent source, 64 sensors for a 20 mw source and so on. This is possible by simply modifying the Labview program and by adding other sensors. The prototype used a PMMA-PMTGA-PMMA film that allowed an accuracy of 1.21 % RH but any other material such as aerogels could be inserted. The system's accuracy could be improved by using a Queensgate piezoelectric actuator coupled with nano sensors allowing a subnanometric resolution. The acquisition system could also be improved by using a dedicated data acquisition card rather than an oscilloscope. Finally the use of a power distributor (fiberoptic switch) interrogating the sensor lines sequentially would reduce the number of detectors to one. Overall this prototype showed to be close to a commercial device and certainly met BNFL's requirements.

8.4 Further possibilities for humidity sensing

Further research could be directed on both, the optical system and on the sensing materials. Aerogels are a route for further research on humidity sensing. During this project the various measurements showed that this material had a good potential for humidity sensing. However other materials could be considered such as novel polymers as the only requirement to be used in the previously described prototype is a repeatable physical or optical thickness change of adequate amplitude over the full range of humidity. Concerning the optics, another route of research could be the measurement of the optical path difference by evaluating the distance between two maximas of the channelled spectrum returned by a Fabry-Perot cavity. The system could be composed of a fibre tree distributing the power in spatially multiplexed Fabry-Perot sensors interrogated sequentially by a power distributor (fiberoptic switch). The channelled spectrum could then be recorded in a computer by using a spectrum analyser computer card. The potential advantage of this method is its simplicity, however accurate data analysis of the channelled spectrum would be necessary to obtain sufficient accuracy in the humidity measurement.

8.5 Overall conclusion

The aim of this project was to explore the possibility of an all fibre optic based humidity sensor. During this project a low cost humidity generator was developed allowing humidity to be tuned over the full range of humidity at a constant flow. Using an accurate dual tandem interferometric system many materials were tested for their possible implementation as a humidity sensors. Sol-gels and aerogels showed to be good candidates and the work reported in this thesis open novel routes for humidity sensing. Also a novel and accurate humidity sensing probe based on the measurement of the refractive index of air has been studied and a dual tandem interferometric system demonstrated offering new possibilities in humidity sensing without using solid state materials. Finally, several polymers were tested and the results showed that the PMMA-PMTGA-PMMA polymer was the best candidate for humidity sensing. This polymer was inserted in a dual tandem multiplexed interferometric system to allow an accurate and absolute measurement of humidity over several independent lines. The final prototype was very close to a commercial device as it was totally independent and gave a continuous reading of the relative humidity on a computer screen of the different sensors that could be in different and remote locations. Finally, this system could easily become a commercial humidity sensing device for use in industry.